



HAL
open science

Binary metal oxides thin films and their role in understanding cell-material interaction

Abhishek Yadav

► **To cite this version:**

Abhishek Yadav. Binary metal oxides thin films and their role in understanding cell-material interaction. Chemical Sciences. Normandie Université, 2024. English. NNT: 2024NORMC208. tel-04720949

HAL Id: tel-04720949

<https://theses.hal.science/tel-04720949v1>

Submitted on 4 Oct 2024

HAL is a multi-disciplinary open access archive for the deposit and dissemination of scientific research documents, whether they are published or not. The documents may come from teaching and research institutions in France or abroad, or from public or private research centers.

L'archive ouverte pluridisciplinaire **HAL**, est destinée au dépôt et à la diffusion de documents scientifiques de niveau recherche, publiés ou non, émanant des établissements d'enseignement et de recherche français ou étrangers, des laboratoires publics ou privés.

THÈSE

Pour obtenir le diplôme de doctorat

Spécialité **CHIMIE**

Préparée au sein de l'**Université de Caen Normandie**

BINARY METAL OXIDES THIN FILMS AND THEIR ROLE IN UNDERSTANDING CELL-MATERIAL INTERACTION

Présentée et soutenue par

ABHISHEK YADAV

Thèse soutenue le 19/01/2024

devant le jury composé de :

M. WILFRID PRELLIER	Directeur de recherche au CNRS - Université de Caen Normandie	Directeur de thèse
MME NATHALIE LEMEE	Professeur des universités - UNIVERSITE AMIENS PICARDIE JULES VERNE	Président du jury
M. KARIM BOUMEDIENE	Professeur des universités - Université de Caen Normandie	Membre du jury
M. RACHEL DESFEUX	Professeur des universités - Université Artois	Rapporteur du jury
M. FRANCK TESSIER	Directeur de recherche au CNRS - UNIVERSITE RENNES 1	Rapporteur du jury

Thèse dirigée par **WILFRID PRELLIER** (Laboratoire de cristallographie et sciences des matériaux (Caen))

ABSTRACT

Understanding how surface chemistry, material composition, and deposition conditions affect cellular function is crucial for building substrates for bio medicine and orthopedic prostheses. This thesis examines the impact of metal oxide thin films on human and bacterial cell behavior, focusing on VO_x , CuTiO , Al_2O_3 , ZnO , and TiO_2 as substrates. With Pulsed Laser Deposition (PLD), we achieved 0.1-0.9 nm surface roughness and evaluated all films' hydrophilic characteristics. This ensures ideal cell adhesion research settings. VO_x adheres to and promotes the proliferation of human bone marrow-derived mesenchymal stem cells (hBMMSCs) when deposited at 400°C , according to our initial research. Additionally, VO_x coatings promoted chondrogenesis while having no effect on adipogenic and osteogenic differentiation. Furthermore, $\text{Cu}_{0.75}\text{Ti}_{0.25}\text{O}_2$ films were tested for antibacterial characteristics. A decrease of 20% in bacterial proliferation indicates that these coatings have the potential to inhibit the growth of biofilms. Following our examination of the bio-compatibility of VO_x and CuTiO films, we proceeded to conduct a more in-depth investigation including cancer cells and the inhibition of cell development on other metal oxide films. For this purpose, we employed thin films composed of binary oxides such as ZnO , Al_2O_3 , CuO_x , VO_x , and TiO_2 to investigate the behavior of cancer cells, yielding diverse outcomes. TiO_2 and Al_2O_3 enhanced adhesion and proliferation to levels that were equivalent to or higher than those observed on a regular polyethylene terephthalate (PET) support. However, CuO_x and ZnO were able to eradicate SKOV3 cells that were seen in ovarian cancer. This extensive investigation demonstrates the intricate and varied biological responses to thin coatings composed of metal oxides. The findings augment our comprehension of the impact of oxide thin films on various cell types, underscoring the significance of material choice in biomedical research.

Acknowledgment

I would like to express my deepest gratitude to my supervisor, Dr. Wilfrid Prellier, whose guidance, support, and mentorship have been invaluable throughout my journey in pursuing a Ph.D. His unwavering commitment to excellence and their insightful guidance have played a pivotal role in shaping my research and academic pursuits.

I am also immensely thankful to my family for their unwavering support and encouragement. Their love and belief in my abilities have been a constant source of motivation. To my friends Krish, Anjali, Mufeed, Yogi, Vasvant, and Someshwer, your friendship has added immeasurable joy to my life, and I appreciate the camaraderie we shared during the highs and lows of this academic endeavor.

A special mention goes to Dr. Oualyd El-Khaloufi (Lulu), who has been more than a friend; he is like a brother to me. I had the privilege of crossing paths with Oualyd when I joined the Ph.D. program on January 04, 2021. From the early days of our friendship, you have been a mentor, a confidant, and a source of inspiration. Your unwavering belief in my potential and your constructive feedback have played a pivotal role in shaping my research and personal growth. The bond we share goes beyond the academic realm, and I am truly fortunate to have you as a best friend.

To Dr. Mudit Upadhyay (Hahahihi), who is not just a friend but a brother in every sense, I am incredibly grateful. His unwavering belief in my abilities and his willingness to share both the challenges and triumphs of this academic pursuit have made the journey more meaningful. Mudit, your friendship is a treasure, and I am thankful for the shared laughter, late-night discussions, and the countless moments that have enriched my Ph.D. experience.

I extend my heartfelt thanks to all those who have played a role, big or small, in my academic and personal life. Your support has been instrumental in reaching this milestone, and I am truly appreciative of the collective effort that has contributed to my success.

List of abbreviations

- hBMMSCs - Human bone marrow-derived stem cells
- DNA - Deoxyribonucleic acid
- ABC - ATP-binding cassette
- MYC- myelocytomatosis
- PIK3CA - phosphatidylinositol-4,5-bisphosphate 3-kinase catalytic subunit alpha
- PI3K/AKT - phosphoinositide-3-kinase-protein kinase B/Akt
- SMAD4 - Suppressor of Mothers against Decapentaplegic 4
- TGF - Transforming growth factor
- KRAS - Kirsten rat sarcoma viral oncogene.
- BRAF- v-raf murine sarcoma viral oncogene homolog B
- CDKN2A - Cyclin-dependent kinase inhibitor 2A
- AFM - Atomic Force Microscopy
- α -MEM - alpha Minimum Essential Medium
- DEPC - Diethyl Pyrocarbonate
- DMEM - Dulbecco's Modified Eagle Medium
- ECM - Extracellular Matrix
- FGF - Fibroblast Growth Factor
- H₂O_d - Distilled water
- HA - Hydroxyapatite
- PBS - Phosphate Buffered Saline
- PFA - Paraformaldehyde
- PLD - Pulsed Laser Deposition
- RNA - Ribonucleic Acid
- ROS - Reactive Oxygen Species
- RT-PCR - Reverse Transcription Polymerase Chain Reaction
- SEM - Scanning Electron Microscopy
- WST - Water-Soluble Tetrazolium
- XPS - X-ray Photoelectron Spectroscopy
- XRD - X-Ray Diffraction
- XRR - X-Ray Reflectivity
- AB - Agrobacterium

Table des matières

CONTENTS	1
1 General Introduction	15
2 Literature Review	19
2.1 Biological matter	19
2.1.1 Stem Cell	20
2.1.2 Cancer Cells	21
2.1.3 Pseudomonas aeruginosa bacterium	24
2.2 Interaction of cellular entities with materials	26
2.3 Exploring Metal Oxides : Unraveling Their Role in Cell-Material Interactions.	28
3 Experimental Technique	33
3.1 Synthesis of PLD target and preparation of Substrate	33
3.2 Thin film preparation	34
3.2.1 Pulsed laser deposition (PLD)	34
3.2.2 Principle of the pulsed laser deposition	35
3.2.3 Growth modes	36
3.3 Characterization techniques	37
3.3.1 X-ray interaction	37
3.3.2 X-ray reflectivity	38
3.3.3 Atomic force microscopy	41

3.3.4	Scanning electron microscopy	42
3.3.5	X-ray photoelectron spectroscopy (XPS)	44
3.3.6	Calculation of contact angle and surface energy	45
3.4	Cell Culture	47
3.4.1	<i>Pseudomonas aeruginosa</i> bacterial cells	47
3.4.2	Mesenchymal stem cells from bone marrow	47
3.4.3	Ovarian and Chondrosarcoma cancer cells	48
3.5	Investigation of bacterial cells adhesion and proliferation	49
3.5.1	Light sheet microscopy imaging	49
3.5.2	Crystal violet (CV) staining of biofilm biomass	50
3.6	Investigation of human stem cells adhesion and proliferation	50
3.6.1	Phase contrast microscopy	50
3.6.2	Histological staining	51
3.6.3	Cell density measurements	53
3.7	Study of human mesenchymal stem cell differentiation	54
3.7.1	Differentiation staining	54
3.7.2	Real time RT-PCR	56
4	Stem Cell Differentiation Using Vanadium Oxide Thin Film	61
4.1	Introduction	61
4.2	Optimization of VO_x thin films with cell adhesion	63
4.3	Structural analysis of optimized VO_x film deposited at 400°C	66
4.4	Cell adhesion and proliferation of hBMMSCs on calibrated sample	72
4.5	Differentiation assays via histological staining	74
4.6	Real-time Reverse Polymerase Chain Reaction	75
4.7	Conclusion	77
5	Antibacterial Properties of Metal Oxides Thin Films	79
5.1	Introduction	79
5.2	Optimization of CuTiO thin films	82
5.3	Bacterial cultivation	83
5.4	Interaction of Cu ions with bacterial cell	83
5.5	Results and Discussion	84
5.5.1	Structure and surface topography of thin films	84

5.5.2	Analysis of surface state by X-ray photoelectron spectroscopy . . .	87
5.5.3	Antibacterial activity of thin films	89
5.6	Interpretation of the results	91
5.7	Conclusion	93
6	Cancer Cells Growth On Binary Metal Oxide Thin Films	95
6.1	Introduction	95
6.2	Experimental techniques	99
6.2.1	Films preparation and characterization	99
6.2.2	Real-time cell imaging of cell morphology	100
6.2.3	Cell death and real-time quantification	100
6.2.4	Nuclei counting after staining by DAPI	100
6.3	Results and discussion	101
6.3.1	Structure and surface topography of thin films	101
6.3.2	Cell proliferation and cell death on oxide films	102
6.4	Discussion	106
7	Conclusions and Perspectives	109
7.1	Conclusion	109
7.2	Future perspective	111

Table des figures

2.1	Schematic representation of Mesenchymal Stem Cells (MSCs) differentiation process into different lineages : Myocytes, Chondrocytes, Osteocytes, Adipocytes, and Neural Cell.	20
2.2	Microscopic image of SW1353 cancer cells.	22
2.3	Microscopic image of SKVO3 cells	23
2.4	Schematic diagram showing the structure of the <i>Pseudomonas aeruginosa</i>	25
2.5	Schematic representation of the cell-material-interaction.	26
2.6	Main steps and molecules involved in cell adhesion to matrix. Cell surface receptors (mostly integrins) interact with specific molecules of the matrix, leading to attachment and spreading of the cell. Attachment is then enhanced through the interaction of focal adhesion (FA) proteins and integrins. Finally, a rearrangement of the cytoskeleton occurs which leads to the spreading of the cell over the surface.	27
3.1	Schematic of PLD system	35
3.2	(a) island : Volmer-Weber growth mod (b) layer by-layer : Van des Merwe growth mode (c) layer plus island : Stranski-Krastanov growth mode.	36
3.3	Bragg's law. Grids represent two-dimensional crystal lattices and imaginary planes. When X-rays strike the crystal at an angle, coherent diffraction (in phase) occurs when the difference in distance ($2d \sin$) equals an integral number of the wavelength (n).	38

3.4	Information provided by X-ray reflectivity.	40
3.5	Schematic representation of AFM.	42
3.6	Zeiss SUPRA 55 scanning electron microscope.	43
3.7	Schematic diagram of X-ray photoelectron spectroscopy (XPS).	44
3.8	Schematic diagram illustrating the components of the contact angle.	46
3.9	Schematic of 24-well plate used during in-vitro experiments.	48
3.10	Schematic of RT-PCR.	56
4.1	Cellular adhesion after 2 hr of incubation period at different temperatures with and without oxygen presence while depositing the thin films. (VN -O ₂ and VN +O ₂ represent the vanadium film deposition without and with the presence of Oxygen in the PLD chamber).	64
4.2	Cellular adhesion after 24 hr of incubation period at different temperatures with and without oxygen presence while depositing the thin films.	65
4.3	Evolution of cells <i>count/mm</i> ² with the incubation period of adhesion on vanadium oxide thin films deposited at different temperatures.	66
4.4	AFM images showing the surface profiles of the glass substrate (control) (a) and VO _x thin films (b). The corresponding average roughness (R _a) is indicated below each figure. Typical VO _x thin films were analyzed for their XRD patterns (c) and XRR curves (d).	67
4.5	Contact angle images of vanadium oxide thin films with different testing liquids (water, ethylene glycol, glycerol) are shown. The thickness of the films are also indicated against each figure.	69
4.6	Variation of the magnitude of contact angle with respect to the thickness of VO _x thin films. The contact angle with water and ethylene glycol is represented by the symbols ■ and ○, respectively.	70
4.7	Evolution of total surface energy (■) and its polar (●) and dispersive (▲) components with varying thickness of the VO _x thin films.	71
4.8	Cell density of hBMMSCs cultured on glass and plastic control and VO _x thin films after 2 hours of culture. (a) Phase contrast images of hBMMSCs on glass control and VO _x surfaces were recorded after 2 and 4 hours of culture (scale bar = 400 μ m). (b) shows the corresponding cell density of glass and plastic control versus VO _x surfaces, respectively (after 10 days).	73

4.9	Cytological staining with Alcian Blue, Alizarin Red, or Oil Red for hBMM-SCs differentiation potential. Microphotographs were taken with a bright field microscope at a magnification of 10X.	75
4.10	chondrogenic (COL2A1, ACAN), Osteogenic (OSTERIX), and adipogenic (CEBP) differentiation of hBMMSCs on Plastic, Glass, and, VO _x thin films substrates after 14 days of culture. Statistical evaluation was performed by comparing the samples with the glass and plastic substrate.	76
5.1	The main mode of mortality in many microorganisms caused by copper nanoparticles.	84
5.2	1 μm x 1 μm AFM images of 20 nm (a), and 24 nm (b) thin CTO films. The roughness values are indicated below each respective figure. Additionally, typical XRR curves for these films, recorded from 0 to 3°, are shown, with experimental data depicted in black and fitted curves in red. The corresponding calculated thicknesses are 20 nm (c) and 24 nm (d).	85
5.3	(a) Variation of surface energy and contact angle with film thickness is depicted, where ■ and ● represent the test liquids water and ethylene glycol, respectively. (b) and (c) display typical contact angle images with water and ethanol, respectively.	86
5.4	XPS scan of Cu _{0.75} Ti _{0.25} O ₂ thin films : (a) Survey scan for 16 nm. (b) to (d) high-resolution spectra of Cu 2p, Ti 2p, and O 1s. (e) Survey scan of 24 nm and (f) to (h) high-resolution spectra of Cu 2p, Ti 2p, and O 1s respectively.	88

5.5	$\text{Cu}_{0.75}\text{Ti}_{0.25}\text{O}_x$ -coating reduces bacterial cell initial attachment and resisted biofilm formation. (a) The bar chart shows the normalized mPAO1 biofilm biomass 24 hours post-incubation under biofilm-inducing conditions. There was larger biofilm biomass compared to $\text{Cu}_{0.75}\text{Ti}_{0.25}\text{O}_x$ -coated glass surfaces. (b) The number of planktonic mPAO1 cells that attached to uncoated and $\text{Cu}_{0.75}\text{Ti}_{0.25}\text{O}_x$ -coated glass surfaces were counted and quantified 6 hours post-incubation under biofilm-inducing conditions. The bar chart depicts the number of adhered planktonic mPAO1 bacterial cells 6 hours post incubation. There were almost 20% more bacterial cell attachments detected on the uncoated glass surface (control) compared to the $\text{Cu}_{0.75}\text{Ti}_{0.25}\text{O}_x$ -coated glass surfaces. (c) The light sheet image shows the initial attachment of fluorescence-labeled mPAO1 bacterial cells (green) on the glass surface in control and $\text{Cu}_{0.75}\text{Ti}_{0.25}\text{O}_x$ -coated glass surface. Each bacterial cell appears as a green dot on a single plane.	90
6.1	Typical XRR curves and $2\mu\text{m} \times 2\mu\text{m}$ AFM image of 20 nm of Al_2O_3 (a), CuO_x (b), TiO_2 (c), and ZnO (d) thin films. XRR recorded from 0 to 2.5, including experimental (black) and fitted (red) curves.	101
6.2	Systematic plot of the contact angle with water and ethylene glycol as the test liquids.	102
6.3	SKVO3 cells growth on PET, Glass, TiO_2 , Al_2O_3 , ZnO and CuO_{xx}	103
6.4	Temporal Assessment of SKOV3 Cell Confluence Post-Seeding and After 48 Hours. The Presence of Green Dots on ZnO and CuO_x Indicates Cell Death Relative to Reference Conditions.	104
6.5	SW1353 Cell proliferation and nuclei count on metal oxide thin films after 90 hrs.	104
6.6	Cell Confluence (%) of SW1353 Cells Over Time Since Seeding.	105
6.7	Kinetics of SKVO3 cells on different metal oxides, plastic and glass coverslips.	105
6.8	Kinetics of SW1353 cells on different metal oxides, plastic and glass coverslips.	106
7.1	XRD profile of various samples of thin films.	113

Liste des tableaux

2.1	Comparison of SW1353 and SKOV3 cell properties.	24
2.2	Comparison of Human Cells and Pseudomonas aeruginosa Bacterial Cells .	25
3.1	Primers sequences used in RT-PCR	57
5.1	Evolution of different parameters for the series of films.	87
5.2	Cu-Ti Ratio Impact on Bacterial Biofilm Growth	89

CHAPITRE 1

General Introduction

Metal oxides have garnered significant interest in both academic and industrial circles due to their diverse physicochemical properties. Their structural flexibility, diverse shapes, and empty lattice structures, combined with the simplicity of introducing dopants, make them promising for technological applications.[1] Additionally, their photocatalytic activity and supermagnetism contribute to their overall utility. Research on the application of metal oxides in medicine has a long history, with initial studies primarily focused on the fundamental characteristics of these materials in large quantities. Historical evidence indicates the use of metal oxides, including ZnO particles, in traditional medicinal systems like Ayurveda for therapeutic purposes, such as in the treatment of diabetes.[2] The exploration of metal oxides in medicine, from conventional bulk materials to advanced nanoparticles and thin films, represents an intersection of materials science and medicine. This interdisciplinary field has emerged from the unique properties of metal oxides and the growing demand for innovative materials in the medical industry. This convergence has led to a vibrant area of research focused on understanding the complex connection between metal oxides and cellular materials, offering exciting opportunities for groundbreaking biomedical applications.[3]

The intriguing properties of metal oxides, including their tunability for electrical, magnetic, and catalytic purposes, have sparked significant interest in their potential applications in medical diagnostics and therapies.[4] Researchers have explored the potential

of metal oxide nanoparticles for various applications, such as targeted drug delivery, imaging, and diagnostics, especially with advancements in nanotechnology. The emergence of nanoscale science has opened up new possibilities for researchers to customize the physicochemical characteristics of metal oxides, resulting in materials with enhanced biocompatibility that can interact with biological entities in precise ways.[5, 6]

Metal oxides find applications in various fields, including catalysts, fuel cells, semiconductors, sensors, piezo-electric devices, biomaterials, and medicines. Several metal oxides, such as Fe_3O_4 , SiO_2 , ZnO , TiO_2 , CuO_x , and CeO_2 have demonstrated impressive bioactivity and biocompatibility, holding great potential for various biomedical applications, including drug delivery, biosensing, bioimaging, biomacromolecule separation, and antimicrobial agents.[7, 8]

The bioactivity of metal oxides is influenced by physicochemical properties such as redox potential, dissolution rate, photocatalytic activity, and surface defects. For example, TiO_2 demonstrates photocatalytic activities applicable in photodynamic therapy for eliminating cancer cells. [9, 10] Conversely, ZnO and CuO_x , with their fast dissolution rate, enhance antimicrobial properties.[11] Additionally, the use of Fe_3O_4 in inducing magnetic hyperthermia in tumors capitalizes on the heightened susceptibility of cancer cells to temperature, providing a precise and focused method for cancer treatment.[12]

In recent decades, engineered metal oxide nanoparticles have overcome technological challenges, offering unique properties not found in larger samples. Engineered nanoparticles, due to their small size, possess exceptional physical and chemical properties, rendering them highly valuable for a wide range of biomedical applications.[13]

However, in the nanoscale realm, toxicity is determined by various factors, including overall characteristics and specific properties related to size, shape, surface coating, and surface charge. Although metal oxides like SiO_2 are generally considered safe, there are reports suggesting potential toxicity at the nanoscale, believed to be due to their heightened chemical reactivity towards cells.[14] The surface area of nanoparticles plays a crucial role in determining toxicity, as research has shown that the increased production of reactive oxygen species (ROS) is a significant factor in their harmful effects.[15]

With the increasing production of engineered metal oxide nanoparticles on an industrial scale, there is a growing need to address concerns regarding potential environmental exposure and the proper handling and disposal of nanoparticle waste to prevent environmental contamination. There is a growing concern about the potential toxicity of metal

oxide nanoparticles due to the increasing number of applications.[16]

In recent years, there has been a significant shift in focus within the field of cell-material interactions, with researchers increasingly investigating metal oxide thin films. Thin films offer a flexible platform for interacting with biological systems at the cellular level due to their nanoscale thickness. This shift is motivated by the recognition that studying thin films provides a valuable chance to investigate the complex relationship between cells and materials. As a result, there is growing interest in examining metal oxide thin films in medical applications to better understand how cells respond to these engineered surfaces.

In the field of biological research, a comprehensive understanding of the substrate used for cell-based experiments is of great importance. This is because the results of these studies are naturally affected by the qualities and properties of the surface on which they are performed.[17] The scientific world has recently become aware that the chemical composition of the topmost atomic layers of a surface can significantly influence cell survival. The study conducted by Nayak *et al.* revealed that the chemical composition of the surface exerted a significant influence on the process of cell proliferation.[18]

In this thesis, we explore the thin metal oxide films grown by Pulsed laser technique and how they interact with human and bacterial cells. Considerable scientific investigation has been devoted to examining the antibacterial properties of many materials, particularly titanium, and copper.[19] The utilization of TiAlV alloys has been well-acknowledged within the realm of biomedical implants. However, it is vital to undertake an inquiry in order to ascertain whether the presence of these components alters the cellular proliferation process or exhibits any cytotoxic properties on human and bacterial cells. In order to better understand how cells react to various metal oxides, such as vanadium, magnesium, and zinc oxide, this thesis will look into how these coatings are used and how they affect cellular interactions.

In Chapter 2, we lay the foundation for our comprehensive investigation of cell-material interactions, with a particular focus on the utilization of metal oxides in the domain of biological implants. The chapter is thoughtfully divided into three distinct sections. Firstly, we delve into the nature of the biological matter employed in our research. Subsequently, we explore the fundamental principles underlying cell-material interactions. Finally, we culminate this chapter with a detailed discussion of the crucial role of metal oxides in the field of biomedicine.

Subsequently, Chapter 3 elucidates the methodology employed in the fabrication and

characterization of the thin films, including the pertinent parameters and primary analysis techniques. The primary objective of this chapter is to provide an overview of the theoretical foundations and technological methodologies employed in this thesis.

Chapter 4 of this manuscript is dedicated to investigating thin films of vanadium oxides. Various techniques, including differentiation staining, phase contrast microscopy, and real-time reverse transcription-polymerase chain reaction (RT-PCR), were employed to analyze the growth, adhesion, proliferation, and differentiation of human bone marrow mesenchymal stem cells (hBMMSCs) on these oxide films throughout the duration of the study.

Bacterial organisms are frequently encountered in diverse environmental reservoirs, including soil and water. Within the various bacterial species, *Pseudomonas aeruginosa* is recognized for its propensity to induce infections in human hosts and exhibit a high degree of surface colonization. In order to tackle this matter, a potential strategy involves the implementation of antibacterial coatings on the surface. In this study, the efficacy of Cu-Ti oxide coatings was examined in Chapter 5. This was achieved by producing $\text{Cu}_{1-x}\text{Ti}_x\text{O}_2$ ($0.25 < x < 0.75$) thin films on glass substrates through the utilization of the pulsed laser deposition (PLD) method.

In chapter 6 we study the growth of cancer cells on Binary oxide thin films of ZnO, Al_2O_3 , CuO_x , VO_x , and TiO_2 deposited on glass substrates. The main focus is to examine the process of creating, describing, and understanding the development of human cancer cells, specifically SW1353 generated from human chondrosarcoma and SKOV3 from human serous ovarian adenocarcinoma.

This thesis work will be brought to a close in the seventh chapter, where we will also provide some future perspectives and a conclusion to this study.

2.1 Biological matter

One thing that makes the Earth special in the known universe is the abundance of biological matter on Earth. This matter refers to any form of matter that consists of living creatures or the substances produced by them. The composition of this entity comprises a diverse array of organic compounds, encompassing proteins, carbohydrates, lipids, and nucleic acids. Biological matter has a vital role in sustaining life, as it serves as the fundamental constituent for cellular and tissue structures. Additionally, it assumes a pivotal function in numerous significant biological processes, including metabolism, reproduction, and immunity.

Biological matter is ubiquitously present in diverse contexts, encompassing the human body, flora, fauna, and the surrounding ecosystem. This thesis expects to understand the effect of various materials on biological matter such as cellular entities. It is important to understand the various cells used in our research, The next section explains the basics about those cells. We will also discuss the cellular entities used in our research like mesenchymal stem cells derived from bone marrow, cancer cells (SW1353, SKOV3), and bacterial cells.

2.1.1 Stem Cell

Stem cells are undifferentiated cells with the capacity to differentiate into specialized cells. They are present in all multicellular organisms, including the human species. There exist two primary categories of stem cells, namely embryonic stem cells and adult stem cells. Embryonic stem cells are obtained from embryos, whereas adult stem cells are present in various tissues and organs inside the human body.

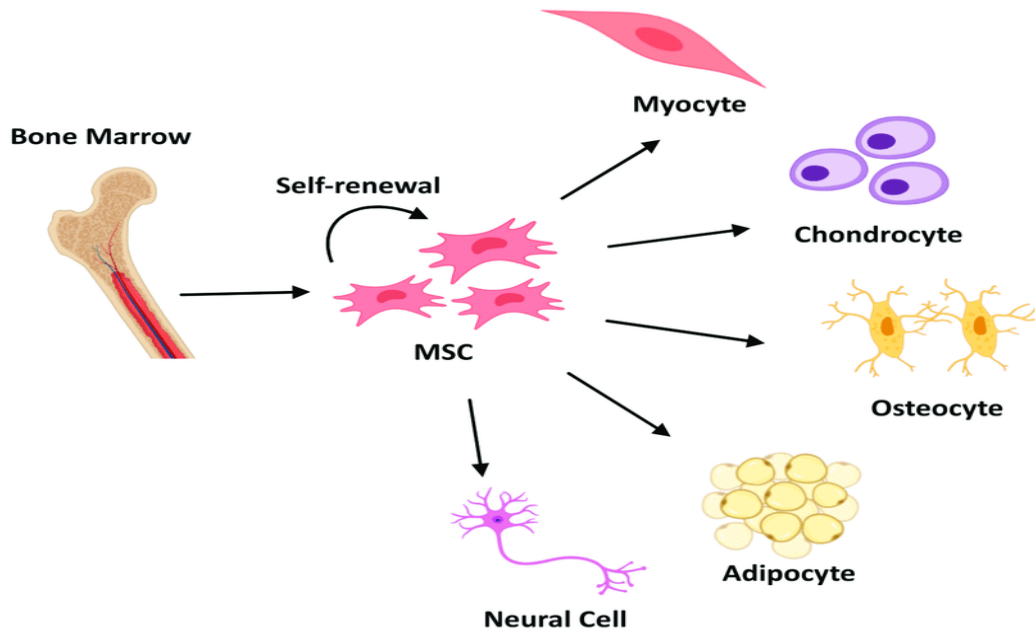


FIGURE 2.1 – Schematic representation of Mesenchymal Stem Cells (MSCs) differentiation process into different lineages : Myocytes, Chondrocytes, Osteocytes, Adipocytes, and Neural Cell.

[20]

Mesenchymal stem cells (MSCs) are a category of adult stem cells. MSCs possess distinct features such as their ability to stick to lenient surfaces, capacity for self-renewal, and potential to differentiate into several lineages including osteogenic, chondrogenic, adipogenic, and other lineages. Furthermore, MSCs exhibited a diminished capacity to provoke an immune response and demonstrated significant potential for modulating immune responses.[21]

MSCs are currently under investigation for a diverse range of therapeutic uses, encompassing :

- Bone and joint illnesses : MSCs have demonstrated efficacy in the therapeutic management of bone and joint diseases, including osteoarthritis and rheumatoid

arthritis.

- Cardiovascular illness : MSCs have demonstrated efficacy in enhancing cardiac function among individuals diagnosed with cardiovascular illness.
- Neurological problems : MSCs have demonstrated efficacy in the therapeutic management of neurological illnesses, including stroke and spinal cord injury.

MSCs are present in bone marrow, adipose tissue, and various other bodily tissues. Bone marrow is the main source of MSCs, and MSCs derived from human bone marrow (hBMMSCs) have several advantages over MSCs derived from other tissues.

- They are more abundant : MSCs are more abundant in bone marrow than in other tissues. This means that more cells can be collected from bone marrow, which can be important for clinical applications.
- They are easier to isolate : MSCs are easier to isolate from bone marrow than from other tissues. This is because bone marrow is a liquid tissue, which makes it easier to extract the cells.
- They are more versatile : hBMMSCs have been shown to be more versatile than MSCs derived from other tissues. This means that they can differentiate into a wider range of cell types.
- They are less immunogenic : hBMMSCs are less immunogenic than MSCs derived from other tissues. This means that they are less likely to be rejected by the body's immune system.

2.1.2 Cancer Cells

Biomedical research has a crucial focus on cancer cells, a group of cells that have undergone genetic changes that can cause uncontrolled development, the ability to invade surrounding tissues, and the capacity to migrate to distant areas in the body. The investigation of cancer cells is vital in order to comprehend the complex nature of cancer biology and formulate approaches for the diagnosis, treatment, and prevention of cancer. Within this framework, the SKOV3 and SW1353 cell lines are two unique cell lines that have emerged as important tools for examining cancer-related events. Gaining a comprehensive understanding of these cell lines and their distinctive properties is crucial in order to further our comprehension of cancer and its associated disciplines regarding material surfaces.

SW1353 Cancer Cells

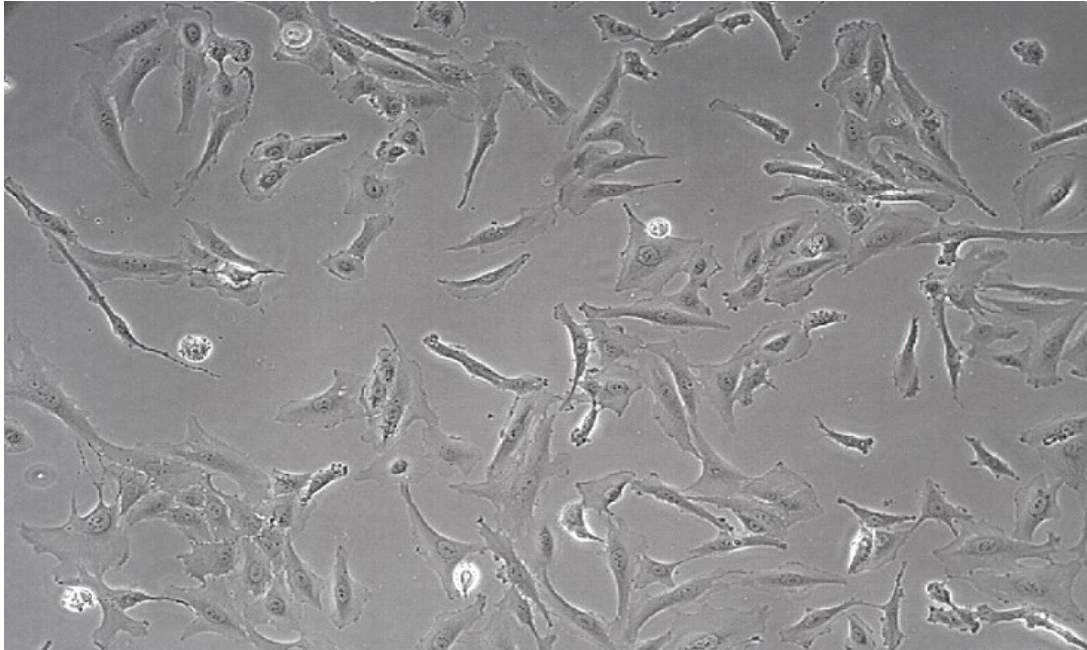


FIGURE 2.2 – Microscopic image of SW1353 cancer cells.

[22]

The SW1353 cell line, derived from human cartilage tissue, serves as a crucial asset within the field of musculoskeletal research, specifically in the sphere of inquiries associated with the biology of cartilage. The SW1353 cell line, which is derived from chondrosarcoma, a malignant tumor originating in cartilage, presents distinctive and valuable opportunities for investigating the complex mechanisms that regulate both normal and pathological cartilage behavior.

The present study focuses on an examination of cells that originate from a cancerous origin. However, it is important to note that these cells do not demonstrate any malignant characteristics themselves. Instead, their primary purpose lies in the elucidation of the complex mechanisms underlying chondrocyte biology, as well as the processes involved in cartilage regeneration and the pathophysiology of disorders associated with cartilage.

The microscopic examination regularly reveals a morphology that is defined by cells that are elongated or spindle-shaped as shown in Figure 2.2. This cellular appearance aligns with the typical findings observed in cases of chondrosarcoma. In addition, the SW1353 cells exhibit a karyotype that is distinguished by complex genetic aberrations, a defining feature commonly observed in chondrosarcomas.

SKOV3 Cancer cells

FIGURE 2.3 – Microscopic image of SKOV3 cells

[23]

The SKOV3 cell line is widely recognized and commonly employed in the field of cancer research, particularly in studies related to ovarian cancer. SKOV3 cells, which were initially isolated from the ascites fluid of a patient suffering from ovarian adenocarcinoma, serve as a promising in vitro model for investigating epithelial ovarian cancer. Ovarian cancer continues to pose a significant health concern, marked by its elevated mortality rate and an urgent demand for enhanced therapeutic approaches.

The observed cells are categorized as epithelial cancer cells and display distinctive traits commonly found in epithelial tissues, hence resembling the histological attributes associated with ovarian adenocarcinoma. These cells have an epithelial-like morphology as shown in Figure 2.3 and are resistant to tumor necrosis factor and to other cytotoxic drugs such as diphtheria toxin, cisplatin, and adriamycin.

A comparison between SW1353 and SKOV3 cells is given in Table 2.1

Property	SW1353 cells	SKOV3 cells
Tissue of origin	Adrenal cortex	Ovarian
Histology	Adenocarcinoma	Serous adenocarcinoma
ER status	Negative	Negative
PR status	Negative	Negative
HER2 status	Negative	Negative
KRAS status	Mutant	Wild-type
BRAF status	Wild-type	Wild-type
PIK3CA status	Wild-type	Mutant
PTEN status	Wild-type	Mutant
Sensitivity to cisplatin	Resistant	Sensitive
Sensitivity to paclitaxel	Resistant	Sensitive
Sensitivity to carboplatin	Resistant	Sensitive
Sensitivity to doxorubicin	Resistant	Sensitive
Sensitivity to gemcitabine	Resistant	Sensitive
Tumorigenic potential	High	High
Metastatic potential	High	High
Growth rate	Rapid	Rapid
Morphology	Epithelial	Epithelial
Adherent	Yes	Yes

TABLE 2.1 – Comparison of SW1353 and SKOV3 cell properties.

2.1.3 *Pseudomonas aeruginosa* bacterium

The bacterium *Pseudomonas aeruginosa* is commonly found in the environment, including in water (including seawater), soil, and plants. It is also found in the human body, where it is normally present in small numbers in the gut and on the skin.

However, this bacterium can become harmful when it enters the body through a break in the skin or when it is inhaled. It can cause a variety of infections, including wound infections, pneumonia, urinary tract infections, and blood infections. *Pseudomonas aeruginosa* is also a major cause of infections in patients with weakened immune systems, such as those with cystic fibrosis or cancer.

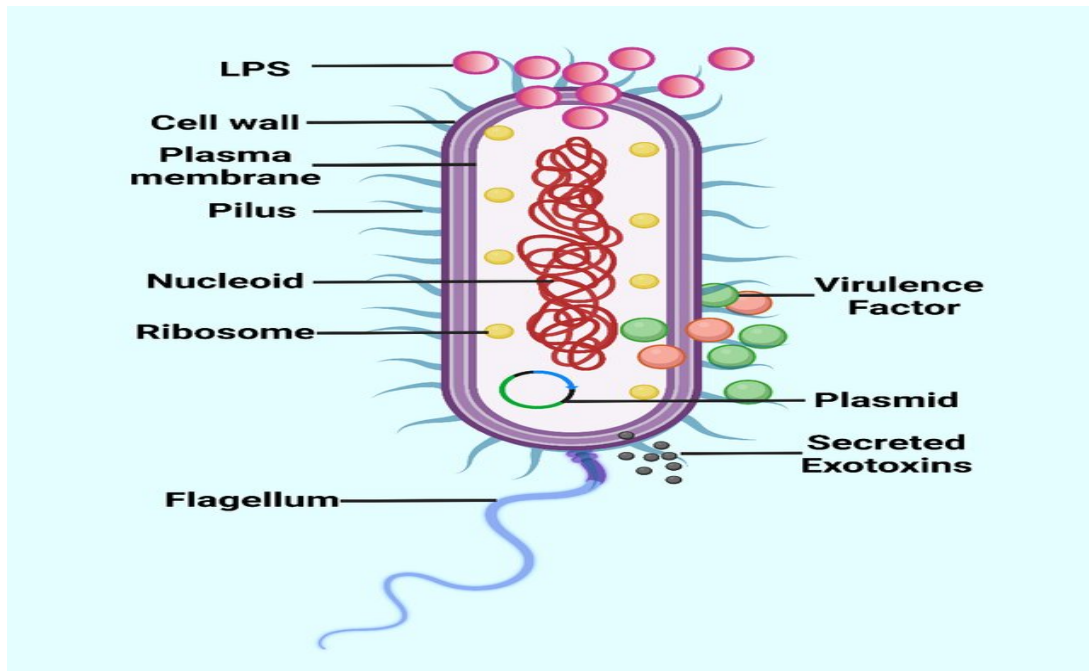


FIGURE 2.4 – Schematic diagram showing the structure of the *Pseudomonas aeruginosa*.

[24]

Pseudomonas aeruginosa can be particularly difficult to treat because it is resistant to many antibiotics.[25] This is due to the fact that it is a very versatile and adaptable bacterium. It is able to mutate quickly to develop resistance to antibiotics.

Difference between the bacterial and human cell

Human cells and *Pseudomonas aeruginosa* bacterial cells, despite being classified as cellular entities, possess inherent distinctions in terms of their cellular structure and arrangement.

Characteristic	Human Cells	<i>Pseudomonas aeruginosa</i> Bacterial Cells
Type of Cell	Eukaryotic	Prokaryotic
Size (micrometers)	10-100	1-10
Complexity	More Complex	Less Complex
Organization	Multicellular	Unicellular
Nucleus	Present	Absent
Membrane-bound Organelles	Present	Absent

TABLE 2.2 – Comparison of Human Cells and *Pseudomonas aeruginosa* Bacterial Cells

It is worth mentioning that human cells are categorized as eukaryotic organisms because they include a distinct nucleus enclosed by a nuclear envelope, along with many membrane-bound organelles such as the endoplasmic reticulum and mitochondria. Conversely, *Pseudomonas aeruginosa* bacterial cells are categorized as prokaryotic organisms due to their lack of membrane-bound organelles and the absence of a well-defined nucleus.

These mentioned prokaryotic characteristics contribute to the comparatively smaller size and reduced complexity observed in bacterial cells as compared to their eukaryotic counterparts.

2.2 Interaction of cellular entities with materials

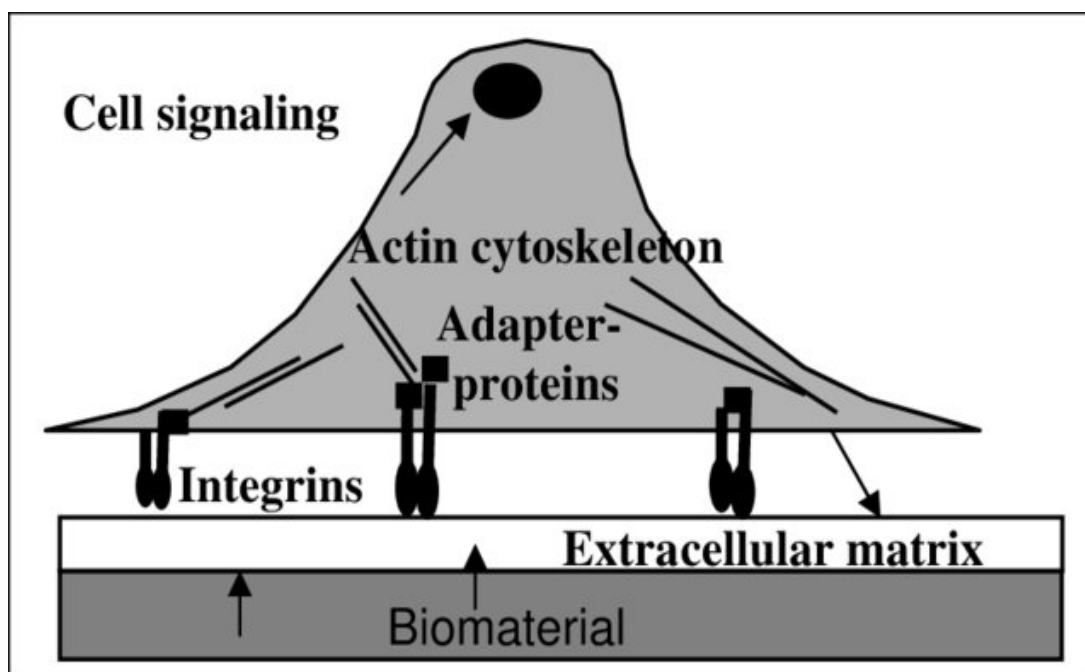


FIGURE 2.5 – Schematic representation of the cell-material-interaction.

[26]

The initial interaction between a living cell and the surface of a material is a highly orchestrated and very complex process that plays a crucial role in various fields, including tissue engineering and biomaterials research. This dynamic interplay involves a series of steps, initiated as the cell approaches the material surface. As the cell nears the surface, it extends filopodia and lamellipodia, specialized protrusions that facilitate surface exploration. These protrusions enable the cell to make contact with the material's surface, marking the commencement of the interaction.

There are specific receptors present on the cell's surface, such as integrins, selectins,

and cadherins, which are poised to recognize and bind to molecular patterns or ligands presented on the material's surface. This binding is characterized by molecular recognition events, akin to a lock-and-key mechanism, where receptor-ligand pairs complement each other's structure as shown in Figure 2.5.

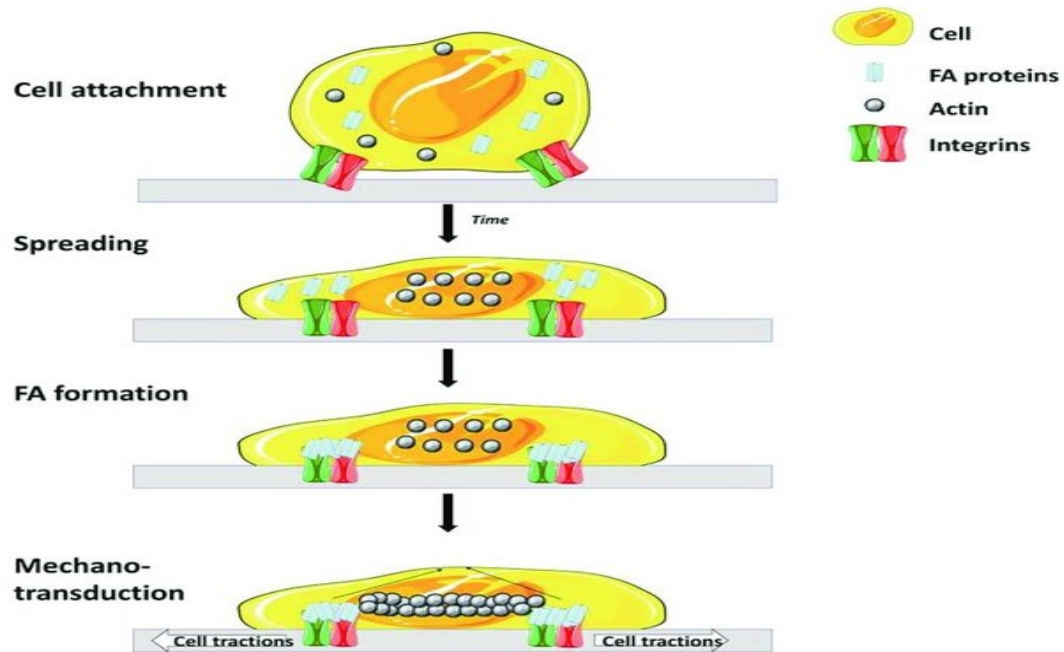


FIGURE 2.6 – Main steps and molecules involved in cell adhesion to matrix. Cell surface receptors (mostly integrins) interact with specific molecules of the matrix, leading to attachment and spreading of the cell. Attachment is then enhanced through the interaction of focal adhesion (FA) proteins and integrins. Finally, a rearrangement of the cytoskeleton occurs which leads to the spreading of the cell over the surface.

[27]

Following successful receptor-material binding, the cell undergoes a remarkable transformation. Focal adhesions, complexes composed of various proteins, including talin, vinculin, and focal adhesion kinase (FAK), begin to form at the site of interaction. These adhesions serve as anchoring points, tethering the cell to the material and providing mechanical stability. Concomitantly, the cell's cytoskeleton, particularly actin filaments, undergoes rearrangements. Stress fibers form, connecting to the focal adhesions and allowing the cell to exert mechanical forces on the material.

Cell spreading and flattening on the material's surface often follow, facilitated by the strengthening adhesions. The cell establishes more extensive contacts, enhancing its attachment to the material. This cellular response is a hallmark of successful adhesion and signifies the commencement of a cascade of intracellular signaling events as described

in Figure 2.6.

Critical to this process is the initiation of intracellular signaling pathways triggered by cell-material interactions. For instance, integrin binding to extracellular matrix proteins can activate downstream signaling cascades involving kinases, such as FAK, and transcription factors. These signaling events play a pivotal role in modulating cellular behavior, including gene expression, proliferation, and differentiation.

In terms of attachment modes, cells can adhere to material surfaces in distinct orientations. In parallel attachment, cells adhere with their basal membrane or underside, parallel to the material surface, forming extensive contact areas. In contrast, perpendicular attachment sees cells initially adhere with their basal membrane oriented at a right angle to the material surface. Over time, cells in this mode often transit to a parallel attachment as they spread and establish focal adhesions.

The choice of attachment mode can significantly impact how cells interact with the material, their ability to migrate, and their responsiveness to surface cues. Researchers frequently manipulate material properties to favor one attachment mode over the other, tailoring these interactions to achieve specific cellular responses in diverse biomedical applications.

2.3 Exploring Metal Oxides : Unraveling Their Role in Cell-Material Interactions.

Metal oxides are a diverse class of materials with a wide range of properties, making them well-suited for a variety of applications, including biomedicine.[28] In recent years, there has been a growing interest in exploring the role of metal oxides in cell-material interactions as we discussed in the above section. This is due to their unique physico-chemical properties, such as their tunable surface chemistry, high biocompatibility, and ability to interact with cells in a variety of ways.[3]

One of the key areas of research in this field is the development of metal oxide-based biomaterials for tissue engineering and regenerative medicine. Metal oxides can be used to fabricate scaffolds, nanoparticles, and Thin films that can promote cell adhesion, proliferation, and differentiation.[29]

Metal oxides nanoparticles

The broad investigation of nanoparticles in both in vitro and in vivo environments has been driven by their particular features, leading to a wide range of different applications. For example, titanium dioxide (TiO_2) scaffolds have been shown to support the growth of bone cells and promote bone regeneration.[30] Zinc oxide (ZnO) nanoparticles have been shown to promote the differentiation of stem cells into adipocytes (fat cells).[31] Iron oxide (Fe_2O_3) nanoparticles have been shown to promote the growth of blood vessels. They have proven to be valuable in magnetic resonance imaging (MRI) and biomolecule purification.[32] Furthermore, gold nanoparticles have been observed to possess significant utility in the areas of bio-molecular recognition, transport, and sensing.[33] Additionally, similar characteristics have been revealed by silver, platinum, and cadmium selenide nanoparticles. Zirconia has emerged as a highly promising biomaterial for dental prostheses owing to its favorable biological and mechanical characteristics. Since the 1970s, the dental field has utilized yttria-stabilized zirconia (YSZ), which is a composite material consisting of zirconia and yttria.[34] Another area of research is the use of metal oxides to develop new diagnostic and therapeutic agents. For example, magnetic nanoparticles can be used to label cells and track their movement in vivo.

The utilization of metal oxide nanoparticles for targeted drug or gene delivery to specific cells presents a promising avenue in biomedical research. For instance, gold nanoparticles can be functionalized with antibodies to precisely target cancer cells and facilitate the delivery of chemotherapeutic drugs.

Metal Oxides thin films

While metal oxide nanoparticles enable precise and targeted delivery at the cellular level, thin films provide versatile platforms for cell-material studies, offering insights into biocompatibility, surface modifications, and biological responses. Metal oxide thin films have emerged as promising candidates in the search for biomaterials. The advent of nanoscale films has opened up new avenues of research across various fields, including drug delivery, tissue engineering, biosensing, antimicrobial coatings, and brain interfaces .[35, 36, 37]

In recent years, the scientific community has increasingly focused on metal oxide thin films for their potential in controlled release systems. These thin films, composed of mate-

rials such as titanium dioxide (TiO_2), zinc oxide (ZnO), and iron oxide (Fe_2O_3), have found utility in encapsulating medicinal drugs .[38, 39] Notably, metal oxide thin films have demonstrated antibacterial properties, making them advantageous in various contexts. For instance, copper oxide thin films can generate reactive oxygen species upon exposure to light or heat, effectively eradicating bacteria, viruses, and other pathogens. In health-care facilities, these films have been employed to enhance infection control measures and maintain cleanliness .[40]

In the field of tissue engineering, the incorporation of metal oxide thin films has led to a significant paradigm shift. Zinc oxide thin films, known for their biocompatibility and antibacterial properties, hold promise for promoting osteoblast proliferation and facilitating bone tissue regeneration .[41, 42] Their anti-inflammatory characteristics further contribute to their favorability in these procedures .[43] Additionally, thin films composed of hydroxyapatite mimic the mineral composition of natural bone, making them suitable for scaffolds in bone tissue engineering. These scaffolds play a crucial role in facilitating the regeneration of damaged bones, a significant advancement in the field of bone tissue engineering.[44, 45]

When it comes to the effort to improve the biocompatibility and performance of brain interfaces, metal oxide thin films are becoming an increasingly significant component of the solution. Coatings such as silicon dioxide (SiO_2) and titanium nitride (TiN) that are applied on brain electrodes assist in minimizing tissue damage and inflammation.[46, 47] This helps to extend the lifespan of neural implants and enhances the seamless passage of signals between electronic devices and neural tissues. Their properties, including antibacterial, biocompatible, and bone-regenerative characteristics, make them valuable tools in fields ranging from controlled drug release to tissue engineering, significantly impacting various aspects of healthcare and biotechnology.

We opted for metal oxide thin films over the nanoparticle approach for studying biocompatibility with cells due to several compelling reasons. Thin films offer a versatile and meticulously controlled framework for in-depth cell-material investigations. Researchers have the ability to precisely manipulate the surface properties, composition, and structure of thin films, granting a high degree of customizability. This level of control facilitates a systematic exploration of how distinct material characteristics influence cellular interactions, simplifying the isolation and study of specific variables.

Furthermore, the fabrication of thin films is typically more straightforward and repro-

ducible when compared to the production of metal oxide nanoparticles. The creation of thin films involves well-established deposition techniques like sputtering, chemical vapor deposition, and Pulsed laser deposition, ensuring a consistent and reliable manufacturing process.

The main goal of this study is to explore metal oxide thin films and their capabilities to affect cellular growth. Moreover to develop efficient tools to study the behavior of cells on surfaces by varying their chemical composition and possibly creating new surfaces for biological implants.

Objectives of the Study :

1. To study how vanadium present in the Ti-Al-V alloy used in implants affects the hBMNCs.
2. To establish combinatorial libraries of metal oxides for investigating various biological studies.
3. To determine the "new" or confirm existing mechanisms of cell/bacteria adhesion to flat surfaces and study interactions of biological matter with surfaces.
4. To find possible commercial applications based on the experimental results.

Expected outcomes and impact :

1. Improved understanding of the true nature of cell-surface interactions, whether chemical, physical, or both.
2. Possibility to control biological organisms by changing the surface on which they are grown, leading to commercial applications.
3. Alternative materials and surfaces can be provided as substrates for biological experiments.
4. The study may have a significant impact on understanding the theory behind cell-surface interactions and lead to the development of new surfaces for biological experiments.

Experimental Technique

The objective of this section is to give a detailed outline of the techniques utilized in this research to fabricate thin films and characterize them. The major objective is to provide a full overview of the several techniques and components used in this study, along with the experimental settings that were essential in generating the intended outcomes. The entire process will be carefully examined and described, from the first stages of synthesis to the final characterizations of the thin films.

3.1 Synthesis of PLD target and preparation of Substrate

The process of depositing thin films onto glass substrates was carried out using the pulsed laser deposition (PLD) technique. The targets, including TiO_2 , Al_2O_3 , ZnO , MgO , CuO_x , and VO_x , were synthesized using a conventional solid-state method. [48] Initially, common commercial compounds such as V_2O_5 , ZnO , MgO , Al_2O_3 , and CuO were meticulously selected. Subsequently, polyvinyl alcohol (PVA) was judiciously incorporated as a binder to enhance the structural integrity of the compounds. Pressing and sintering processes were meticulously executed under optimized conditions tailored for each compound. V_2O_5 underwent sintering at 600°C for 12 hours, while ZnO , MgO , and Al_2O_3 were subjected to sintering temperatures of 1450°C and 1500°C for 4 hours, respectively. CuO ,

on the other hand, underwent sintering at 900°C for 24 hours. Notably, for the CuTiO target, a stoichiometric mixture of CuO and TiO₂ was meticulously prepared through ball milling, followed by binder addition and subsequent sintering at 850°C for 10 hours. Each step was meticulously executed to ensure the reproducibility and quality of the targets, thereby laying a robust foundation for subsequent PLD deposition techniques.

The experimental setup involved the use of substrates measuring 12 mm in diameter, specifically microscope glass round coverslips. Prior to deposition, the substrates were subjected to a cleaning process involving a 10-minute treatment with distilled water, followed by an additional 10-minute treatment with ethanol using an ultrasonic vibrator. In order to mitigate any potential interaction between the specimens and the silver (Ag) coating on the heater, the specimens were securely attached to the corner using silver paste. Each specimen was treated with three dots of silver paste.

3.2 Thin film preparation

The fabrication of thin films has a significant role in formulating the properties and potential of the material. Thin films can be created using a variety of methods, including chemical vapor deposition, sputtering, and molecular beam epitaxy. Each strategy has advantages and disadvantages that make it suitable for different objectives.

High deposition speeds and exact control over the layer's thickness, content, and structure are achieved with the help of chemical vapor deposition (CVD) technology, which involves reacting vapor-phase chemicals on a heated substrate.^[49] Sputtering is the process of ejecting atoms from a target material onto a substrate by bombarding it with high-energy ions. This process offers exceptional control over the film's growth and thickness, making it appropriate for a variety of uses. Atoms are deposited onto a substrate using a vacuum-based technique called molecular beam epitaxy (MBE), which enables atomic-scale control over the makeup and structure of the film. In our research, we used the Pulsed Laser Deposition (PLD) process, a highly flexible and regulated way to create thin films with accuracy and consistency.

3.2.1 Pulsed laser deposition (PLD)

In the Pulsed Laser Deposition (PLD) system, a high-intensity pulsed laser beam is precisely aimed at the desired material within a vacuum chamber. This focused laser beam

causes the target material to vaporize, generating a plume of evaporated material. This vapor plume is then carefully directed towards a substrate, where it condenses to form a thin film layer.

The process operates on a layer-by-layer ablation mechanism, where each laser pulse removes a minute amount of material from the target surface, creating a cloud of vapor. This vapor is then transported to the substrate, where it settles and forms a thin layer. This sequential deposition of nanometer-thick layers enables the precise fabrication of thin films with tailored properties.

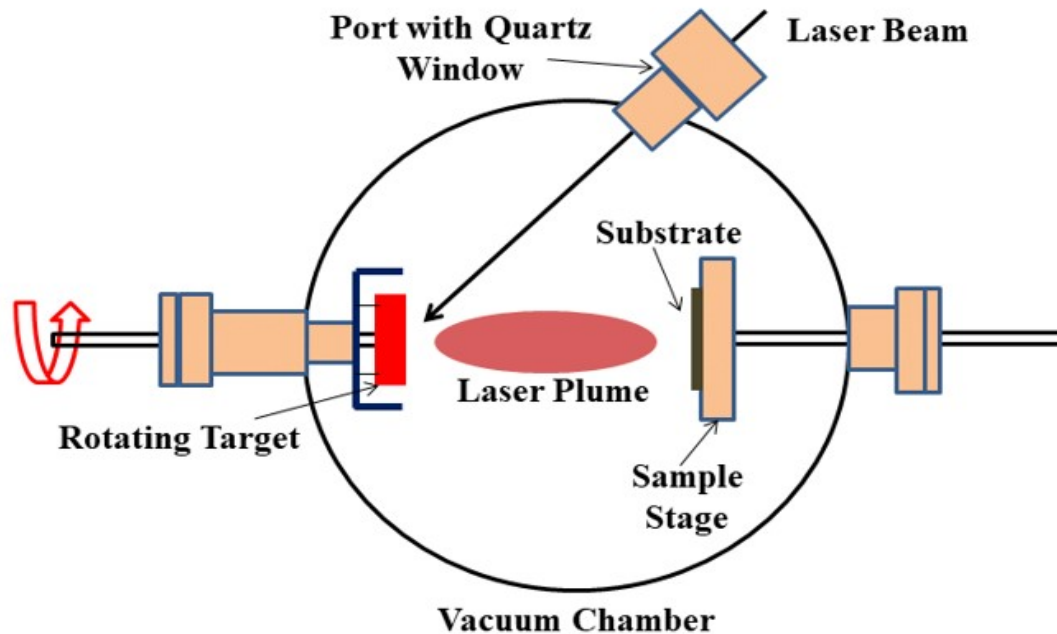


FIGURE 3.1 – Schematic of PLD system

High-temperature superconductors, oxides, metals, nitrides, semiconductors, carbides, polymers, and fullerenes are just a few of the many materials that may be deposited using the very adaptable PLD process. PLD is an appealing choice for many applications due to its high deposition rates.^[50]

3.2.2 Principle of the pulsed laser deposition

Within a vacuum chamber, a high-power pulsed laser beam is focused in order to strike a target with the material that is going to be deposited by the PLD Machine. The process is broken down into three stages : vaporizing the target materials, transporting the vapor plume, and growing the film on the substrate. Laser pulses that are used in a clean layer-by-layer fashion are what eliminate the material. The target material will get

vaporized as a result of the laser pulse. When the laser pulse is focused on the material to be vaporized, the material to be vaporized vaporizes and generates a plume of the evaporated material. After that, the plume is carried to the substrate, and there, a very thin layer of it is put there. After that, a series of tiny layers, each one only a few nanometers in thickness, are used to develop the film. PLD has the advantage of being able to deposit a large variety of materials, including high-temperature superconductors, oxides, metals, nitrides, semiconductors, carbides, and even polymers or fullerenes at high deposition rates. This ability to deposit a wide range of materials is a significant benefit of PLD.

3.2.3 Growth modes

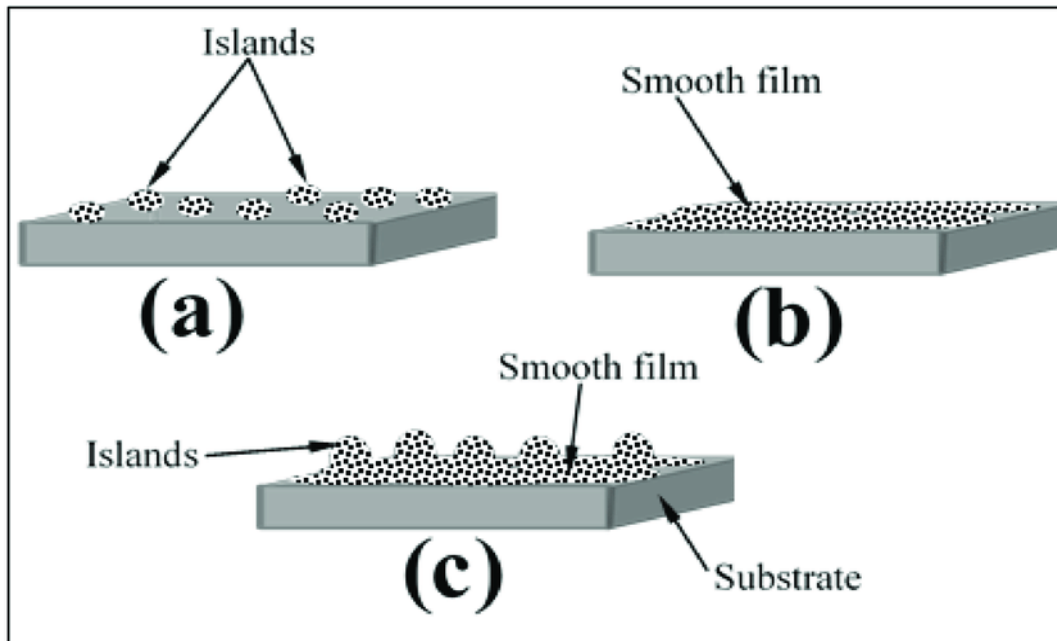


FIGURE 3.2 – (a) island : Volmer-Weber growth mod (b) layer by-layer : Van des Merwe growth mode (c) layer plus island : Stranski-Krastanov growth mode.

[51]

The growth mechanisms observed in thin film deposition play a crucial role in determining the structural and morphological characteristics of the resulting films. Among these mechanisms, three primary modes stand out : Volmer-Weber growth, Van der Merwe growth, and Stranski-Krastanov growth.

Volmer-Weber growth, often referred to as the island growth mode, occurs when the deposited material forms discrete islands or clusters on the substrate surface. In this

mode, individual islands nucleate and grow independently, leading to a non-uniform film thickness and surface roughness. This mechanism is commonly observed in systems where the interaction between the deposited material and the substrate is weak, resulting in poor adhesion and limited lateral growth.

Conversely, Van der Merwe growth, also known as layer-by-layer growth, involves the sequential deposition of atomic or molecular layers with continuous coverage over the substrate surface. In this mode, the adatom-substrate interaction is strong, facilitating the formation of a coherent and uniform film. This growth mechanism typically occurs when the lattice mismatch between the deposited material and the substrate is minimal, allowing for the accommodation of additional layers without significant strain.

The Stranski-Krastanov growth mode represents a hybrid scenario, combining elements of both island and layer-by-layer growth. Initially, the deposited material forms a continuous monolayer on the substrate surface, following the Van der Merwe growth mode. However, as the thickness of the film increases, strain begins to accumulate, leading to the formation of three-dimensional islands on top of the initial layer. This mode is commonly observed in systems characterized by a moderate lattice mismatch between the deposited material and the substrate, resulting in a transition from coherent to strained growth.

3.3 Characterization techniques

3.3.1 X-ray interaction

Crystalline substances are characterized by a highly structured periodic lattice structure that extends across all three dimensions and is made up of atoms that are arranged in a convoluted pattern at each lattice point. This lattice is defined by three lattice vectors that create a fundamental elementary cell. The dimensions of this lattice are specified by three lattice parameters (a , b , and c) and three interaxial angles (α , β , and γ). The fundamental elementary cell is the building block of this lattice. The configuration of atoms within the crystal structure results in the formation of fourteen different Bravais lattice modes, each of which has a unique symmetry.

A lattice plane is any plane that passes through three lattice points, and a family of lattice planes is formed by an infinite number of identical planes that have an inter-

lattice spacing of d_{hkl} and are recognized by their Miller indices (hkl). A lattice plane can be described as any plane that passes through three lattice points. Diffraction of the incident beam occurs as a result of the interaction of X-rays with a crystalline lattice that has a wavelength that is equivalent to the inter-lattice spacing. This can either result in constructive or destructive interference, depending on the circumstances. Only when the path difference between two diffracted rays from two planes of the same family is an integer multiple of the wavelength of the incident X-ray can a lattice plane qualify as being in a diffraction position, also known as d_{hkl} . This phenomenon is known as Bragg's law, and it enables the estimation of the lattice parameter and the interplanar distance d_{hkl} . As a result, it is an extremely useful instrument for the characterization of the crystal structure of various materials. [52]

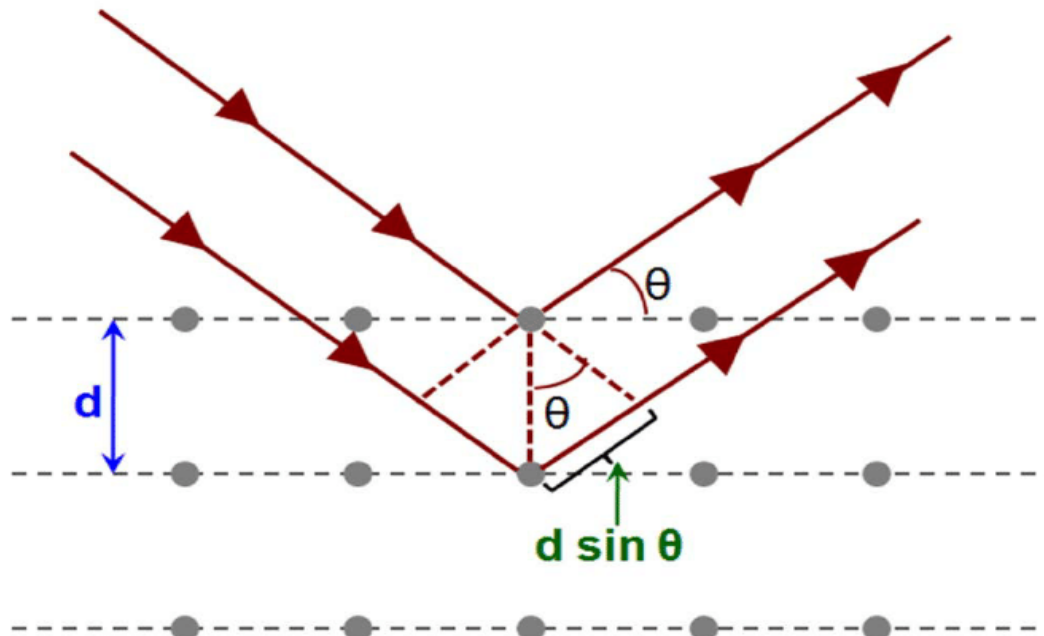


FIGURE 3.3 – Bragg's law. Grids represent two-dimensional crystal lattices and imaginary planes. When X-rays strike the crystal at an angle, coherent diffraction (in phase) occurs when the difference in distance ($2d \sin$) equals an integral number of the wavelength (n).

[53]

3.3.2 X-ray reflectivity

The structural features of our PLD-produced samples were analyzed with the assistance of a BRUKER four-circle D8 discover diffractometer. A Johansson Ge (111) monochromator and an X-ray source are both components of the diffractometer. These

components work together to make it possible to generate a parallel, monochromatic incident beam that has a wavelength of equal to 1.54059 Å.

Principle

Depending on the angle of incidence and material properties, X-rays can bounce off a material contact. A sample's surface and inside can scatter and reflect X-rays. Incident and reflected angles determine reflected X-ray intensity. This characterizes the material's surface and interface features, including thickness, roughness, and density.

Thickness estimation

In X-ray reflectivity (XRR) measurements, the thickness of the samples is figured out by studying the oscillations in the intensity of the reflected X-rays as a function of the square of the order number. This helps to ensure that the results are accurate. Interference between X-rays that are scattered from the surface of the thin film and X-rays that are scattered from the interface between the substrate and the thin film is what causes these oscillations to occur.

In order to get the film thickness from the slope of the oscillation maxima, a mathematical model must be applied to the relative position of the oscillation maxima with the square of their order number. This path difference (Δl) is what regulates the number of fringes that may be observed, and it is affected by the thickness of the film that is being measured.

$$\Delta l = 2d\sqrt{(n^2 - \cos^2 \theta)} \quad (3.1)$$

It is possible to compute the connection between the film thickness (d) and the number of fringes (N) by rearranging the equation that involves the film thickness (d) and the refractive index (n) and taking into consideration the need for constructive interference, as shown here :

$$\sin^2 \theta_M = \frac{(\lambda^2)}{(4d^2)} N^2 - \delta^2 - 2\delta \quad (3.2)$$

Plotting the square of the product of the refractive index and the film thickness ($n^2 d$) against the order number ($N = 1, 2, 3, 4, \dots$) yields a linear connection when the angle of

the fringes' maxima theta (M) is known. The film's thickness is shown by the slope of this line. Consequently, the thickness of the film may be estimated in XRR measurements by estimating the slope of this linear connection. Prior to data collection, the exact alignment of the sample height and incidence angle was done in order to guarantee the correctness of the data acquired. During a θ - 2θ scan extending from 0° to 6° , the detector was employed to capture the intensity profile as a function of angle 2θ . The equation was used to compute the value of $\sin(2\theta \text{ m})$ and the angle ($\theta \text{ m}$) corresponding to each fringe's maximum intensity. $\sin(2\theta \text{ m})$ was shown for N values ranging from 1 to 5 since the order number of the fringe (N) was not clearly established. The data were then subjected to linear regression, and the appropriate value of N was determined using the slope of the best-fit line.

$$d = \frac{\lambda}{2\sqrt{b}} \quad (3.3)$$

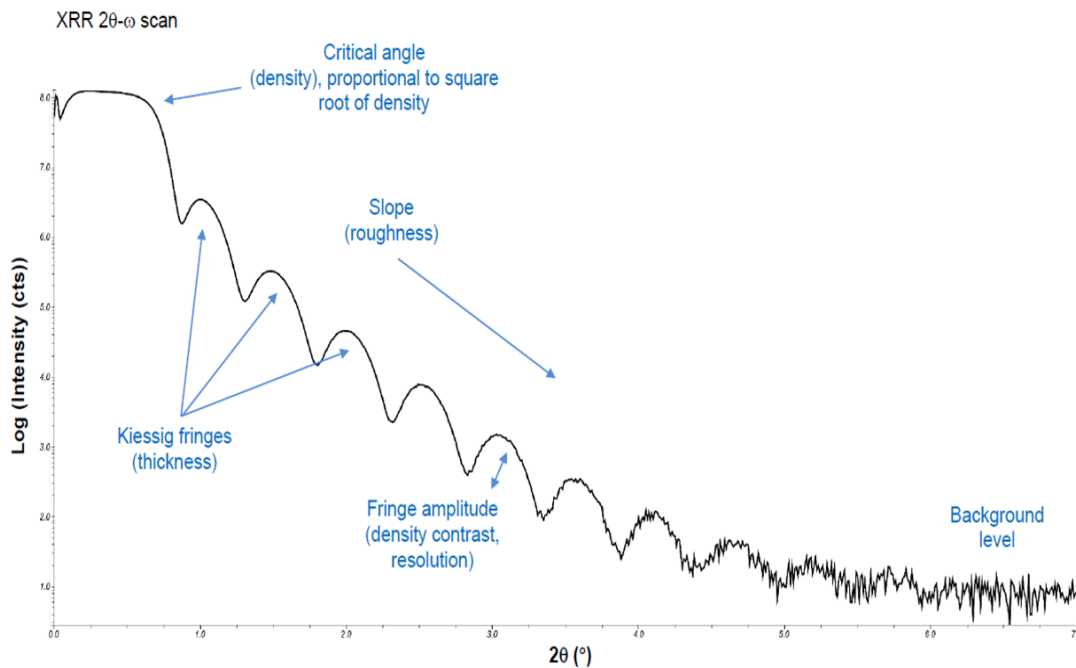


FIGURE 3.4 – Information provided by X-ray reflectivity.

[54]

Reflectivity curves were recorded in this investigation using a Bruker™ D8 Discover diffractometer with radiation K α ($\lambda = 1.5406 \text{ \AA}$) and a 2Θ angle range that went from 0 to 6° .

The X-ray beam will normally hit the sample at an angle of a few degrees, and the reflected X-rays will be caught by a detector that is positioned at a constant angle. After that, the XRR curve is found by determining the intensity of the X-rays that were reflected

as a function of the angle at which they were incident.

The XRR curve is a useful tool for determining the thickness, density, and roughness of thin films. It is possible to assess the thickness of the film by doing an in-depth analysis of the oscillations that appear in the XRR curve. Measurements of XRR are utilized extensively in the fields of materials science and engineering for the purpose of characterization of thin films and coatings.

3.3.3 Atomic force microscopy

Using the Atomic Force Microscopy (AFM) technique, the surface morphology of deposited thin films is investigated in this study. AFM is a potent imaging instrument that can produce images of surfaces and their features with atomic-scale resolution. AFM relies on the interaction between a sample's surface and a sharp probing tip affixed on a flexible cantilever. As the point scans across the surface of the sample, it encounters numerous forces, including van der Waals, electrostatic, and repulsive forces, which cause the cantilever to bend. Using an optical or piezoresistive sensor, the deformation of the cantilever is detected and measured, producing a topographic image of the sample surface. The Atomic Force Microscopy (AFM, PicoSPMTM) technology was utilized in order to conduct the surface morphology investigation. The action of forces from the sample surface on the tip of the scanning cantilever lies at the heart of the atomic force microscope's (AFM) working mechanism.

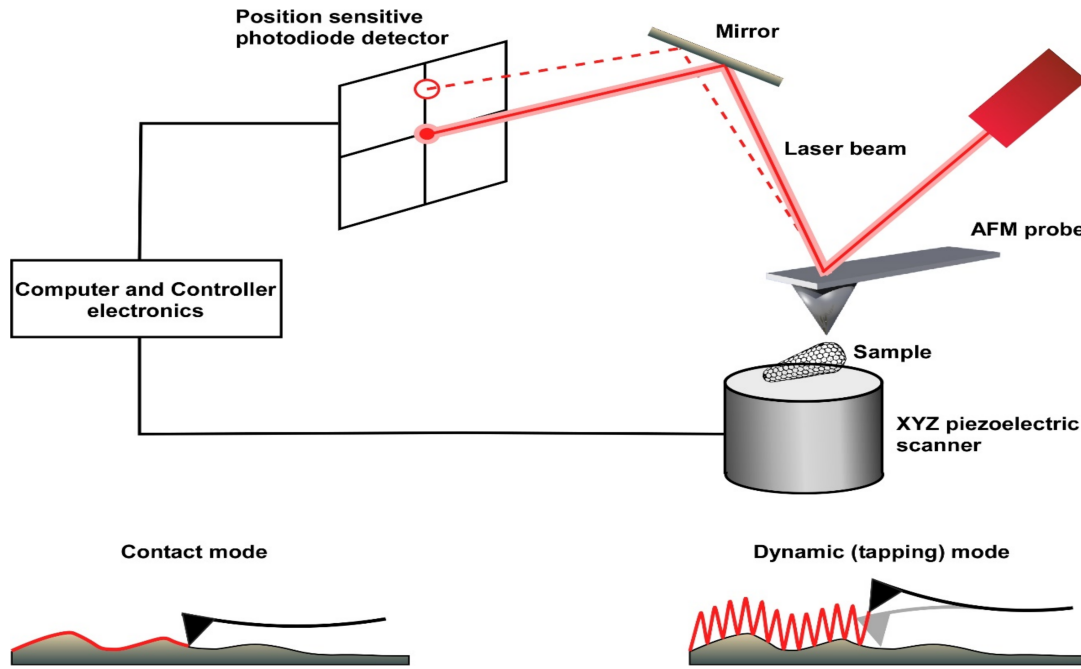


FIGURE 3.5 – Schematic representation of AFM.

[55]

There are numerous AFM operation modes, like contact mode, non-contact mode and tapping mode each with its own advantages and disadvantages. In this investigation, tapping mode AFM was utilized, which is a nondestructive imaging technique that minimizes tip-sample interaction and minimizes the danger of surface damage to the sample. Tapping mode AFM operates by oscillating the cantilever at its resonance frequency while maintaining a constant distance between the tip and sample. This enables high-resolution imaging of the surface of the sample without producing considerable damage or wear on the sample itself.

AFM measurements were taken of a $1 \mu\text{m}^2$ area using the tapping mode, and the root-mean-square (RMS) roughness was determined using WSxM 5.0 software.

3.3.4 Scanning electron microscopy

Scanning electron microscopy is a commonly used technique for surface characterization. In this particular form of microscopy, the image is created through a series of signals that are generated one after another as an electron beam, which is carefully focused, scans the surface of the sample using a set of deflection coils. The electron beam, with a range of energies from a few hundred eV to 50 keV, is precisely directed onto the sample's surface, creating an incredibly tiny spot measuring approximately 5 nm in diameter. Si-

signals primarily arise from the movement of electrons generated through interaction with a material. Based on the type of electrons, such as backscattered and secondary, various information can be obtained. The SEM method enables a comprehensive analysis that combines qualitative and quantitative aspects. It allows for the simultaneous examination of grain size and shape, phase composition, grain size distribution, and the determination of chemical element distribution within its area. The morphology of MSCs cultured onto oxide thin films was examined using a Scanning Electron Microscope (SEM) Zeiss™ SUPRA 55. The microscope was operated within a voltage range of 2.0 - 10.0 kV, and at a distance of 4 - 10 mm.

For our study, we fixed hBMMSCs cultured for 2 weeks using 2.5% glutaraldehyde in 0.1 M cacodylate buffer (pH = 7.4) at 4°C. After that, we rinsed them with cacodylate buffer and postfixed them in 1% osmium tetroxide. Next, the samples underwent a dehydration process using a series of ethanol concentrations ranging from 70% to 100%. They were then dried using a critical point dryer (CPD 030 LEICA Microsystem). The samples underwent sputtering with platinum (Pt) and were then examined using a SUPRA 55 scanning electron microscope (Zeiss™).



FIGURE 3.6 – Zeiss SUPRA 55 scanning electron microscope.

3.3.5 X-ray photoelectron spectroscopy (XPS)

The working principle of X-ray photoelectron spectroscopy (XPS) involves the analysis of the elemental composition and chemical states of a solid surface specimen. The determination of atom percentage concentrations can be easily achieved by utilizing the relative sensitivity factor. The detection capabilities of this system encompass all elements with the exception of hydrogen and helium. When the surface of the specimen is exposed to X-rays with adequate energy, electrons in particular bound states become excited and dislodge the photoelectron from the nuclear attractive force of an element. A portion of the electrons that are ejected from the photoelectric process experience inelastic scattering within the sample as they travel toward the surface.[56] Conversely, some electrons undergo immediate emission without any loss of energy as they escape the surface and enter the surrounding vacuum. After being emitted from the photosensitive material, these electrons are subsequently captured within a vacuum environment and subsequently analyzed by an electron analyzer to determine their respective kinetic energy levels.

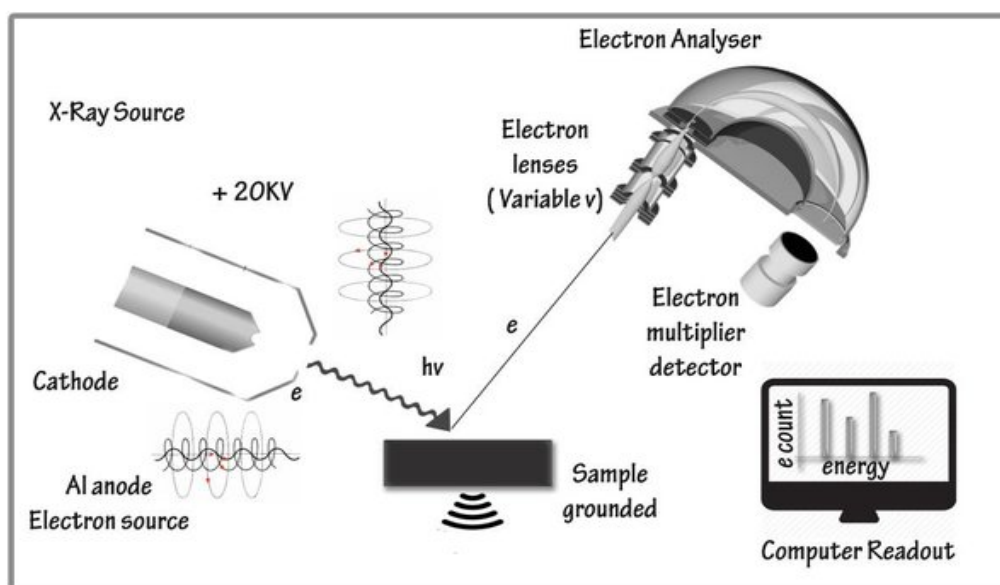


FIGURE 3.7 – Schematic diagram of X-ray photoelectron spectroscopy (XPS).

[57]

The electron energy analyzer generates an energy spectrum that depicts the relationship between the intensity of photo-ejected electrons over time and their corresponding binding energy, which refers to the energy possessed by the electrons prior to their departure from the atom. Each distinct energy peak observed on the electromagnetic spec-

trum is indicative of a particular chemical element. The determination of the constituent elements comprising the microstructure of the material. The composition, or elemental concentration, of each element can be determined by analyzing the specific energy of a core level transition within the element. This transition occurs at a binding energy that is unique to each element and, in some cases, can be quantified.

3.3.6 Calculation of contact angle and surface energy

Temperature and oxygen pressure are two of the most essential factors in the process of film growth ; nevertheless, the surface interfacial energy between the film and the substrate is also highly important. Because the interactions between water and metal oxides with low electronegativity are mostly electrostatic, surface characteristics such as roughness, wettability, and surface energy should be expected to be dependent on the thickness of the material. We were able to further investigate this link by measuring the contact angles (also known as the wetting angles) of several different liquids using the Shape Analyzer DSA 25-KRUSS GmbH. Some of the liquids that were measured included water, glycerol, and ethylene glycol, amongst others. To determine the contact angle, the tangent to the solid-liquid-vapor triple point was utilized. Young's equation (see eq. 2.5) was utilized to carry out the form analysis of the drop.

$$\cos(\theta) = \frac{\gamma_s - \gamma_{sl}}{\gamma_l} \quad (3.4)$$

where θ is the contact angle and γ_s , γ_{sl} and γ_l are the surface energies of the substrate, the substrate-liquid interface, and the liquid, respectively.

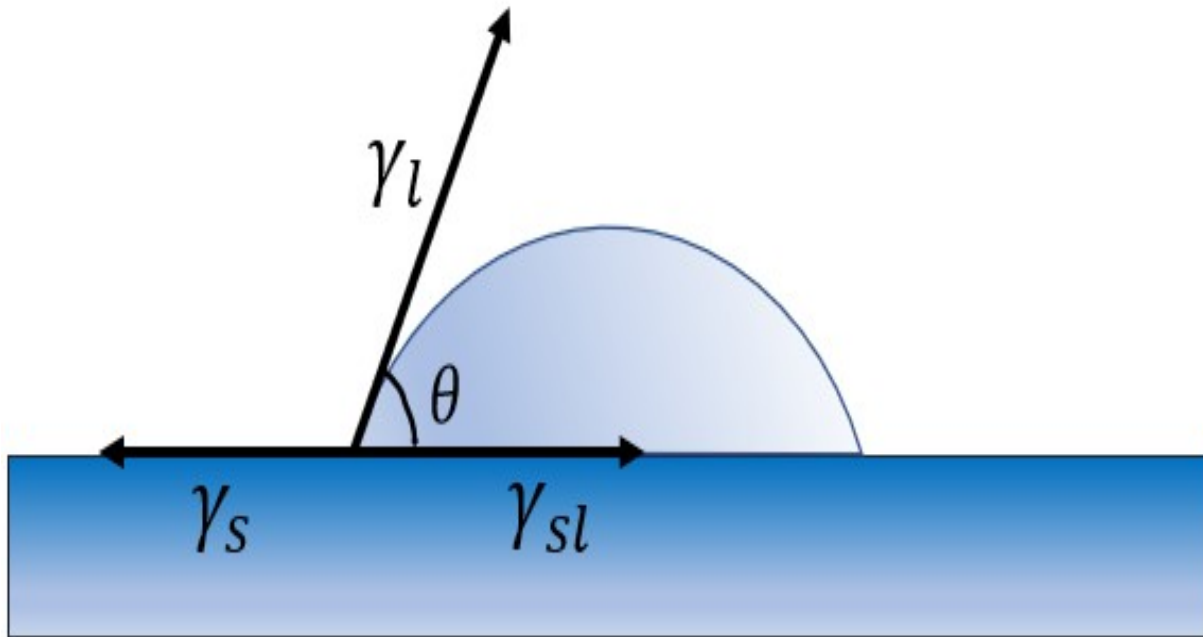


FIGURE 3.8 – Schematic diagram illustrating the components of the contact angle.

By observing the contact angle between a solid surface and a liquid drop on the surface, it is possible to calculate the surface tension and wettability of a given solid material. A substrate is considered hydrophilic if the contact angle is less than 90° , indicating a high affinity for water molecules. Hydrophilic materials have active polar functional groups that enable them to adsorb water molecules. On the other hand, hydrophobic materials behave in the opposite way when interacting with water compared to hydrophilic materials, and parameters such as surface topography and energy determine the wetting behavior of the surface. The Owens-Wendt method (also known as the Kaelble-Owens-Wendt method) [58, 59] is one of the few methods available for calculating surface energy components, namely, the dispersion and polar components. These components result from the Coulomb and Van der Waals interactions between permanent and induced dipoles, and from temporary fluctuations caused by the charge distribution in the atom or molecules on the surface. The method is based on Berthelot's hypothesis, which assumes that the work of adhesion between a solid and a liquid is equal to the geometric mean of the cohesion work of a solid and the work of cohesion of the measuring liquid.

The geometric mean of the polar component (γ^p) and dispersive component (γ^d) of surface tensions of liquids and of the surface energy of solids is given by the following equation :

$$\gamma_{sl} = \gamma_s + \gamma_l - 2\sqrt{(\gamma_s^d \gamma_l^d)} - 2\sqrt{(\gamma_s^p \gamma_l^p)} \quad (3.5)$$

Using equations 2 and 3, a linear equation like $y = ax + b$ is attained.

$$\frac{(\gamma_l(1 + \cos(\theta)))}{(2\sqrt{(\gamma_l^d)})} = \sqrt{(\gamma_l^d)} \frac{\sqrt{(\gamma_l^p)}}{(\sqrt{\gamma_l^d})} + \sqrt{\gamma_s^d} \quad (3.6)$$

Where $y = \frac{(\gamma_l(1 + \cos(\theta)))}{(2\sqrt{(\gamma_l^d)})}$ and $x = \frac{\sqrt{\gamma_l^p}}{\sqrt{\gamma_l^d}}$ contain the known values like the contact angle, the dispersive γ_l^d and polar γ_l^p parts of the liquid surface tension for each liquid. The linear regression of equation 4 primes straight to the components of the solid surface energy $\gamma_s^p = a^2$ and $\gamma_s^d = b^2$ with total surface energy given by,

$$\gamma_s = \gamma_s^p + \gamma_s^d \quad (3.7)$$

Where γ_s is total surface energy, γ_s^p and γ_s^d are the polar and dispersive components, respectively.

3.4 Cell Culture

3.4.1 Pseudomonas aeruginosa bacterial cells

Pseudomonas aeruginosa bacteria (mPAO1) were grown in LB broth overnight with agitation at 37 °C. Before imaging, the bacteria were diluted to an optical density of OD600 = 1.5 and stained with Vybrant Dycycle Green stain (Invitrogen) for 30 min under agitation.

3.4.2 Mesenchymal stem cells from bone marrow

In accordance with the recommendations of the regional ethical commission, bone marrow was harvested from the iliac crests of adult donors undergoing arthroplasty who had previously completed a consent form. After aspirating the bone marrow, the cells were separated using a density gradient composed of Hypaque and Ficoll. Isolated mononuclear cells were cultured in a medium consisting of alpha-MEM, 10% fetal calf serum (manufactured by Invitrogen™ and located in Cergy-Pontoise, France), 2 mM L-glutamine, 1 ng/ml fibroblast growth factor-2 (manufactured by Sigma™), and antibiotics. Trypsinization (0.25% trypsin/1 mM EDTA, Invitrogen™) was used to harvest the cells when they

reached close to 80% confluency. The cells were then plated at a density of $2 \times 10^3 - 5 \times 10^3$ cells/cm². Following five cell passages, an RT-PCR analysis was performed to look for the absence of hematopoietic markers. hBMMSCs were plated at a density of 5×10^4 cells/cm² in the 24-well plate for the *in vitro* tests. The culture medium was replaced three times per week, and the temperature was maintained at 37 degrees Celsius with 5% carbon dioxide.

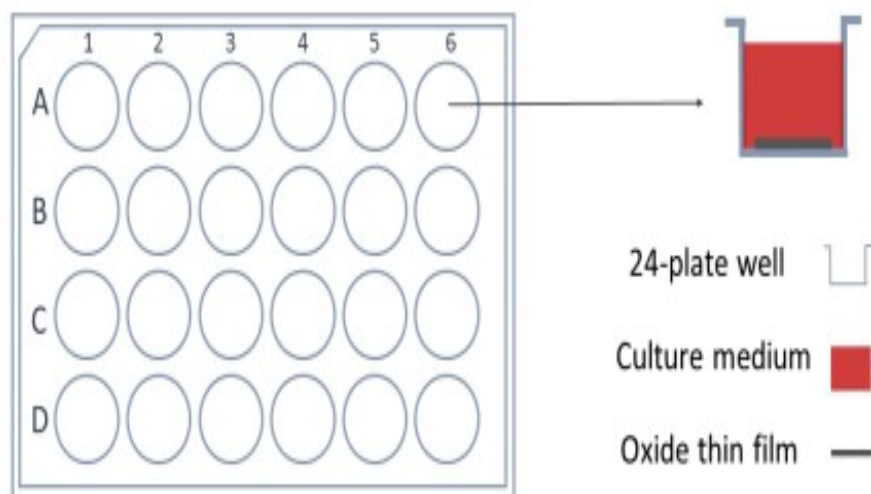


FIGURE 3.9 – Schematic of 24-well plate used during in-vitro experiments.

3.4.3 Ovarian and Chondrosarcoma cancer cells

The SKOV3 (ovarian) and SW1353 (chondrosarcoma) cell lines, were cultured in RPMI 1640 medium supplemented with 2 mM Glutamax™ (Fisher Scientific Bioblock, Illkirch, France), 10% fetal calf serum (Fisher Scientific Bioblock), 20 mM HEPES, and 33 mM sodium bicarbonate (Gibco BRL, Lyon, France). The cells were maintained in a 5% CO₂ humidified atmosphere at 37°C. The SW1353 cells were seeded at a density of 55×10^3 cells per well in 24-well plates using RPMI-1640 medium in order to investigate the kinetics of cytotoxicity. Similarly, the SKOV3 cells were seeded at a density of 30×10^3 cells per well. The cells were cultivated in a culture dish under controlled conditions of 37°C and 5% carbon dioxide. The monitoring of the cells was conducted using an Essen BioScience IncuCyte S3 instrument. After the introduction of the CellTox™ Green Cytotoxicity Assay reagent (manufactured by Promega), photographs were taken using a 10x objective to establish the baseline. The plate underwent scanning, resulting in the acquisition of fluorescence and phase-contrast images in real time from nine discrete

positions within each well. The aforementioned procedure was iterated at hourly intervals. The CellTox™ Green reagent is utilized to label deceased cells, resulting in the generation of green fluorescence.

The live-cell phase contrast images were utilized for the purpose of providing morphological data and calculating confluence through the utilization of the IncuCyte program. The experiment was conducted in triplicate, with the objective of comparing the temporal accumulation of CellTox™ Green with the cell count at the confluence.

3.5 Investigation of bacterial cells adhesion and proliferation

3.5.1 Light sheet microscopy imaging

The light sheet microscopy imaging technique utilized in this study necessitates the use of a specially designed apparatus, which consists of a bacteria inoculation chamber and a Zeiss light sheet Z.1 microscope (manufactured by Carl Zeiss).[60] In order to establish a bacteria inoculation chamber, a solution of 1% liquid agarose was introduced into a syringe with a volume capacity of 1 ml. Subsequently, the tip of the syringe, also measuring 1 ml, was incised and subsequently sealed using parafilm. Subsequently, a styrene square rod was introduced into a yellow tip holder and subsequently inserted into the central agarose cylindrical column, thereby establishing a hollow chamber intended for bacterial inoculation. Once the agarose had undergone solidification, the styrene square rod was extracted, and subsequently, a lengthy strip of glass, either coated or uncoated, was positioned adjacent to the agarose wall. Subsequently, the syringe plunger was utilized to push the imaging chamber out to a length that was deemed appropriate, approximately half the size of the agarose chamber, in preparation for light sheet imaging.

To facilitate the process of biofilm formation, the bacteria that had been stained were collected by centrifugation, and then suspended in a specifically designed AB minimal medium. This medium was further enriched with 2 g of glucose per liter and 2 g of Casamino Acids per liter, referred to as ABTGC. Finally, the suspended bacteria were introduced into the agarose chamber. Following a 6-hour incubation period at a temperature of 37 °C, the agarose chamber was affixed to the Zeiss light sheet Z.1 microscope. During the imaging process, the focal plane was adjusted to specifically target the glass surface where

the bacteria adhere and commence the process of biofilm formation. The experiment was conducted three times independently in order to perform quantification analyses.

3.5.2 Crystal violet (CV) staining of biofilm biomass

The experimental setup involved the placement of 15 mm glass cover slips, both coated and uncoated, within a 24-well microplate with a flat bottom. A volume of 200 μL of bacterial suspension was introduced into each well and subjected to incubation for a duration of 24 hours at a temperature of 37°C, while ensuring that the lid remained in place. Subsequently, the contents of the wells were removed by aspiration, followed by a washing step. A 0.1% aqueous solution of CV (Sigma-Aldrich) was then introduced into the wells of a 24-well microplate containing the biofilm. The microplate was incubated at room temperature for a duration of 30 minutes. Subsequently, the CV solution was eliminated and the wells underwent a meticulous triple washing procedure using 200 μL of sterile water, ensuring minimal disruption to the biofilm. The plate was allowed to undergo natural evaporation for a duration of 30 minutes. Subsequently, a volume of 200 μL of glacial acetic acid with a concentration of 30% (v/v) was introduced into each well in order to dissolve the dye that had become bound to the biofilm adhered to the surface. Values for absorbance measurements were acquired at a wavelength of 570 nm. The experiment was conducted three times, each time with three replicates.

3.6 Investigation of human stem cells adhesion and proliferation

3.6.1 Phase contrast microscopy

Phase contrast microscopy is a sophisticated optical method that enables the observation of transparent specimens, which are typically challenging to visualize with traditional bright field microscopy. This methodology demonstrates significant utility in the examination of dynamic biological processes occurring within living cells and tissues. The core concept of phase contrast microscopy is based on the utilization of the natural phase shifts experienced by electromagnetic waves when they interact with transparent specimens. This allows for the conversion of these phase differences into changes in the distribution of light intensity within the resulting image. Through the utilization of this fundamen-

tal principle, phase contrast microscopy effectively amplifies contrast and facilitates the comprehension of intricate structural intricacies that would otherwise be difficult to perceive or comprehend using alternative imaging techniques. As a result, this methodology has emerged as a fundamental aspect within the field of biomedical research, enabling thorough examinations of the dynamic characteristics and intricate structures of living biological entities.

The monitoring of cell adhesion and proliferation was conducted using a phase contrast VisiScope™ series 400 microscope (VWR) and an EVOS™ FL Auto 2 Imaging system (Thermo Fisher Scientific). To assess the diameter of multicellular structures, human bone marrow-derived mesenchymal stem cells (hBMMSCs) were cultured at a density of 10^4 cells/cm². The cells were seeded onto a 24-well plate that contained thin films of VO_x. The media underwent three alterations per week and were maintained in a 5% CO₂ environment at a temperature of 37°C for a duration of 26 days. Multicellular structures were observed for each sample using a phase contrast VisiScope™ series 400 microscope (VWR).

3.6.2 Histological staining

The experiment involved the application of histological staining techniques to human bone marrow-derived mesenchymal stem cells (hBMMSCs) that were cultured in a 24-well plate at a cellular density of 10,000 cells per square centimeter. The substrates employed for the process of seeding encompassed uncoated glass slides, as well as slides coated with oxide thin films. The media experienced a tri-weekly alteration and were kept in a regulated setting with a carbon dioxide concentration of 5% at a temperature of 37 degrees Celsius for a period of 14 days. Following that, the cells were subjected to two rinses using phosphate-buffered saline (PBS) and subsequently fixed using a 4% paraformaldehyde solution for a period of 15 minutes. After fixation, the cells were rinsed once more with phosphate-buffered saline (PBS) and subsequently kept in this buffer until further analysis.

Histological staining techniques, namely Van Gieson, Hematoxylin phloxine saffron, and Masson's Trichrome, were employed for staining purposes on every individual sample. The stained specimens were mounted onto microscopic histological glass slides using a solution containing an acrylic polymer. The slides were subsequently examined utilizing the EVOS™ FL Auto 2 Imaging system, which is produced by Thermo Fisher Scientific.

In the Van Gieson staining technique, the glass slides were successively submerged in xylene for a period of three minutes. Subsequently, the slides were submerged in a solution of 99% ethanol, undergoing a series of 20 immersions, with each immersion being repeated twice. Following that, the slides were immersed in Weigert's iron hematoxylin staining solution for a period of 10 minutes. After undergoing a rinsing process with tap water, the slides were immersed in a picrofushin (Van Gieson) solution for a duration of two minutes. Following that, the slides were submerged in distilled water on ten separate occasions, subsequently undergoing two consecutive rinses in 99% ethanol. Ultimately, a sequence of twenty immersions in xylene, accompanied by periodic alterations, was executed.

In the case of the hematoxylin phloxine staining technique, the slides were immersed in xylene for a duration of 3 minutes on two separate occasions. Subsequently, they were subjected to two successive immersions in 99% alcohol, with each immersion consisting of 10 dips. Finally, the slides were rinsed with tap water. Following this, the specimens were immersed in Harris hematoxylin solution for a duration of 3 minutes, followed by a thorough rinsing with tap water. After three immersions in acid alcohol to eliminate excessive staining, the glass slides were subsequently immersed ten times in tap water and a solution containing 1% lithium carbonate. Following a second wash with tap water, the samples were subjected to a 5-minute incubation period in a 2% phloxine solution. Following this, the samples were rinsed with water and dehydrated using three successive changes of 99% alcohol. The slides underwent the same dehydration procedure following a 2-minute incubation in a saffron staining solution. Ultimately, two sets of ten immersions in xylene were conducted.

The staining technique employed in this study is Masson's Trichrome staining. The glass slides underwent two cycles of immersion in xylene for a duration of 3 minutes each, followed by a series of 20 dips in 99% ethanol, repeated twice. Subsequently, the specimens were immersed in Weigert staining solution for a duration of 3 minutes, followed by thorough rinsing with tap water. They were then submerged in Ponceau-Fuchsin (Masson) solution for a period of 5 minutes. The subsequent procedure involved rinsing the slides with a solution of 1% acetic acid before subjecting them to treatment with phosphomolybdic acid for a duration of 5 minutes. The slides underwent a second rinsing process using a solution of acetic acid, followed by a 1-minute immersion in aniline blue. Subsequently, following an additional rinsing procedure involving the use of acetic acid,

the slides underwent a process of dehydration utilizing 99% ethanol, with a total of two sets of ten dips. Finally, the slides were subjected to a clearing process involving xylene, with two sets of ten dips.

3.6.3 Cell density measurements

In order to assess the population growth of mesenchymal stem cells, HBMMSCs were introduced into a 24-well plate at a density of 10^4 cells/cm². The plate consisted of thin films of TiO₂ and Al₂O₃, while a glass substrate was used as a control. The media were replaced on a daily basis over a period of five days to ensure the use of fresh medium.

The cells were collected and individually quantified using a Malassez counting chamber. The doubling time (T_d) was determined by analyzing the cell growth curve over a period of five days, employing the following equation :

$$T_d = \frac{(T_f - T_i) \times \log 2}{(\log N_f - \log N_i)} \quad (3.8)$$

where T_f represents the final time, T_i represents the initial time, N_f represents the final cell number, and N_i represents the initial cell number.

In subsequent stages of the study, experiments were conducted to investigate the use of the same deposition temperature for oxide thin films. hBMMSCs were cultured in α -MEM medium at a density of 10^4 cells/cm². The cells were seeded onto various substrates, namely thin films of TiO₂, VO_x, and Al₂O₃, as well as uncoated glass slides, using a 24-well plate. Following a two-hour incubation period, the media was extracted and the cells were subsequently rinsed with phosphate-buffered saline (PBS) in order to eliminate any non-adherent cells. The hBMMSCs were then collected through trypsinization, using a solution consisting of 0.25% trypsin and 1mM EDTA from Invitrogen™. The cells were then individually counted using trypan blue staining and the Countess™ II Automated Cell Counter from Thermo Fisher Scientific. The identical methodology was employed to quantify cellular populations subsequent to the process of culturing at varying time intervals, specifically 2, 4, and 7 days.

3.7 Study of human mesenchymal stem cell differentiation

3.7.1 Differentiation staining

To evaluate the impact of oxide thin films on the differentiation potential of MSCs into different cell types, a differentiation staining technique was employed. In this study, mesenchymal stem cells (MSCs) were cultured using standard α -MEM media for a duration of 7 days, without the addition of basic fibroblast growth factor. Subsequently, the chondrogenic, osteogenic, and adipogenic differentiation media were introduced to facilitate alcian blue, alizarin red, and oil red stainings, respectively. The media were replaced every 2-3 days in both instances. Following a 14-day culture period, the cells were treated with a 4% solution of paraformaldehyde (PFA). Subsequently, the cells were washed with phosphate-buffered saline (PBS) and then immersed in 1.5 ml of PBS for subsequent differentiation staining experiments. An acrylic polymer solution was employed for the purpose of repairing stained samples on microscopic histological glass slides.

The utilization of the Alcian blue staining technique was employed to ascertain the occurrence of chondrogenic differentiation in mesenchymal stem cells (MSCs). Alcian blue staining selectively visualizes acid mucopolysaccharides, serving as indicators of the chondrogenesis process. Mucopolysaccharides, also known as glycosaminoglycans, are intricate linear polysaccharides that play a structural role in connective tissues. For Alcian blue staining, a 1% solution of Alcian blue (pH = 2.5) was prepared by dissolving 1 gram of Alcian blue powder in 100 milliliters of 3% acetic acid. After removing the paraformaldehyde, the cells underwent a washing process using distilled water (H_2O), followed by staining with the alcian blue solution for a duration of 30 minutes.

Subsequently, the cells underwent four washes with distilled water (H_2O), and the samples were affixed onto glass slides intended for microscopic examination. In the process of optical density analysis, the samples underwent four rounds of washing with 1 ml of H_2O . Subsequently, a solution containing 1% sodium dodecyl sulphate (SDS) was introduced, and the resulting solutions were then transferred to a 48-well plate. In order to conduct cellular analysis, the absorbance at a wavelength of 616 nm was measured for triplicate samples using a Multiskan GO spectrophotometer manufactured by Thermo Scientific.

The utilization of the Alizarin red staining technique is employed for the purpose of identifying the osteogenic differentiation of cells. Undifferentiated mesenchymal stem cells (MSCs) lacking extracellular calcium deposits typically exhibit a slightly reddish appearance, while MSC-derived osteoblasts possessing extracellular calcium deposits are expected to display an orange-red hue. The Alizarin red solution was prepared by dissolving 2 grams of Alizarin red S in 50 milliliters of distilled water. Subsequently, the pH was adjusted to a range of 4.1-4.3 through the introduction of HCl or NH₄OH. To stain the cells, the H₂O was meticulously aspirated following the washing process, and subsequently, the Alizarin red staining solution was applied to fully cover the cellular monolayer. The incubation process was conducted for a duration of 30 minutes in a lightless environment at ambient temperature. Subsequently, the staining solution was removed by aspiration, and the cells were subjected to four washes with distilled water. Following this, the samples were affixed onto microscopic glass slides. In order to conduct optical density tests, the cells underwent a series of four washes using 1 ml of distilled water (H₂O), followed by the addition of an additional 1 ml of distilled water (H₂O).

The measurement of absorbance at a wavelength of 490 nm was conducted on three separate samples to obtain triplicate data.

Oil red staining is a widely employed technique for the visualization of lipids and assessment of adipogenic differentiation. Initially, a stock solution of Oil red was prepared by dissolving 0.3 g of Oil red O powder in 100 ml of 99% isopropanol. Next, a combination of three portions of stock solution was mixed with two portions of distilled water and subsequently filtered using a Whatman filter paper to create the working solution. Subsequently, the H₂O was aspirated following the washing procedure. A volume of 2 ml of isopropanol solution with a concentration of 60% was introduced into each well and allowed to incubate for a duration of 5 minutes. Subsequently, the isopropanol was eliminated and the cells were subjected to staining by adding 2 ml of Oil red working solution to each well.

The stained cells were subjected to a 30-minute incubation period at room temperature under light-free conditions. Subsequently, the staining solution was meticulously aspirated, and the cells were subjected to four washes using 1 ml of H₂O. Following this, the samples were affixed onto microscopic glass slides for observation.

3.7.2 Real time RT-PCR

The real-time reverse transcription polymerase chain reaction (RT-PCR) is a commonly employed molecular biology method utilized to measure and quantify gene expression levels. The methodology is dependent on the amplification of complementary DNA (cDNA) sequences, followed by the subsequent detection of the amplified products. (see figure 3.10)

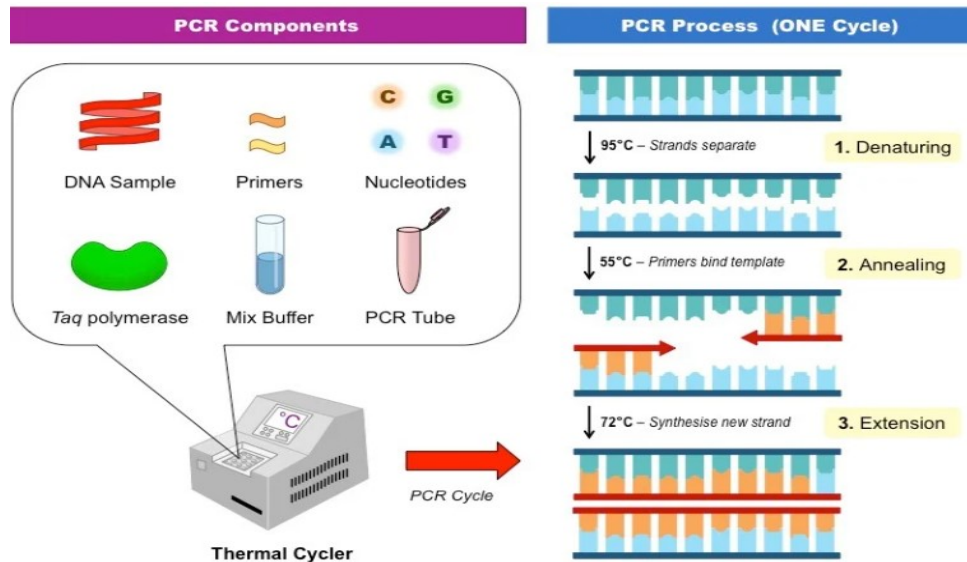


FIGURE 3.10 – Schematic of RT-PCR.

[61]

The template DNA of interest is synthesized and subjected to a process of amplification involving multiple cycles of heat denaturation. This process continues until the reaction reaches a plateau, at which point the quantity of template DNA has doubled compared to its initial amount. The fluorescence-based methodology is utilized to quantify the amplified product, with a notable augmentation in the fluorescence signal indicating the presence of a sufficient quantity of the target gene. A greater initial copy number results in a decreased number of amplification cycles necessary. RNA was extracted by Qiagen kit (RNeasy® mini kit 250), according to the manufacturer's protocol. Total RNA (1µg) was treated with DNase before reverse transcription into cDNA using MMLV enzyme (Invitrogen by Thermo Fisher Scientific) and oligo T primers. Specific transcripts were then amplified by real-time PCR on the StepOnePlus apparatus (ThermoFisher Scientific) targeting (RUNX2), chondrogenic (COL2A1), and adipogenic (CEBP/a) genes. Reactions were done using Power SYBR Green mix (ThermoFisher Scientific) for 40 cycles (30s at 95°C/1min at 60°C). GAPDH, RPL13, and B2MG housekeeping genes were used to

normalize mRNA expression levels calculated by $2^{-\Delta\Delta Ct}$ method. The sequences of the primers used are given in Table 1.

Standard α -MEM medium was used for cell culture, and differentiation media were introduced after one week of culture. The media were refreshed twice a week. Total RNA was extracted from cells cultured in osteogenic and chondrogenic media for 16 days using the RNeasy Mini kit (Qiagen), according to the manufacturer's instructions. Next, 500 ng of the extracted RNA was reverse transcribed into cDNA using the Invitrogen kit after DNase I treatment. The $2^{-\Delta\Delta Ct}$ method was used to calculate mRNA expression levels, which were normalized using GAPDH, RPL13, and B2MG housekeeping genes.

Table 1	
Gene	Primer
OST (Osterix)	F : GGCTCAGCTCTCTCCATCTC
	R : GGGGACTGGAGCCATAGTG
CBPa (CCAAT enhancer-binding protein alpha)	F : ACTGGGACCCTCAGCCTTG
	R : TGGACTGATCGTGCTTCGTG
ACAN (aggrecan)	F : GTGCCTATCAGGACAAGGTCT
	R : GATGCCTTTCACCACGACTTC
GAPDH (glyceraldehyde-3-Phosphate Dehydrogenase)	F : ATGGGGAAGGTGAAGGTCTG
	R : TAAAAGCAGCCCTGGTGACC
RPL13 (ribosomal protein L13)	F : GTTCGGTACCACACGAAGGT
	R : CTGGGGAAGAGGATGAGTTTG
B2MG (beta-2-microglobulin)	F : GAGGCTATCCAGCGTACTCCA
	R : CGGCAGGCATACTCATCTTTT
COL2 (Collagen type II)	F : TGGACGATCAGGCGAAACC
	R : GCTGCGGATGCTCTCAATCT

TABLE 3.1 – Primers sequences used in RT-PCR

The process of quantifying RNA entails the determination of the concentration or quantity of RNA molecules present in a specific sample. The Multiskan GO spectrophotometer, manufactured by Thermo Scientific, was utilized for this study.

To ascertain the concentration of RNA, measurements of absorbance were performed at a wavelength of 260 nm, a widely employed approach in quantification methodologies. The values obtained in this study represent the quantification of RNA in each sample from the conducted experiments. The concentration chosen for subsequent procedures was determined based on the provided sample and was denoted as 100, 500, or 1000 nanograms per microliter (ng/ μ l).

The primary area of investigation in this study pertains to the DNase treatment procedure and the subsequent assessment of its effectiveness. The objective of DNase treatment is to thoroughly eradicate any remaining traces of genomic DNA (gDNA) contamination present in the extracted RNA material obtained from the samples.

In order to accomplish this, the RNA samples were mixed with a DEPC-treated H₂O solution in the appropriate volume. The sample was supplemented with a mixture comprising a 10-fold concentrated reaction buffer and DNase I, Amplification Grade. This addition resulted in a final volume (V_{total}) of 15 μ l. The solution was gently agitated and subjected to incubation for a duration of 15 minutes at ambient temperature. Following that, a volume of 1 μ l of Stop Solution was introduced into the mixture in order to facilitate the binding of calcium and magnesium ions and to render the DNase I enzyme inactive. Subsequently, the mixture was subjected to a temperature of 70 degrees Celsius for a duration of 10 minutes. In order to validate the successful elimination of genomic DNA (gDNA) via DNase treatment, a polymerase chain reaction (PCR) was performed utilizing b-actin primers. The polymerase chain reaction (PCR) was conducted both prior to and subsequent to the application of DNase treatment. The samples were subsequently subjected to electrophoresis on a 1% agarose gel stained with GelRed dye in order to facilitate visualization.

Real-time PCR, also referred to as quantitative PCR, is a commonly employed molecular biology methodology utilized to assess and quantify levels of gene expression. The process encompasses three primary stages :

1. Denaturation refers to the process by which the double-stranded DNA is subjected to elevated temperatures exceeding 90°C, leading to the dissociation of the two DNA strands.

2. Annealing is a process in which the temperature is reduced to a level slightly below the melting temperature. This facilitates the binding of forward and reverse primers to their respective target sequences on the DNA template.

3. Elongation is a process facilitated by the DNA polymerase enzyme, which serves as a catalyst for the incorporation of nucleotides into the primers. This enzymatic activity leads to the formation of complementary DNA strands.

Stem Cell Differentiation Using Vanadium Oxide Thin Film

The phenomenon of altering cellular growth by materials, as previously stated in Chapter 2, has been the subject of investigation in relation to several metals within the scope of this research. In this chapter, our objective was to comprehensively investigate the characteristics of bone marrow-derived human stem cells when utilizing vanadium oxide thin films as a substrate deposited by pulsed laser deposition (PLD). Cell culture and RT-PCR were done by Eva Lhuissier in the BioConnect lab at the University Hospital Center of Caen with the help of Dr. Maria Khokhlova and Dr. Mira Hammad under the supervision of Dr. Karim Boumédiene.

4.1 Introduction

Oxide materials possess an extensive array of applications, spanning diverse fields such as sensors, solar cells, and electronics. However, it is intriguing to note that their vast potential in the realms of medical and biological sciences remains largely uncharted territory.[29] Titanium oxide (TiO_2), in the form of nanotubes or thin films, has been extensively studied and utilized in biomedical implants because of its bio inertness and good biocompatibility.[62, 63, 64]

Pure titanium possesses desirable characteristics such as a high specific strength-to-weight ratio and high corrosion resistance. However, its practical utility is constrained

by its restricted mechanical and tribological properties, as well as its susceptibility to high oxidation rates when exposed to extreme temperatures.[65] Typically, the resolution of this issue involves the creation of composite alloys through the incorporation of elements. Elements such as Aluminum, Silicon, and Nitrogen exhibit α -stabilizing properties that contribute to the expanded temperature range in which the α -phase of titanium can persist. These properties include enhanced thermal stability and improved corrosion resistance. By incorporating these elements into titanium alloys, we can modify materials to endure a broader spectrum of temperatures while benefiting from resistance to degradation in corrosive environments.[66] A significant portion of transition metals, including molybdenum, niobium, vanadium, chromium, iron, and several others, are renowned for their β -stabilizing properties. These distinctive characteristics encompass attributes such as enhanced alloy hardenability and an increase in high-temperature performance. In contrast to elements that stabilize the α phase, these β -stabilizing elements extend the temperature range within which the β -phase of titanium can maintain its structural integrity. There is a significant need in the industry for titanium alloys that consist of a combination of low-temperature (α) and high-temperature (β) phases, commonly referred to as ($\alpha+\beta$)-alloys.[66] The properties of alloys are influenced by a diverse variety of factors, including the type of alloying elements and the relationship between phases and the microstructure of the alloy. Ti-6Al-4V alloys exhibit a distinctive amalgamation of qualities, including reduced density, favorable resistance to corrosion, and heightened strength. The alloy Ti-6Al-4V is classified as a ($\alpha+\beta$) alloy, wherein the aluminum (Al) atoms constitute the majority (6wt%) and primarily form a solid solution within the α phase. Conversely, the vanadium (V) atoms, comprising 4wt%, mostly form a solid solution inside the β phase. The use of aluminum leads to strength enhancement, whereas the inclusion of vanadium facilitates the retention of plasticity. The Ti-6Al-4V alloy is extensively employed in the medical field for the fabrication of dental and orthopedic implants.[67]

The main problem of the Ti-6Al-4V use in medicine is the presence of toxic elements like aluminum and Vanadium. While most metal implants are inert, the release of vanadium ions from the surface of a biomaterial can lead to adverse effects.[68, 69] Conversely, some studies have shown that vanadium compounds can effectively enhance cell growth at relatively low concentrations of released vanadium ions (up to 10 μM).[70, 71] Therefore, understanding the interfacial interactions between vanadium oxide compounds and living

materials is crucial. So far, only TiO_2 and Al_2O_3 have been investigated for their potential to modulate cell growth and differentiation depending on their composition.[29] Therefore, more research into alternative oxide surfaces is required. In addition, bio-interface engineering relies heavily on being able to exert command over cellular architecture, particularly in the context of shrunken dimensions.[72]

The objective of this chapter is to examine the cytotoxicity impact and growth differentiation alteration of hBMMSCs when exposed to a vanadium oxide thin film deposited on a glass substrate using the PLD technique. Our objective is to examine the adhesion, proliferation, and differentiation of hBMMSCs on the surfaces of these films and compare them to uncoated glass and plastic cover slides.-

4.2 Optimization of VO_x thin films with cell adhesion

The deposition process was conducted at several temperatures, specifically (500, 400, 300, 200, and 100) $^{\circ}C$ keeping the same pluses of 5000. Before every deposition, the vacuum chamber was evacuated down with a turbo pump to a base pressure lower than 1.33×10^{-4} Pa (10^{-6} Torr). During experiments involving deposition with O_2 , gas was introduced in the chamber with a flow rate that led to the pressure 10^{-4} - 10^{-5} Torr. Prior to conducting the cytological experiment, it is important to determine the growth temperature of the VO_x film at which cell adhesion reaches its highest level.

Following the successful deposition of thin films at various temperatures, maintaining a consistent number of deposition cycles both in the presence and absence of oxygen, we embarked on a vital calibration process. This calibration aimed to assess the affinity of cells for the vanadium oxide thin films deposited at various temperatures. To achieve this, we employed bone marrow samples collected from adult donors undergoing arthroplasty, specifically gathered from the iliac crests.

It is crucial to emphasize that the donors had willingly provided their samples and had received prior approval from the local ethical committee, thereby adhering to ethical research practices. The marrow was aspirated and the cells were fractionated using a Hypaque-Ficoll density gradient as described in section 3.4.2.

Cellular adhesion after 2 hr of incubation

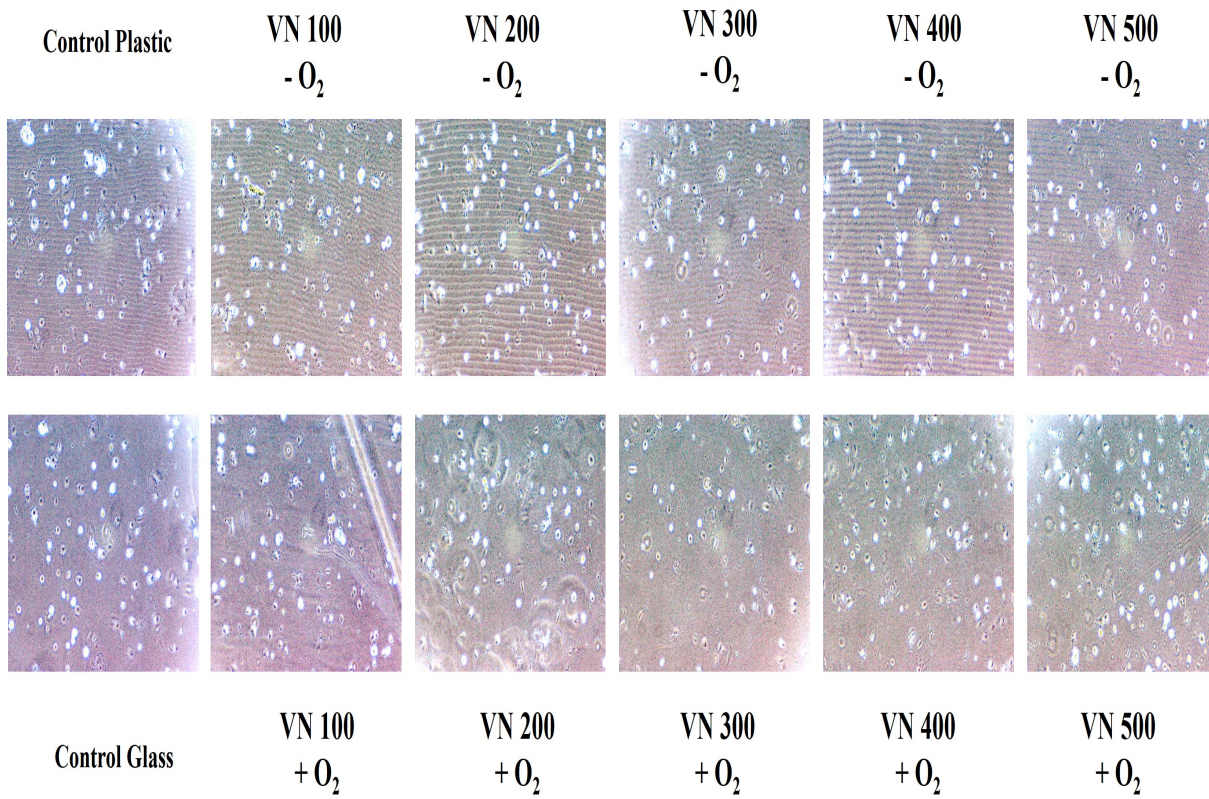


FIGURE 4.1 – Cellular adhesion after 2 hr of incubation period at different temperatures with and without oxygen presence while depositing the thin films. (VN -O₂ and VN +O₂ represent the vanadium film deposition without and with the presence of Oxygen in the PLD chamber).

In our experimental investigation, the evaluation of cell adhesion on vanadium oxide thin films was conducted with meticulous attention to detail. Cells were precisely cultivated on each film, spanning distinct durations of 2 hours, 24 hours, 48 hours, and 74 hours. This extensive time frame was chosen to comprehensively assess the adhesion characteristics exhibited by the diverse vanadium film samples.

The observation of cell adhesion of hBMNCs was carried out at discrete time intervals to capture the dynamic nature of cellular interaction with the vanadium substrates, plastic, and uncoated glass. Notably, cells were seeded onto vanadium thin films, previously deposited on glass substrates at various temperatures, as visually depicted in Figures 4.1 and 4.2.

In our analysis, the presence of cellular entities (hBMNCS) was visually represented

by white dots. Preliminary observations indicated that the vanadium thin film deposited at 400 degrees Celsius without the presence of oxygen exhibited a higher density of these white dots. Furthermore, this trend persisted even after a 24-hour incubation period, as illustrated in Figure 4.2.

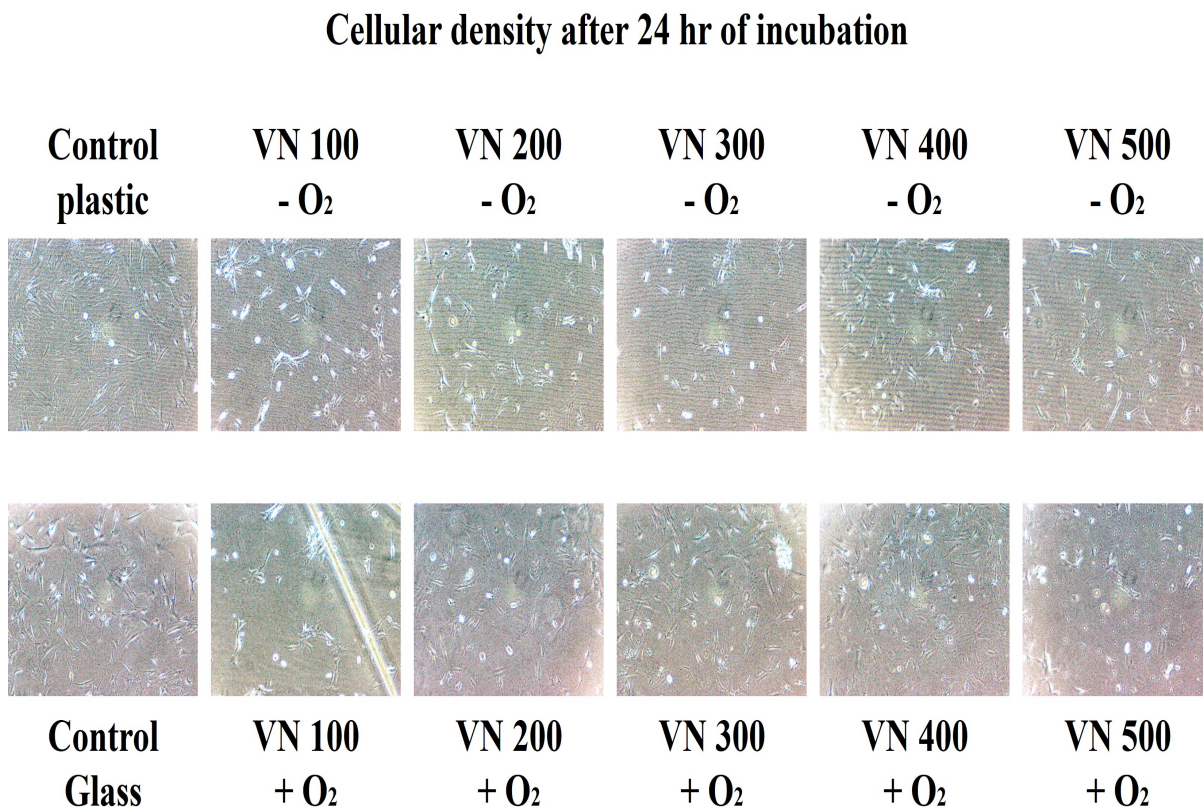


FIGURE 4.2 – Cellular adhesion after 24 hr of incubation period at different temperatures with and without oxygen presence while depositing the thin films.

However, it is imperative to note that quantitative assessments necessitated a more rigorous approach than a mere visual inspection of white dots. Subsequently, following the incubation period, an extensive series of microphotographs were successfully acquired. These images served as the basis for a systematic cell counting procedure, quantifying the adhesion per square millimeter of the various samples.

Normalization of cell counts per mm^2 across distinct time intervals, as exemplified in Figure 4.3, yielded a comprehensive distribution analysis of cellular units across the sampled areas. Our analyses led to the compelling conclusion that the vanadium oxide thin film, particularly when deposited at 400 degrees Celsius (without the presence of oxygen), indeed exhibited a notably higher degree of adhesion in comparison to other temperatures with respect to reference surfaces. This finding underscores the importance

of deposition conditions in influencing cellular behavior on thin film substrates.

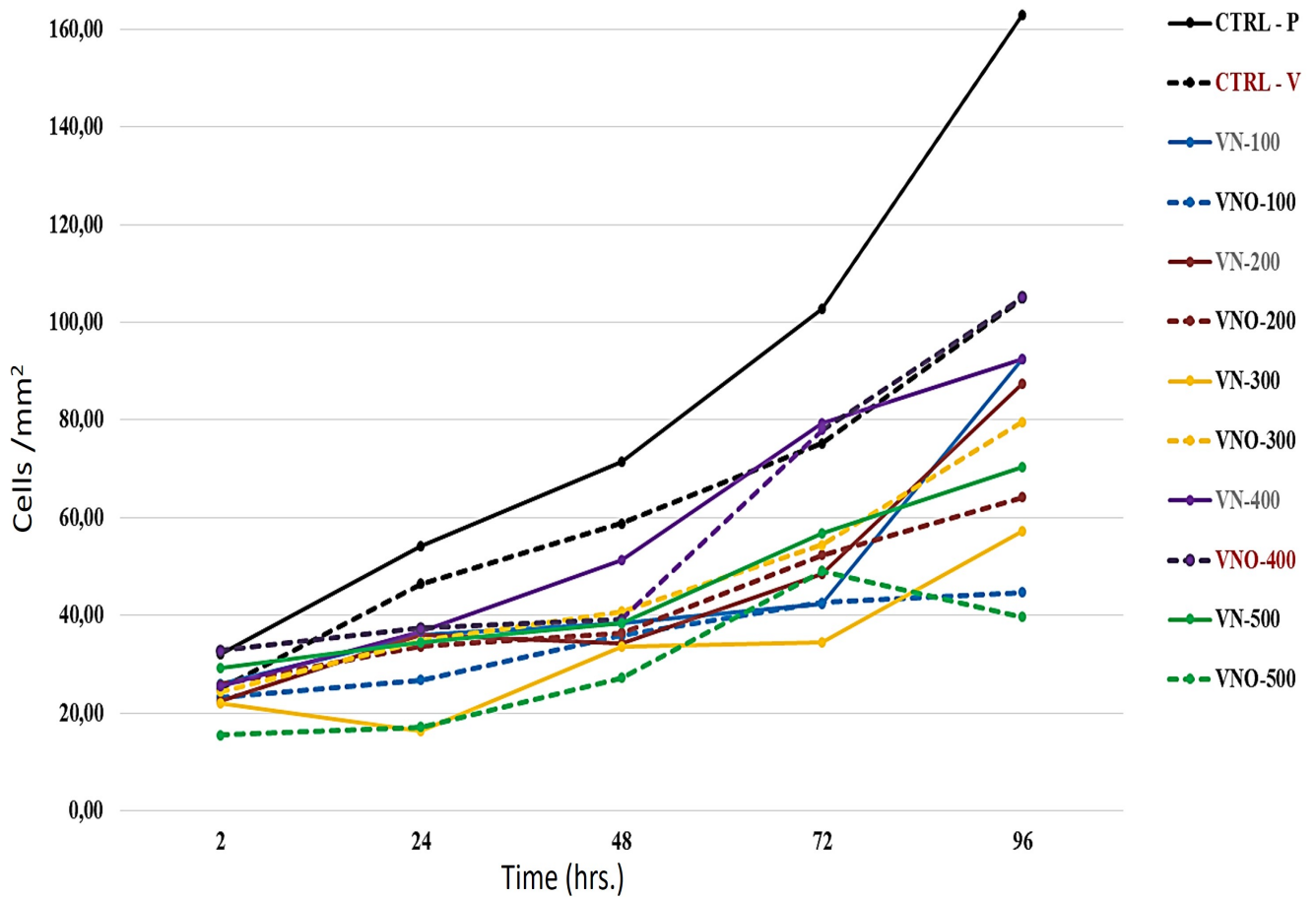


FIGURE 4.3 – Evolution of cells $count/mm^2$ with the incubation period of adhesion on vanadium oxide thin films deposited at different temperatures.

After optimizing the deposition temperature by cell adhesion, we proceeded to study the structural features of vanadium oxide thin films deposited at a temperature of 400 degrees. This analysis included examining parameters such as film roughness and surface energy.

4.3 Structural analysis of optimized VO_x film deposited at 400°C

Subsequent to the successful calibration of deposition temperature for vanadium thin films, our research endeavor extended to the determination of the most suitable film thickness for further investigation of the cell adhesion using surface morphology. To achieve this, a series of thin films was prepared using PLD at a precisely controlled temperature

of 400 degrees Celsius. These films were fabricated with varying thicknesses, achieved by modulating the laser pulse parameters during deposition.

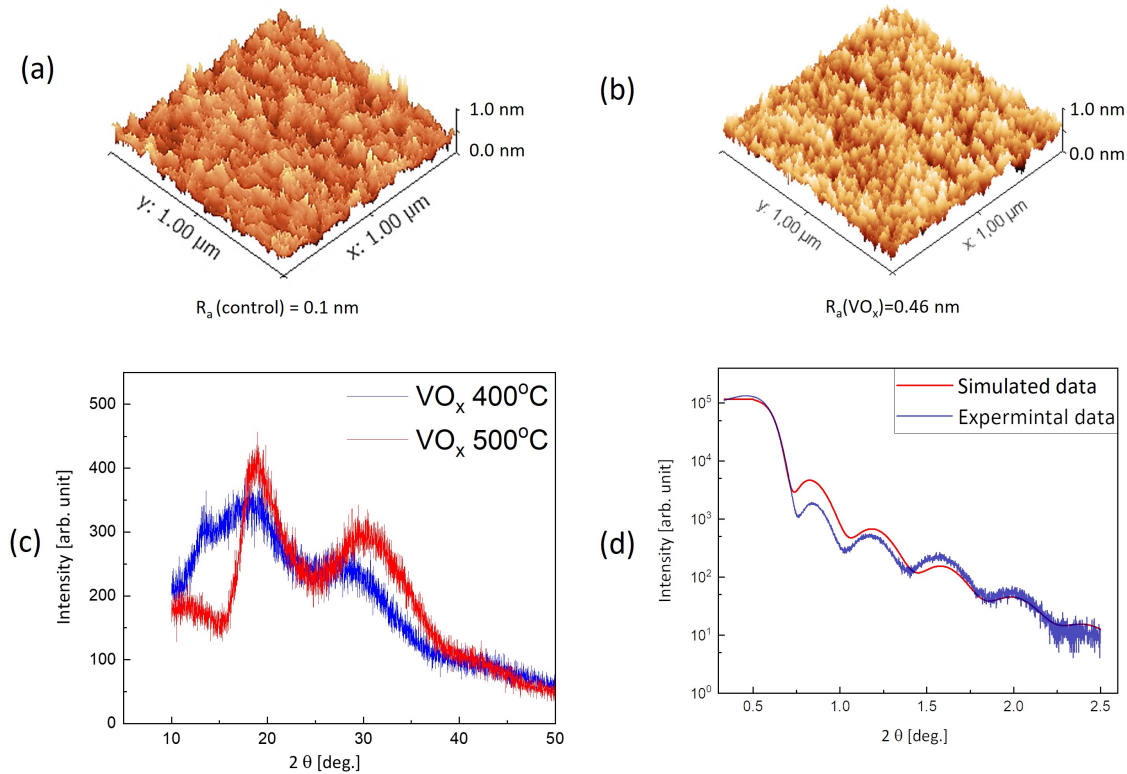


FIGURE 4.4 – AFM images showing the surface profiles of the glass substrate (control) (a) and VO_x thin films (b). The corresponding average roughness (R_a) is indicated below each figure. Typical VO_x thin films were analyzed for their XRD patterns (c) and XRR curves (d).

Following the deposition process, we conducted a comprehensive characterization of these thin films, employing advanced techniques outlined in Chapter 3 of our study. Specifically, we performed Atomic Force Microscopy (AFM) and X-ray Reflectivity (XRR) to acquire detailed insights into the surface morphology and structural properties of the films. These analytical methods allowed us to ascertain the films' thicknesses and structural integrity with a high degree of precision as we describe in Chapter 3. Subsequently, our investigation delved into the assessment of surface wettability, a critical parameter that significantly influences cell adhesion. It has been well-documented that hydrophilic surfaces tend to exhibit enhanced cell adhesion properties. Therefore, we quantified the wettability of the vanadium thin films. In our analysis, we were particularly interested in the contact angle, as it has been reported that surfaces with contact angles falling

within the range of 50 to 60 degrees are considered favorable biomaterials, demonstrating superior adhesion characteristics compared to hydrophobic surfaces.

Figure 4.4 (a) and (b) present a comparison of the surface profiles of the control sample (uncoated glass slide) and the VO_x film deposited at 400°C . The study revealed a positive correlation between film thickness and roughness. Specifically, the roughness measurements for a 6 nm film were about 0.20 nm, while those for a 26 nm film were 0.79 nm. The uncoated glass substrate exhibited a roughness of around 0.1 nm, but the VO_x samples displayed roughness values ranging from 0.2 to 0.8 nm. This suggests that the films possess a smooth surface and are of high quality, showing successful growth of VO_x thin films using pulsed laser deposition (PLD) technique. Although vanadium oxides can exhibit different stoichiometries depending on temperature and other growth conditions, XRD measurements revealed that the deposited thin films had an amorphous structure (Fig.4(c)). This is evident from the two broad peaks of low intensity, indicating the absence of long-range ordering in the structure. Hence, X-ray diffraction analysis does not provide information about the stoichiometry or structure of the vanadium oxide, and the composition of the vanadium oxide thin films will be referred to as VO_x in the following. The thickness of the films was extracted from Fig.4(d) using the XRR technique, ranging from 6-26 nm, resulting in a deposition rate of approximately 0.012 nm/laser pulse.

We continued our investigation into the surface energy and wettability of the vanadium oxide thin films by depositing them at a temperature of 400 degrees. The observation of the sample's wettability is considered significant due to the established relationship between material wettability, protein adsorption, and cell adhesion. It is well documented that biomaterial surfaces exhibiting moderate hydrophilicity tend to enhance cell growth and exhibit enhanced biocompatibility. It was shown in the previously reported articles that surfaces with hydrophilic properties exhibit a greater tendency for cellular adhesion.[73]

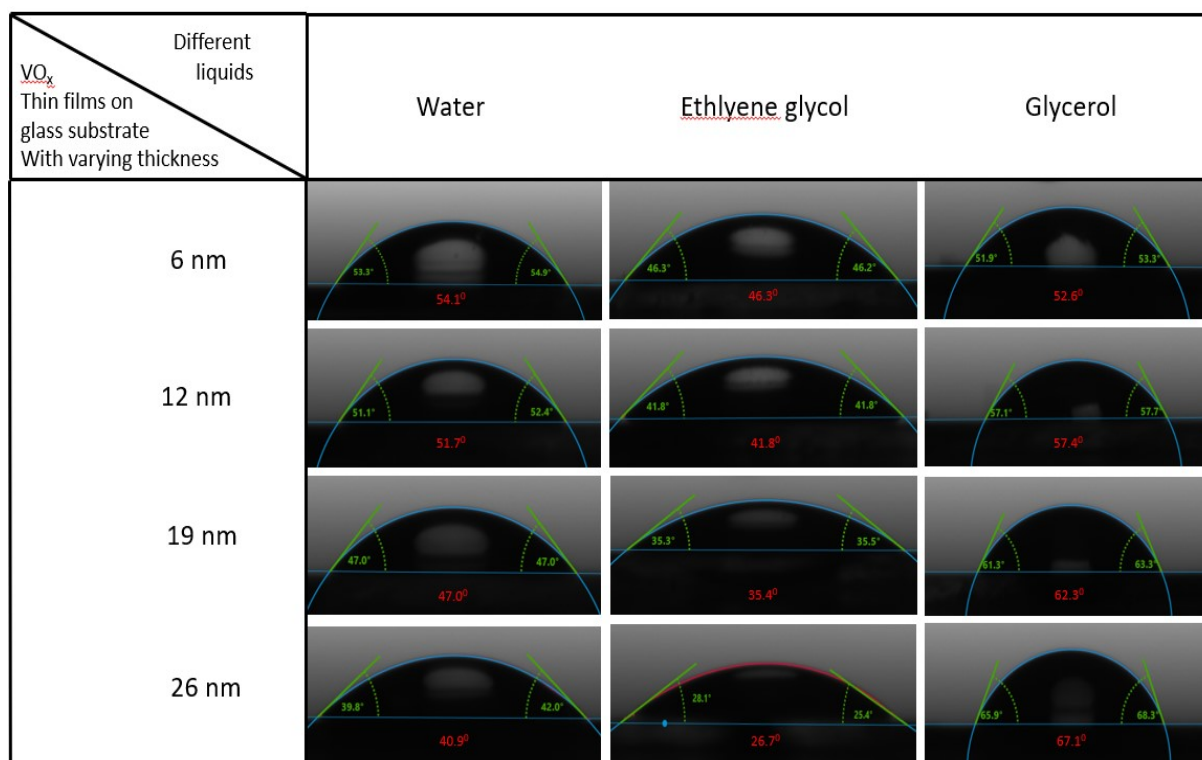


FIGURE 4.5 – Contact angle images of vanadium oxide thin films with different testing liquids (water, ethylene glycol, glycerol) are shown. The thickness of the films are also indicated against each figure.

The experimental setup involved placing droplets of distilled water, ethylene glycol, and glycerol over VO_x thin films with different thicknesses as described in Chapter 3. The results, as depicted in Figure 4.5, revealed that the contact angle of all droplets was below 90° , suggesting that the films exhibited hydrophilic properties. The hydrophilic nature of these metal oxide thin films can be ascribed to the existence of surface hydroxyl groups, which readily establish hydrogen bonding interactions with water molecules.[74]

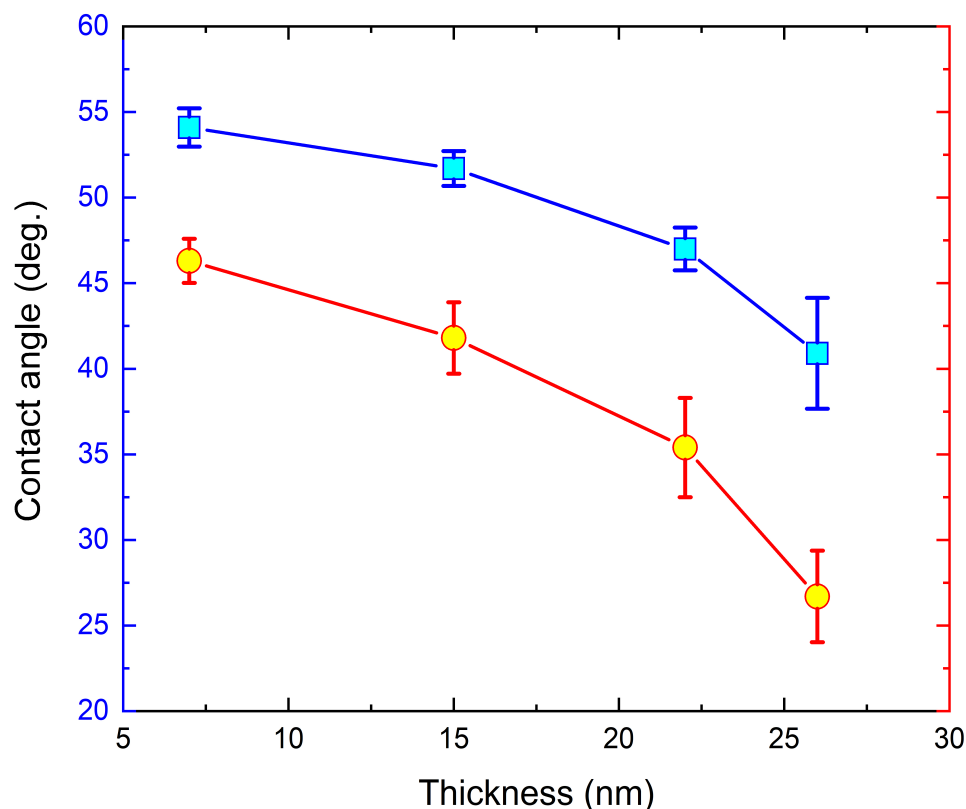


FIGURE 4.6 – Variation of the magnitude of contact angle with respect to the thickness of VO_x thin films. The contact angle with water and ethylene glycol is represented by the symbols ■ and ○, respectively.

Fig.4.6 displays the evolution of the contact angle with the thickness of VO_x thin films. The contact angle values of distilled water droplets on VO_x thin films with thicknesses of 6, 15, 22, and 26 nm were 54.1° , 51.7° , 47.0° , and 40.9° , respectively, and with ethylene glycol 46.3° , 41.8° , 35.4° , and 26.7° , respectively. It was observed that the contact angle decreased with increasing thickness. Tungsten-doped vanadium dioxide (VO_2) thin films deposited on fused quartz were found to be extremely hydrophilic, yielding similar results. Also, iron dopants in VO_2 thin films resulted in smaller water contact angles, indicating superior hydrophilic properties.[75] This phenomenon can be explained by the Wenzel equations mentioned earlier in chapter 3 which indicates that an increase in roughness with thickness results in increased hydrophilicity of these surfaces as observed.

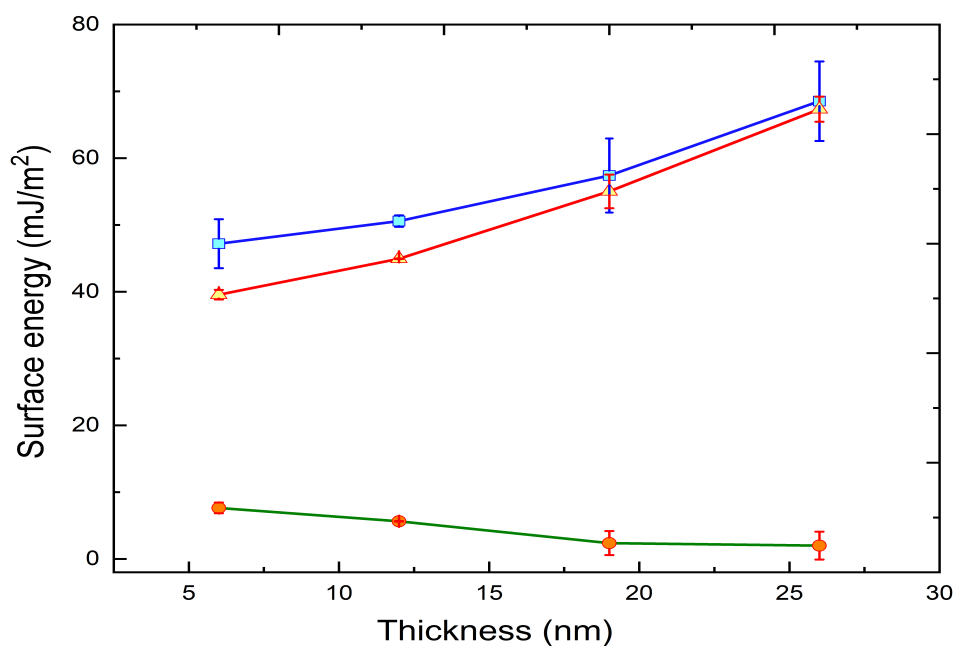


FIGURE 4.7 – Evolution of total surface energy (■) and its polar (●) and dispersive (▲) components with varying thickness of the VO_x thin films.

Following the measurement of the contact angle, we proceeded to determine the surface energy of each sample and subsequently plotted it against the thickness of the vanadium oxide thin films.

We used equations (6, 7, 8) described in Chapter 3 to calculate the total surface energy of VO_x thin films, which varied from 47 to 69 mJ/m^2 . To obtain the surface free energy, we employed the dispersive (γ_i^d) fractions reported previously, which were 21.8, 34, 29 for water, ethylene glycol, and glycerol, respectively, as well as the polar (γ_i^p) fractions, which were 51.0, 30.4, and 19.3 mJ/m^2 for the same liquids.

For the 6nm VO_x thin film, the polar, dispersive, and total surface energies were 7.63, 39.56, and 47.19 mJ/m^2 , respectively. For the 26 nm thin film, the polar, dispersive, and total surface energies were 1.20, 67.32, and 68.52 mJ/m^2 , respectively, as shown in Figure 4.7. The polar component of the surface energy decreased with increasing thickness due to weaker Coulomb interactions between permanent and induced dipoles. Figure 4.7 also revealed that the dispersive component contributed significantly to the surface energy, which was related to van der Waals interactions resulting from charge motion at the thin film surface.

The reason for this phenomenon could be attributed to the different oxidation states

of vanadium, which react differently to liquids depending on their polarity. Additionally, the variation in particle size distributions during pulsed laser deposition (PLD) growth of VO_x thin films could lead to higher packing efficiency of powder beds, resulting in a lower wetting effect, decreased contact angle (better wetting), and increased surface energy. [76]

The surface investigations that have been conducted offer valuable information regarding the most favorable film thickness for enhancing cell adhesion. The vanadium thin films utilized in this investigation were deposited at a temperature of 400 degrees Celsius and had a thickness of 19 nm. The thickness was selected for further investigation in order to observe cellular response. This decision is based on past research findings which have shown that surfaces exhibiting contact angles ranging from 40 to 60 degrees are considered more favorable for the processes of cell adhesion and proliferation.[77] The contact angle of the 19 nm vanadium thin films was measured to be 47 degrees.

4.4 Cell adhesion and proliferation of hBMMSCs on calibrated sample

To assess cell adhesion and proliferation, hBMMSCs were seeded onto various substrates, including thin films of VO_x of thickness 20 nm, uncoated glass, and plastic wells as a control, at a density of 10^4 cells/cm² in 24-well plates with α -MEM medium. After a two-hour incubation period, non-adherent cells were removed by washing them with phosphate-buffered saline. Adherent hBMMSCs were subsequently harvested by trypsinization (0.25% trypsin/1 mM EDTA, InvitrogenTM) and counted using the CountessTM II Automated Cell Counter (Thermo Fisher Scientific) and trypan blue staining. The same procedure was repeated at different time points (2 hours, 4 hours, and 10 days) to monitor cell proliferation.

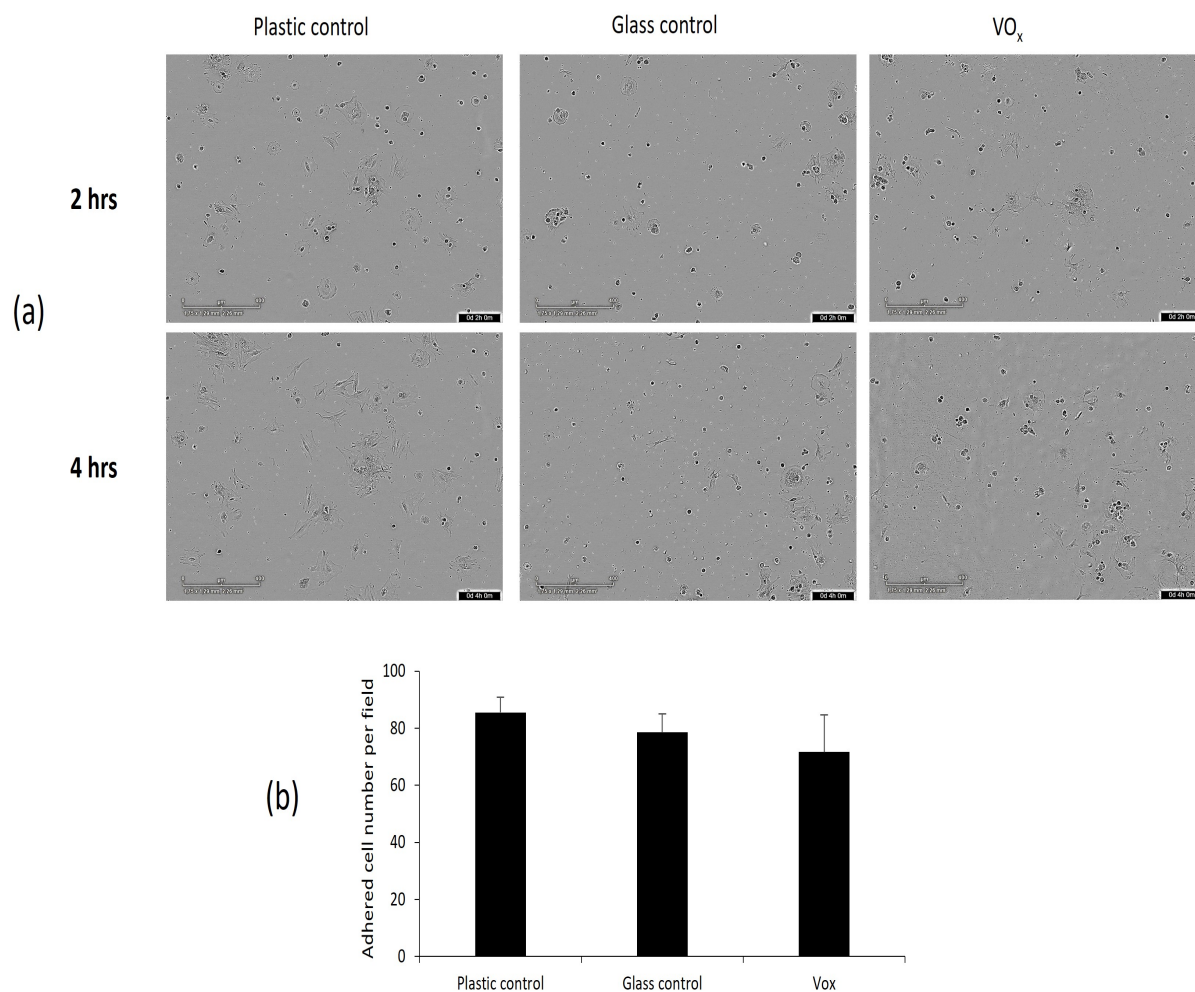


FIGURE 4.8 – Cell density of hBMMSCs cultured on glass and plastic control and VO_x thin films after 2 hours of culture. (a) Phase contrast images of hBMMSCs on glass control and VO_x surfaces were recorded after 2 and 4 hours of culture (scale bar = 400 μm). (b) shows the corresponding cell density of glass and plastic control versus VO_x surfaces, respectively (after 10 days).

We assessed the initial adhesion of cells onto substrates at 2 and 4 hours (see Fig. 4.8(a)) and captured several microphotographs. Cell counting was performed, and indicated that there were only slight differences in cell adhesion between vanadium oxide films and bare glass or plastic substrates. However, the adhesion of hBMMSCs to vanadium appeared to be somewhat less, although the difference was not significant.

4.5 Differentiation assays via histological staining

Seven days after seeding, differentiation (adipogenic, chondrogenic, and osteogenic) media were added and cells were cultured for an additional 2 weeks, with media change twice a week. Afterward, they were prepared for staining and gene expression. Composition media : Osteogenic medium (MEM α supplemented with, 0.1% antibiotics, 10% FBS, 100 nM dexamethasone, 50 μ g/ml ascorbic acid-2 phosphate, β -glyceraldehyde 10 μ M), Adipogenic medium : (MEM α with 0.1% antibiotics, 10% FBS, 100nM dexamethasone, 0.5mM Isobutylmethylxanthanine) or Chondrogenic medium : (Dulbecco's Modified Eagle's Medium-high glucose with glutamine and sodium pyruvate (DMEM, Dutcher), 0.1% antibiotics, 100nM dexamethasone, 50 μ g/ml ascorbic acid-2 phosphate, 40 μ g/ml proline, Transforming growth factor β -3 (TGF beta 3 and Insulin Transferrin Selenium media supplement, $x(ITS + 1)$). (all materials are from Sigma-Aldrich unless mentioned).

To investigate the differentiation activity of cells on oxide thin films, Oil red, Alizarin red, and Alcian blue staining was done. After 2 weeks of differentiation assay, the cells were fixed with 4% paraformaldehyde (PFA) and after being washed with phosphate-buffered saline (PBS), cells were kept at 4°C in PBS. The staining tests consist of washing with distilled water (H_2O_d) and incubation with Alcian blue, Alizarin red, or Oil red solutions for 30 minutes. After Alizarin red and Oil red staining, samples were washed 4 times with H_2O_d and fixed on microscopic histological glass slides. After Alcian blue staining, samples were washed with H_2O_d , and cell layers were analyzed in 1% sodium dodecyl sulfate (SDS). Aliquots of the lysates were transferred to the 48-well plate, and absorbance at 616 nm was determined for triplicate samples (Multiskan GO spectrophotometer, Thermo Scientific TM). To assess the influence of VO_x oxide films on the differentiation potential of hBMMSCs, cells were seeded on VO_x thin films, uncoated glass, or regular plastic wells. After adhesion for 48 hours, they were cultured for 2 weeks under a regular medium (control) before fixing and preparing the cell layers for cytological staining, namely Alcian blue (proteoglycans accumulation), Alizarin red (calcium-rich sites of mineralization), and Oil red. Figure 9 illustrates that culturing hBMMSCs on VO_x substrate affects their differentiation. They exhibit more proteoglycan accumulation (Alcian blue staining) and fewer calcium sites of mineralization (Alizarin red), while calcium sites of mineralization (Alizarin red) and the number of lipidic vesicles remain unchanged (Oil red) (lipidic vesicles staining). Parallel cultures were also conducted under specific media

that direct the cells toward chondrogenic, osteogenic, or adipogenic differentiation. When seeded on plastic or glass wells, hBMMSCs show good trilineage differentiation, with clear staining with Alcian blue, Alizarin red, and Oil red in comparison to respective controls. However, culture on VO_x thin films alters the behavior of the cells by altering osteogenic differentiation while enhancing adipogenic differentiation.

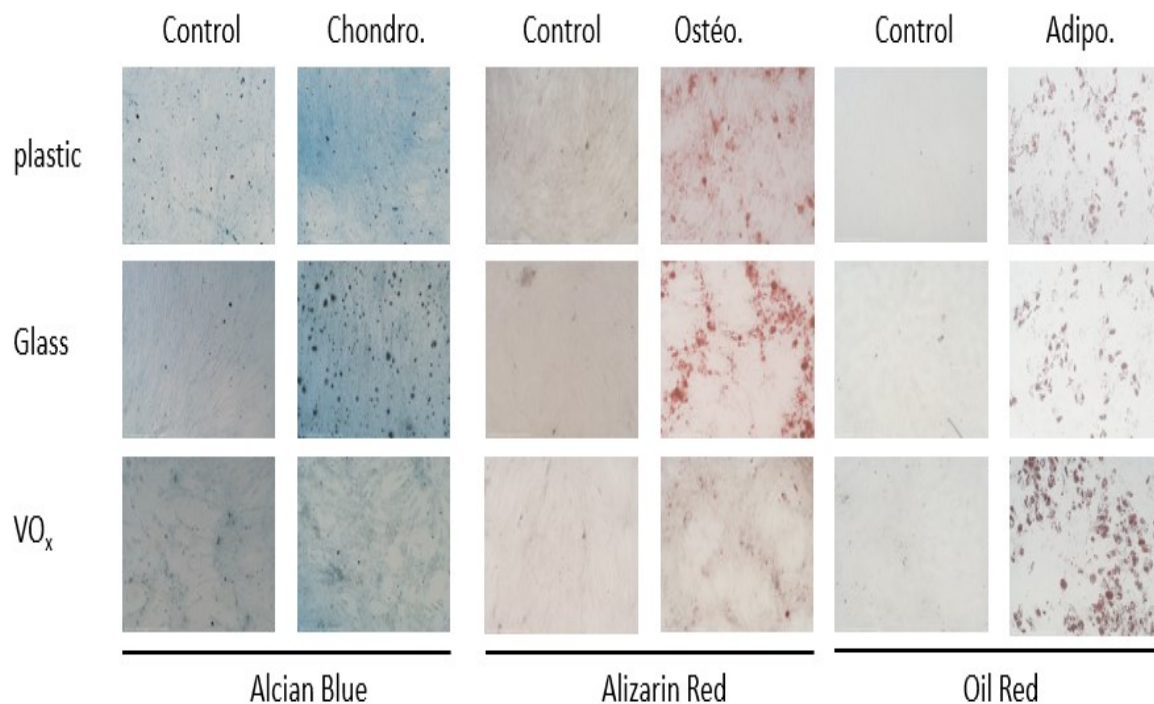


FIGURE 4.9 – Cytological staining with Alcian Blue, Alizarin Red, or Oil Red for hBMMSCs differentiation potential. Microphotographs were taken with a bright field microscope at a magnification of 10X.

4.6 Real-time Reverse Polymerase Chain Reaction

To confirm the observations made by cytological staining gene expression analysis was done on parallel cultures. For this, RNA was extracted by Qiagen kit (RNeasy® mini kit 250), according to the manufacturer's protocol. Total RNA ($1\mu g$) was treated with DNase before reverse transcription into cDNA using MMLV enzyme (Invitrogen by Thermo Fisher Scientific) and oligo T primers. Specific transcripts were then amplified by real-time PCR on the StepOnePlus apparatus (ThermoFisher Scientific) targeting (RUNX2), chondrogenic (COL2A1), and adipogenic (CEBP/a) genes. Reactions were done using Power SYBR Green mix (ThermoFisher Scientific) for 40 cycles (30s at $95^{\circ}C$ /1min at $60^{\circ}C$).

GAPDH, RPL13, and B2MG housekeeping genes were used to normalize mRNA expression levels calculated by $2^{-\Delta\Delta Ct}$ method. The sequences of the primers used are given in Table 3.1 of Chapter 3.

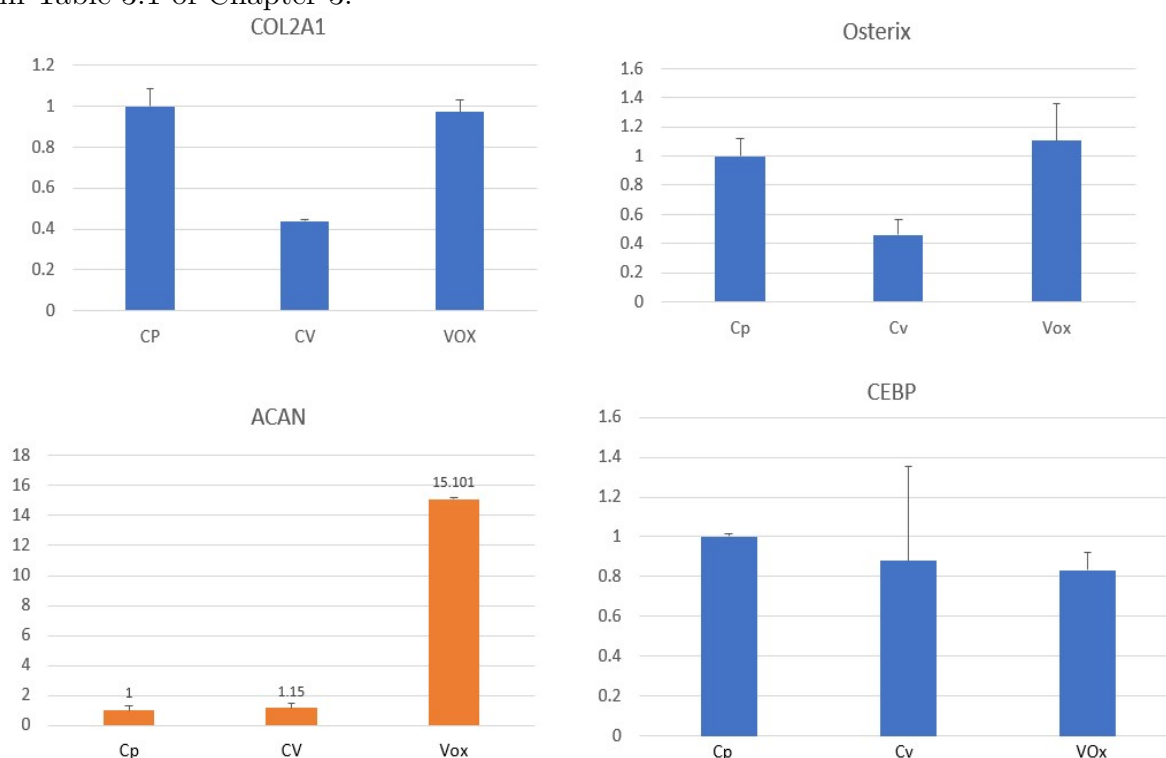


FIGURE 4.10 – chondrogenic (COL2A1, ACAN), Osteogenic (OSTERIX), and adipogenic (CEBP) differentiation of hBMSCs on Plastic, Glass, and, VO_x thin films substrates after 14 days of culture. Statistical evaluation was performed by comparing the samples with the glass and plastic substrate.

hBMSCs were cultured on VO_x thin films, uncoated glass, and plastic wells for 2 weeks. In order to observe the net effect of the oxides Vs. control on differentiation, we culture the cells only with regular media, without those that enhance their differentiation. RNA was extracted, and real-time RT-PCR analysis was performed for specific gene expression. Figure 10 shows the normalized expression of COL2A1 and ACAN (for chondrogenic lineage), Osterix (for osteogenic), and C/EBPalpha (for adipogenic lineage) with GAPDH, RPL13, and B2MG as housekeeping genes. While Osterix and C/EBPa expression is unaffected, ACAN expression is greatly enhanced when the cells are in contact with VO_x (as shown in Figure 10). These observations are consistent with cytological staining that showed more proteoglycan production under culture onto VO_x while no mineralization nor lipidic vesicles were seen.

4.7 Conclusion

To summarize, we employed the pulsed laser deposition technique to create thin films of vanadium oxide (VO_x), which we then used as substrates for the development of human bone marrow mesenchymal stem cells (hBMMSCs). The VO_x coatings had flat surfaces that were hydrophilic in nature. According to the findings of our comprehensive investigation, the VO_x films had a marginally inhibitive effect on the adhesion and proliferation of hBMMSCs, although this effect was not statistically significant. Moreover, our investigation has revealed that VO_x coatings exert a notable promotion of chondrogenesis, while simultaneously exerting discernible but relatively modest influences on osteogenic or adipogenic differentiation. These compelling findings have been substantiated through a combination of cytological staining techniques and real-time RT-PCR gene expression analyses.[78]

The implications of our findings underscore the imperative need for a comprehensive understanding of the underlying mechanisms and interactions governing the influence of vanadium oxide on cell behavior. Particularly noteworthy is the pivotal role played by surface chemistry and morphology in dictating the dynamic interplay between materials and cells.

In the context of constructing cell culture substrates for screening tests and, potentially, orthopedic prostheses, this knowledge assumes paramount significance. The precision with which these surfaces can be engineered to modulate cellular responses holds great potential for biomedical applications.

The outcomes of this study have far-reaching implications, potentially catalyzing further research into the optimal content of vanadium elements in implants. Our observations have demonstrated that vanadium exerts no inhibitory effect on human bone marrow-derived mesenchymal stem cells (hBMMSCs) and, intriguingly, augments the chondrogenesis differentiation process within these cells. This breakthrough insight presents a promising avenue for future research endeavors aimed at enhancing the biocompatibility and performance of implant materials, with the potential to significantly impact the field of orthopedics and beyond.

Antibacterial Properties of Metal Oxides Thin Films

This chapter investigates the issue of bacterial infection on implants and analyzes the potential of metal oxide coatings to offer a solution. Bacteria, specifically found on natural surfaces such as dirt and water, can lead to human ailments, such as the bacterium *Pseudomonas aeruginosa*. This resilient Gram-negative bacteria is responsible for several infections acquired in hospitals, particularly in locations where TiAlV implants are present. The bacteria culture was done in the School of Biological Sciences, College of Science, Nanyang Technological University, Singapore with Dr. Soak Kuan Lai and Li Hoi Yeung . XPS was done at IIT Madaras by Mr. Souman Pradhan under the supervision of Professor M.S.R. Rao.

5.1 Introduction

Bacterial infections pose a significant concern in various fields, ranging from health-care facilities to industrial sectors. The impressive ability of bacteria to attach to surfaces form persistent biofilms, and display resistance to traditional therapies poses a substantial and intricate problem. Furthermore, the extensive growth of bacterial biofilms, which are known for their accumulation on various surfaces, occurs not only in everyday residential water pipes but also in important industrial medical equipment, leading to long-lasting health problems and infections. The field of surgical implants is plagued by the com-

plex and enduring problem of implant-associated infections, principally caused by the existence of biofilms. This issue continues to be a notable concern in current healthcare methods. The six prominent pathogens, namely (*Pseudomonas aeruginosa*, *Escherichia coli*, *Staphylococcus aureus*, *Klebsiella pneumonia*, *Streptococcus pneumonia*, and *Acinetobacter baumannii*) were responsible for a significant 929,000 deaths worldwide in 2019, primarily due to antimicrobial resistance.

Pseudomonas aeruginosa, among various *Pseudomonas* species, is the most common cause of infections in humans, affecting the bloodstream, lungs, and other organs.[79] Consequently, extensive research has been conducted on this particular pathogen and its biofilm formation on surfaces. For instance, Kim *et.al*, demonstrated that *Pseudomonas aeruginosa* forms denser biofilms under microgravity conditions compared to those on earth.[80] Additionally, *Pseudomonas aeruginosa* biofilms are commonly found in chronic wounds and contribute to conditions like chronic osteomyelitis, an infection where microorganisms attach to dead bone.[81] In general, it is widely accepted that organisms associated with biofilms are accountable for more than 65% of microbial infections. These organisms demonstrate significant resistance to antimicrobial agents as well as components of the host defense system, encompassing both innate and adaptive immunity.[82]

Pseudomonas aeruginosa is particularly concerning as a highly troublesome infection among several bacterial causes. This Gram-negative bacterium is well-known for its exceptional capacity to adapt and its preference for causing infections that are acquired in hospitals, especially in areas where medical devices are used. These chronic infections frequently result in severe consequences, emphasizing the urgent necessity to investigate and create efficient remedies to counteract their persistence.

Due to the aforementioned challenges,[83] effectively controlling germ growth has become a critical concern, and extensive efforts are being directed toward combating biofilm formation.[84, 85, 86] Developing methods to modify the surfaces of biomaterials or materials while preserving their mechanical properties is essential in addressing this issue. Various strategies have been employed to combat the detrimental effects of biofilm contamination, including anti-adhesion techniques, contact activation, and the release of biocidal agents.[87] However, these treatments often exhibit limited efficacy, as incomplete eradication of bacteria can lead to increased resistance against cleaning agents.[88] As a result, alternative approaches such as surface coating with anti-biofilm agents and related materials have been developed.[89] Among these approaches, thin film techno-

logy has shown significant promise in enhancing antibacterial activity. Furthermore, the preparation of thin films at the molecular level can play a crucial role in determining the interaction between human biology and materials, making it an essential aspect to consider.

In biomedical applications, the choice of coating material remains a significant consideration. Polymer surfaces are widely accessible, cost-effective, and effective in combating biofilm growth.[90] However, they tend to exhibit lower strength and are prone to degradation in the body's biochemical environment.[91]

Alternatively, other compounds such as metals, alloys, or ceramics can be utilized as coatings. Various metal ions, including Zn^{+2} , Cu^{+2} , Al^{+3} , Ti^{+4} , and Ag^{+} , have been extensively investigated for their antimicrobial properties [92, 93, 94]. Recent research has shown that Cu is more effective than Ag in combating bacteria under typical indoor settings, including humidity and temperature. Research has demonstrated that incorporating copper(Cu) surfaces in a pediatric intensive care unit (PICU) can effectively minimize the amount of harmful microorganisms.[95, 96] Additionally, another study found that using linens and uniforms infused with copper oxide led to a notable reduction in the prevalence of hospital-associated infections (HAIs).[97, 98]

Copper-based coatings, for instance, show promise as biocompatible materials for developing anti-biofilm coatings, effectively protecting surfaces against harmful biofilm pathogenesis.[99] Several studies have demonstrated the antimicrobial activity of copper or copper oxide against a wide range of bacteria.[100, 101, 102]

Additionally, Ti-based coatings are frequently employed as biomaterials in implant applications. Doping copper into the TiO_2 host offers several advantages. Copper serves as an antibacterial agent, while TiO_2 helps reduce the recombination of charge carriers, which is crucial for antibacterial activity.[100] These synergistic effects contribute to the enhanced antibacterial properties of Cu-doped TiO_2 coatings. Overall, the choice of coating material is a critical factor in biomedical applications, with both polymer and metal-based coatings offering distinct advantages in terms of antimicrobial properties and biocompatibility with the TiAlV alloys used in implants.[100, 101, 102]

In this chapter, we utilized the Pulsed Laser Deposition (PLD) technique to grow (Cu,Ti) oxide films on glass surfaces. These coated surfaces were then subjected to exposure to *Pseudomonas aeruginosa*, a specific bacterium of interest. Our main objective was to investigate the antimicrobial activity of the coatings against this bacterium, focusing

on the influence of surface properties and varying Cu/Ti ratios. Remarkably, we observed a significant 20% reduction in biofilm formation by bacterial cells on $\text{Cu}_{0.75}\text{Ti}_{0.25}\text{O}_x$ coated glass surfaces compared to the control glass samples in the initial steps. We attribute this reduction to the alteration of copper content present at the surface of the films. Our findings highlight the potential of these coatings to effectively inhibit biofilm formation by *Pseudomonas aeruginosa*, emphasizing the significance of surface modifications and the specific Cu/Ti ratio in achieving such antimicrobial effects which can be further used for bioimplants. The correlation between identifying the issue of implant-related infections, specifically those caused by bacteria such as *Pseudomonas aeruginosa*, and the implementation of metal oxides as an effective remedy, highlights the potential of these coatings in preventing bacterial adhesion, hindering the formation of biofilms, and suppressing the growth of *Pseudomonas aeruginosa*.

5.2 Optimization of CuTiO thin films

Thin films of different thicknesses were created on a 12 mm diameter glass substrate using PLD, as explained in Chapter 2. Before being introduced into the vacuum chamber, the glass substrate was subjected to ultrasonic cleaning using ethanol, followed by rinsing in deionized water and subsequent drying using compressed air. Several $\text{Cu}_x\text{Ti}_{1-x}\text{O}_x$ (CTO) compositions were examined, specifically with x values of 0.25, 0.5, and 0.75. The preparation of (Cu, Ti) O_2 targets included utilizing a typical solid-state procedure. This process involved grinding CuO_x and TiO_2 powders to achieve the desired stoichiometry and subsequently subjecting them to numerous firing cycles at a temperature of 800° C in an air environment. The final product was thereafter compressed and put to sintering for a duration of 24 hours at a temperature of 1100° C. Throughout the process of depositing the film, a KrF excimer laser with a wavelength of 248 nm and a frequency of 3 Hz was moved across the surface of the target at a fluence of 2.45 J/cm². The substrate was placed 4.5 cm away from the target and kept at a temperature of 200° C. The base pressure was maintained at 1.1x10⁻⁷ bar in vacuum. In order to obtain various film thicknesses, the quantity of laser pulses was adjusted within the range of 4500 to 10000, while utilizing a low deposition rate of 0.0024 nm/pulse to avoid any splashing or the creation of particles on the films.[103]

5.3 Bacterial cultivation

In order to promote the formation of biofilm, the bacteria that were stained were initially gathered and placed in a specifically designed AB minimum medium. This medium consisted of 2 grams of glucose per liter and 2 grams of casamino acids per liter. Subsequently, the bacterial suspension was put inside a chamber made of agarose. Before imaging, the bacteria were diluted to an optical density of $OD_{600} = 1.5$ and then stained with a Vibrant Dye cycle Green stain (Invitrogen) for 30 minutes while being agitated. Following a 6-hour incubation period at a temperature of 37°C , the agarose chamber was positioned on the Zeiss light-sheet microscope (Z.1) as we already discussed in Chapter 3.

5.4 Interaction of Cu ions with bacterial cell

Every cell, whether a single-cell organism like a bacterium or a more sophisticated eukaryotic cell, has a consistent electrical phenomenon known as the "transmembrane potential." This refers to the disparity in voltage between the inner and exterior of the cell. There is compelling data indicating that the interaction between bacteria and a copper surface can interfere with the conduction of electric current through the cell membrane.[104, 105, 106] This disturbance compromises the integrity of the membrane and can result in the development of holes. A different approach to generating openings in the membrane involves the utilization of a technique known as targeted oxidation. This phenomenon takes place when a copper ion, an individual copper molecule, is liberated from the copper surface and comes into contact with a fundamental constituent of the cell membrane, such as a protein or a fatty acid.

Due to the reduced integrity of the cell's outer membrane, copper ions continuously enter the cell. The rapid increase of this inflow quickly fills the intracellular environment, inhibiting its regular metabolic processes. Enzymes are essential for aiding and executing the metabolic events within a cell. The excessive binding of copper to these enzymes hinders their regular functioning within the cell. Consequently, this limits the bacteria's capacity to respire, acquire nutrients, carry out metabolism, or produce ATP (adenosine triphosphate), which serves as the main energy unit of the cell. Essentially, the presence of copper interferes with the regular operation of the cell's membrane and its internal metabolic processes, finally causing the bacteria to lose the ability to carry out vital life

tasks.

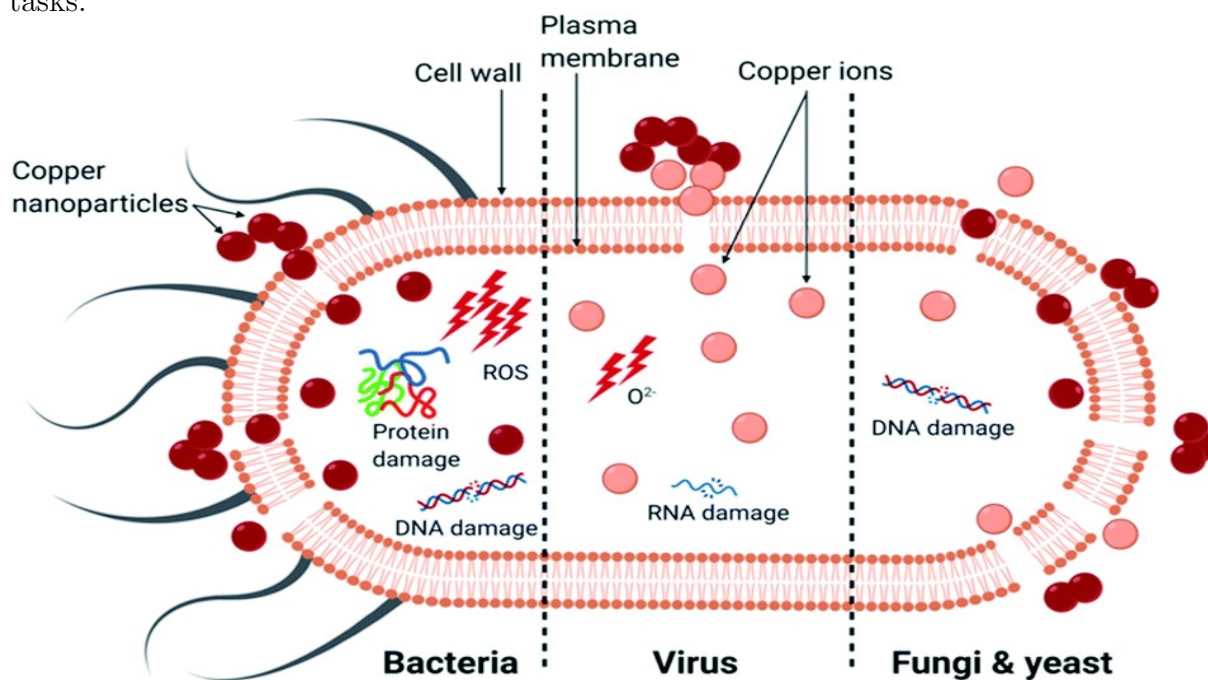


FIGURE 5.1 – The main mode of mortality in many microorganisms caused by copper nanoparticles.

[107]

5.5 Results and Discussion

5.5.1 Structure and surface topography of thin films

After successfully depositing thin films of $\text{Cu}_x\text{Ti}_{1-x}\text{O}_x$ with varying thicknesses, we conducted structural characterization using X-ray Reflectivity (XRR), surface energy, and Atomic Force Microscopy (AFM), as previously described in Chapter 3. Figure 5.2 (a) and 1(b) present representative images of $\text{Cu}_{0.75}\text{Ti}_{0.25}\text{O}_2$ films with thicknesses of 20 nm and 24 nm, respectively. These images illustrate that the films exhibit a uniform coverage with a yellow transparent color, indicating a homogeneous deposition without any presence of pin-hole defects. Moreover, all the films display excellent adhesion to the glass substrate. The roughness measurements of both samples reveal values less than 1 nm, indicating remarkably smooth surfaces. The thicknesses of the films were determined using X-ray Reflectivity (XRR) analysis, revealing measurements of 11 nm, 16 nm, 20 nm, and 24 nm, respectively. Referencing Figures 5.2(c) and (d) allows for visual representation of the 20 nm and 24 nm thicknesses.

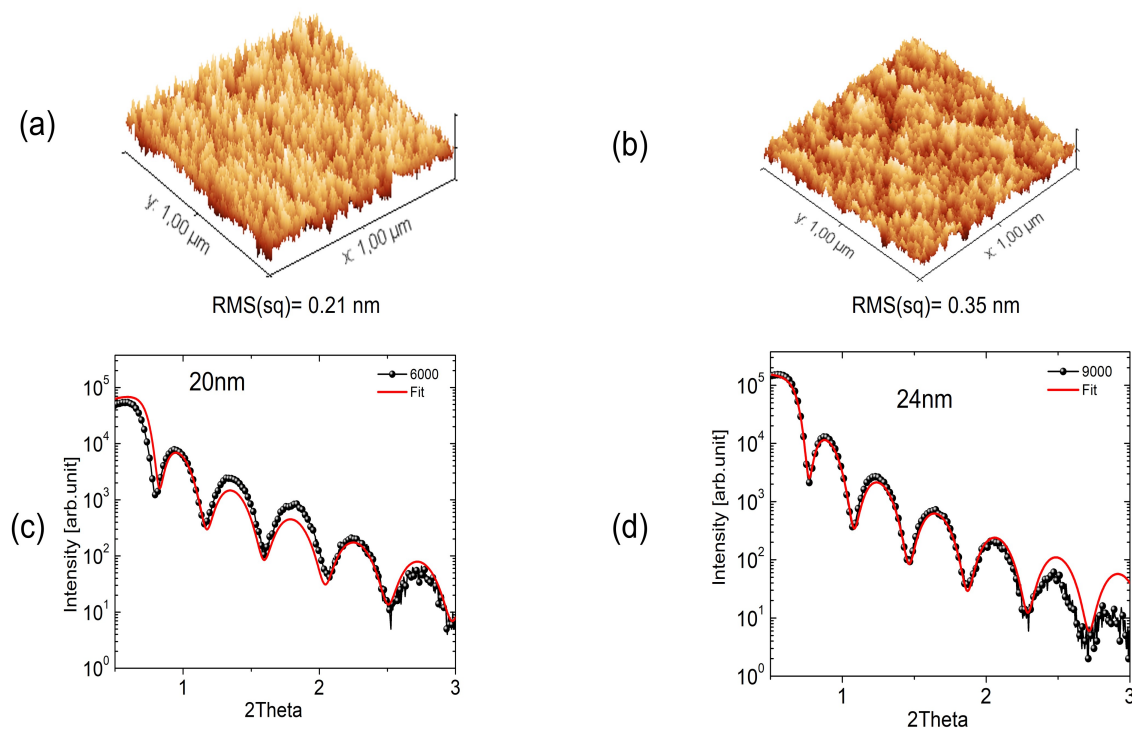


FIGURE 5.2 – $1\mu\text{m} \times 1\mu\text{m}$ AFM images of 20 nm (a), and 24 nm (b) thin CTO films. The roughness values are indicated below each respective figure. Additionally, typical XRR curves for these films, recorded from 0 to 3° , are shown, with experimental data depicted in black and fitted curves in red. The corresponding calculated thicknesses are 20 nm (c) and 24 nm (d).

Figure 5.3 illustrates the variation of contact angle with respect to film thickness. For distilled water, the contact angles were measured to be 60.4° , 67.5° , 76.1° , and 81.3° for film thicknesses of 11 nm, 16 nm, 20 nm, and 24 nm, respectively. Similarly, for ethylene glycol, the contact angles were found to be 42.2° , 53.7° , 55.5° , and 65.7° for the same respective film thicknesses. Figures 3b and 3c depict typical images used to measure the contact angle for water and ethylene glycol, respectively (Table 1). The obtained data suggests that the thin $\text{Cu}_{0.75}\text{Ti}_{0.25}\text{O}_2$ films exhibit inherent hydrophilicity, as indicated by contact angles less than 90° . The surface, serving as the point of contact between bacteria and the material, plays a crucial role in promoting or preventing bacterial adhesion. Surface wettability, a fundamental property, governs the interactions between solid and liquid phases in biological systems, as hydrophilic surfaces facilitate adhesion as we saw in Chapter 3.

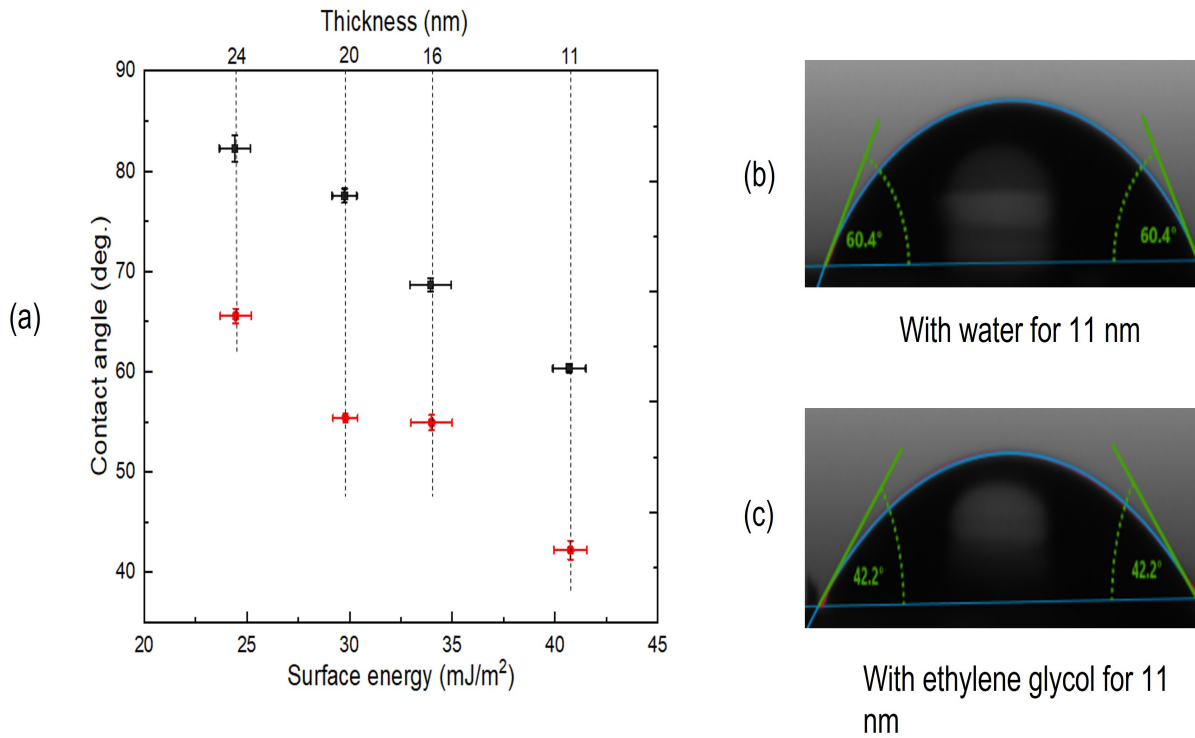


FIGURE 5.3 – (a) Variation of surface energy and contact angle with film thickness is depicted, where ■ and ● represent the test liquids water and ethylene glycol, respectively. (b) and (c) display typical contact angle images with water and ethanol, respectively.

By using the Owens-Wendt equation and the contact angles of these films, the surface energy was calculated. We utilized the dispersive (γ_i^d) and polar (γ_i^p) fractions to calculate the surface energy, which was found to be 21.8 and 51 mJ/m² for water, and 34 and 30.4 mJ/m² for ethylene glycol, respectively, as previously reported.[58] By considering these components, the total surface energy was determined, resulting in surface energies of 40.75, 33.98, 29.79, and 24.45 mJ/m² for Cu_{0.75}Ti_{0.25}O₂ films with thicknesses of 11 nm, 16 nm, 20 nm, and 24 nm, respectively (Fig. 3). Table 1 clearly demonstrates that increasing the film thickness leads to modifications in both surface energy and contact angle. In fact, the contact angle and surface energy exhibited an inverse relationship. These changes can be explained by Eq. (1), where an increase in θ leads to a decrease in the term $\cos(\theta)$. As a result, the surface tension of the solid decreases. The variation in contact angle strongly depends on surface roughness, which is influenced by factors such as the density of layers, the preparation method of thin films, and geometric factors.[108]

TABLE 5.1 – Evolution of different parameters for the series of films.

Thickness (nm)	11	16	20	24
Contact angle with water (deg.)	60.4	67.5	76.1	81.3
Contact angle with ethylene glycol (deg.)	42.2	53.7	55.5	65.7
Surface energy (mJ/m ²)	40.75	33.98	29.79	24.45

5.5.2 Analysis of surface state by X-ray photoelectron spectroscopy

XPS analysis was conducted at the Indian Institute of Technology, Madras (IIT Madras) on $\text{Cu}_{0.75}\text{Ti}_{0.25}\text{O}_2$ thin films with two different thicknesses (16 nm and 24 nm), and the resulting spectra are presented in Figure 5.4. The survey scans revealed the presence of Cu, Ti, O, and C elements without any unexpected peaks. The binding energy of all elements was calibrated using the C 1s peak (284.6 eV). Figures 5.4 (b-d) and (f-h) exhibit high-resolution spectra for Cu 2p, Ti 2p, and O 1s of the films. In the Cu 2p core-level spectrum, two distinct peaks correspond to Cu $2p_{1/2}$ and $2p_{3/2}$, each of which can be further deconvoluted into two peaks, indicating the presence of both Cu(I) and Cu(II) species in the samples. The binding energies (BEs) located at 932.14 and 952.09 eV correspond to Cu $2p_{3/2}$ and $2p_{1/2}$ spectra of Cu(I) associated with Cu_2O . Conversely, the BEs at 934.09 and 954.44 eV correspond to Cu $2p_{3/2}$ and $2p_{1/2}$ spectra of Cu(II) related to $\text{Cu}(\text{OH})_2$. Additionally, peaks at 942.39 and 962.09 eV represent the shake-up satellite peaks, which are also associated with Cu(II) species. The relative concentration of Cu(I) and Cu(II) species on the surface of the thin film can be calculated using the equation proposed by Ghodselahe et. al, [109] :

$$Cu(II) = \frac{Cu_2 + S}{Cu_1 + Cu_2 + S} \cdot 100\% \quad (5.1)$$

The relative concentration of Cu (I) species, Cu(I), Cu (II) species, Cu_2 , and the total area of the shake-up satellite peak, S, were used to calculate their respective proportions. The calculated relative concentration of Cu (I) species was determined to be 38.03% and 39.28% on the surfaces of the 16 nm and 24 nm thick films, respectively.

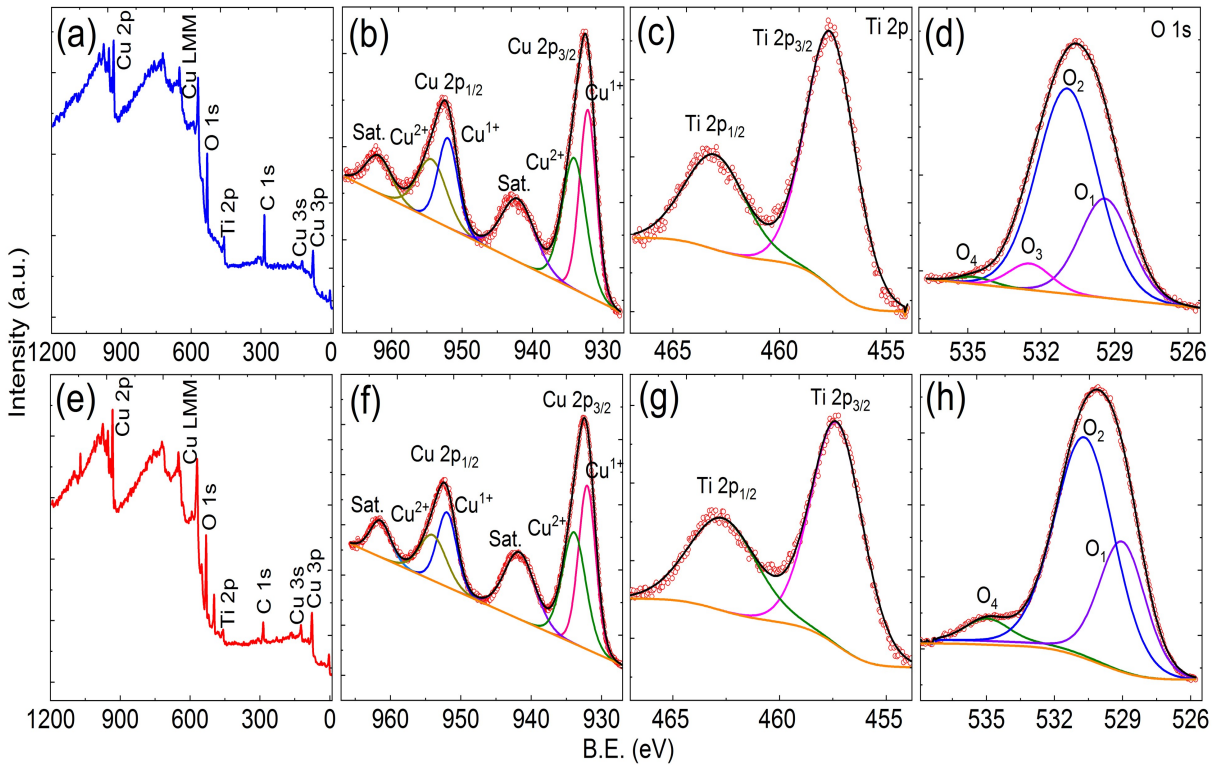


FIGURE 5.4 – XPS scan of $\text{Cu}_{0.75}\text{Ti}_{0.25}\text{O}_2$ thin films : (a) Survey scan for 16 nm. (b) to (d) high-resolution spectra of Cu 2p, Ti 2p, and O 1s. (e) Survey scan of 24 nm and (f) to (h) high-resolution spectra of Cu 2p, Ti 2p, and O 1s respectively.

The Ti 2p spectrum exhibited two peaks at approximately 457.71 eV ($2p_{3/2}$) and 463.21 eV ($2p_{1/2}$), with a difference of approximately 5.5 eV, closely matching the 5.6 eV difference for Ti (IV) species. Thus, the peak fitting confirmed the presence of only Ti (IV) species on the film surface, ruling out the presence of any Ti (0)-metallic species. This observation suggests the presence of Ti^{4+} -O bonds within the system. The experimental Cu/Ti ratio in the samples was determined as 70.32/29.68 for the 16 nm film and 80.11/19.89 for the 24 nm film. This indicates a deviation of approximately $\pm 5\%$ from the nominal composition of the target used during the deposition. The deviation primarily arises from two factors : the XPS experiment, which relies on proper background selection and accurate peak positioning, and the variation in experimental conditions, such as pressure, energy calibration of the laser, scan range, etc., between different depositions. These results confirm the reliability of the experimental composition of the thin films. Furthermore, the O 1s peak could be deconvoluted into multiple peaks, where O1 and O2 correspond to lattice oxygen of CuO_x and Cu_2O , while O3 and O4 represent oxygen vacancies and adsorbed oxygen, respectively.

5.5.3 Antibacterial activity of thin films

To investigate the ability of $\text{Cu}_x\text{Ti}_{1-x}\text{O}_X$ coatings ($x = 0.25, 0.50, 0.75$) to resist biofilm formation, we conducted an experiment using round glass slides, both coated and uncoated, placed in microtiter plates. The biofilm generation efficiency was evaluated at NTU Singapore utilizing the Crystal Violet Biofilm Detection Assay. mPAO1 bacteria were cultured under conditions that promote biofilm formation and incubated for 24 hours at 37 °C in the microtiter plates. The bacterial cells adhering to the glass surfaces were stained and quantified to evaluate the extent of biofilm formation. Our findings consistently demonstrated that the biomass of the biofilm was significantly lower on the glass surfaces coated with $\text{Cu}_x\text{Ti}_{1-x}\text{O}_X$ (specifically, ($x = 0.75$)) compared to the uncoated control surfaces (refer to Fig. 5.5 (a)). It is widely recognized that the initial attachment of bacteria to a surface is crucial for biofilm formation. Therefore, we tested the hypothesis that a $\text{Cu}_x\text{Ti}_{1-x}\text{O}_X$ coating with ($x = 0.75$) could hinder the initial attachment of mPAO1 bacteria, while the other two compositions ($x = 0.25, 0.50$) did not significantly alter the attachment (see Table 5.2). To examine the initial attachment of mPAO1, we visualized the adhesion of individual bacteria to both the control and $\text{Cu}_{0.75}\text{Ti}_{0.25}\text{O}_2$ -coated glass surfaces using a light sheet microscope. The mPAO1 cells were incubated for 6 hours in a specially prepared light sheet chamber under conditions favorable for biofilm formation.

TABLE 5.2 – Cu-Ti Ratio Impact on Bacterial Biofilm Growth

No	Composition ratio Cu-Ti-O	Deposition temperature (°C)	Comparative assessment of antibacterial activity
1	Cu : Ti = 3 : 1	200	20% reduction in growth of bacteria compared to glass control
2	Cu : Ti = 1 : 3	200	Active growth of bacteria
3	Cu : Ti = 1 : 1	200	Partial growth of bacteria but no significant change compared to glass control
4	Glass Control		Active growth of bacteria

Our results revealed a significant reduction in the adhesion of mPAO1 bacterial cells to the surface with $\text{Cu}_{0.75}\text{Ti}_{0.25}\text{O}_2$ compared to the uncoated glass surface.

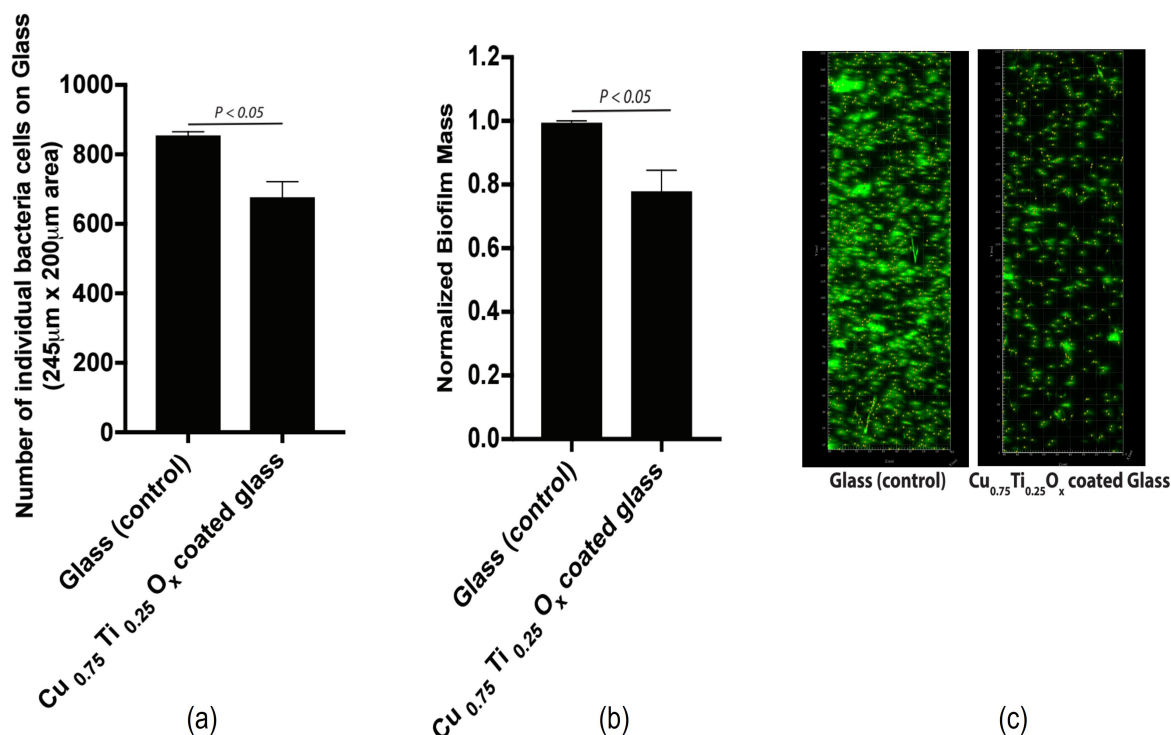


FIGURE 5.5 – $\text{Cu}_{0.75}\text{Ti}_{0.25}\text{O}_x$ -coating reduces bacterial cell initial attachment and resisted biofilm formation. (a) The bar chart shows the normalized mPAO1 biofilm biomass 24 hours post-incubation under biofilm-inducing conditions. There was larger biofilm biomass compared to $\text{Cu}_{0.75}\text{Ti}_{0.25}\text{O}_x$ -coated glass surfaces. (b) The number of planktonic mPAO1 cells that attached to uncoated and $\text{Cu}_{0.75}\text{Ti}_{0.25}\text{O}_x$ -coated glass surfaces were counted and quantified 6 hours post-incubation under biofilm-inducing conditions. The bar chart depicts the number of adhered planktonic mPAO1 bacterial cells 6 hours post incubation. There were almost 20% more bacterial cell attachments detected on the uncoated glass surface (control) compared to the $\text{Cu}_{0.75}\text{Ti}_{0.25}\text{O}_x$ -coated glass surfaces. (c) The light sheet image shows the initial attachment of fluorescence-labeled mPAO1 bacterial cells (green) on the glass surface in control and $\text{Cu}_{0.75}\text{Ti}_{0.25}\text{O}_x$ -coated glass surface. Each bacterial cell appears as a green dot on a single plane.

The light sheet image illustrates the initial accumulation of fluorescently labeled mPAO1 bacterial cells (depicted in green) on both the control and $\text{Cu}_{0.75}\text{Ti}_{0.25}\text{O}_2$ -coated glass surfaces. Each bacterial cell is visualized as a green dot on a single plane (Fig.5 (c)).

5.6 Interpretation of the results

Structural studies initially revealed that the $\text{Cu}_{0.75}\text{Ti}_{0.25}\text{O}_2$ films deposited on glass substrates by PLD are amorphous, as evidenced by their X-ray diffraction patterns. Additionally, AFM images displayed a remarkably low surface roughness of approximately 1 nm. Moreover, all the films exhibited hydrophilic properties, although the thicker ones displayed higher contact angles (81.3° for the 24 nm film compared to 60.4° for the 11 nm film). In a related study, Maltage et al. reported that biomaterials with contact angles exceeding 65° can be classified as hydrophobic, and such surfaces have the potential to inhibit cell attachment.[110] Conversely, surfaces with contact angles ranging from approximately 40° to 80° tend to exhibit adhesive properties, promoting relatively high cell and bacterial attachment.[111] This corroborates our findings, as the contact angles of the $\text{Cu}_{0.75}\text{Ti}_{0.25}\text{O}_2$ films were less than 90° , indicating their hydrophilic nature. Therefore, we can infer that the surface topography of the Cu-Ti oxide layer facilitates cell adhesion.

Our comprehensive data analysis supports the conclusion that the $\text{Cu}_{0.75}\text{Ti}_{0.25}\text{O}_2$ films possess a hydrophilic surface, making them favorable for promoting cell attachment and potentially enhancing biomedical applications.

Based on the XPS data, our analysis revealed that the films predominantly contain Cu and Ti elements. Notably, the Cu/Ti ratio increases with film thickness, indicating the migration of copper ions towards the film surface. Furthermore, the presence of both Cu^+ and Cu^{+2} ions on the surface was confirmed, with the thicker film exhibiting a slightly higher proportion of Cu^+ ions. This phenomenon could potentially enhance the penetration of copper ions through bacterial cell membranes, leading to the disruption of cellular processes and eventual cell death. The initial attachment of bacteria plays a critical role in biofilm formation as it establishes the foundation for inter-bacterial interactions and communication within the community.[112] Previous studies have attributed the toxicity of copper to the release of copper ions under wetting conditions. Our findings reinforce the significance of copper by confirming its essential presence. The interaction between copper ions on the film surface and proteins in *Pseudomonas aeruginosa* bacteria can be described as follows. One important mechanism involves the formation of copper complexes that generate radicals capable of inactivating viruses. Additionally, copper can bind to thiol and other protein groups, leading to the disruption of enzyme structure and function, similar to other transition metals. Copper ions can also chelate with proteins by binding

to amino and carboxyl groups, resulting in protein inactivation. Thus, our study highlights the presence and role of copper ions in the films. Their ability to interact with proteins in *Pseudomonas aeruginosa* bacteria through complex formation, radical generation, and protein binding contributes to the disruption of bacterial processes, emphasizing their potential as antimicrobial agents.

Furthermore, the antimicrobial activity of copper is closely linked to its interaction with DNA. Copper ions, specifically Cu^{+2} , possess the capability to form chelates with phosphate groups, resulting in the disruption of hydrogen bonds within DNA and subsequent microbial death. Copper ions exhibit a distinct affinity for DNA, enabling them to bind and disturb the helical structure of DNA and integrate within and between DNA strands. Moreover, copper can form complexes with mRNA, contributing to the degradation of viruses. This multifaceted interaction of copper with genetic material underscores its potent antimicrobial properties.[113, 114]

Copper's antimicrobial effects are not limited to nucleic acids; they also extend to lipids. In the presence of copper, lipids can undergo peroxidation, leading to the formation of gaps in the cell membrane and consequent disruption of cellular integrity. XPS analysis confirmed the presence of Cu^+ ions on the surface, which exhibited higher cytotoxicity against bacteria compared to Cu^{+2} ions. The combination of Cu^+ ions and OH^- ions (active oxygen) effectively destroyed microbial membranes and DNA by interacting with proteins that contain -CH and -SH groups. This interaction resulted in the disruption of microbial cellular components, further emphasizing copper's antimicrobial properties.

In addition, adding Ti to a thin coating improves adherence with implant-use TiAlV alloy. The thin film and TiAlV alloy are compatible and chemically affine due to their titanium-based chemical compositions. Titanium naturally creates oxide layers, improving its adherence. The thin film's titanium oxide layers interact with the TiAlV alloy's titanium oxide layer to promote adhesion and bonding. Titanium aids interface atomic interdiffusion. Titanium atoms travel between the thin film and alloy, forming intermetallic compounds and strengthening their link. Titanium in the thin coating enhances surface roughness, which increases contact points and surface area, improving mechanical interlocking with the TiAlV alloy.

Furthermore, our light sheet microscope imaging setup is well-suited for studying the initial attachment and behavior of bacterial cells on various surfaces, including walls and tilted surfaces.[60] In line with this, using the light sheet microscope, we demonstrated

a reduction in the initial attachment of mPAO1 bacterial cells on $\text{Cu}_{0.75}\text{Ti}_{0.25}\text{O}_2$ -coated glass surfaces compared to uncoated control surfaces. These findings align with previous reports highlighting the antimicrobial activities of copper-plated surfaces.[115] We observed similar antimicrobial activity of the $\text{Cu}_{0.75}\text{Ti}_{0.25}\text{O}_2$ coating in preventing initial biofilm formation on vertical surfaces. Ongoing efforts are focused on improving the performance of copper coatings through modifications in compound compositions, as reported in previous studies.[115, 113] These observations further support the crucial role of copper ions in exerting toxicity against bacteria.[116]

5.7 Conclusion

In this study, we investigated the growth of *Pseudomonas aeruginosa* bacteria on thin Cu-Ti films deposited on glass coverslips. Our findings shed light on the interaction between bacterial cells and the Cu-Ti films, providing valuable insights into their antimicrobial properties. The deposited films exhibited a hydrophilic and smooth surface, which are favorable characteristics for bacterial cell attachment. XPS analyses confirmed the presence of active Cu^+ and Cu^{2+} ions on the film surface. These ions were found to penetrate the bacterial cells, leading to the destruction of their DNA and RNA, effectively inhibiting bacterial growth.[117]

By utilizing our light sheet microscope imaging setup, we observed a remarkable 20% reduction in bacterial growth on the $\text{Cu}_{0.75}\text{Ti}_{0.25}\text{O}_2$ coated surfaces compared to uncoated surfaces, as demonstrated by the crystal violet test. This provides evidence that the $\text{Cu}_{0.75}\text{Ti}_{0.25}\text{O}_2$ surfaces exhibit resistance to biofilm formation. We attribute this reduction in biofilm formation to the inhibition of the initial attachment of individual mPAO1 bacterial cells, consistent with previous reports on the antimicrobial activities of copper-plated surfaces.

While our experimental conditions may not fully replicate real-life scenarios, we believe that these findings have significant implications for various applications, particularly in the healthcare industry and in the prevention of surgical implant-related infections. Biofilm formation poses a substantial risk, and our study contributes to the understanding of strategies to mitigate this risk.

Finally, our study provides valuable insights into the antimicrobial properties of Cu-Ti films and their impact on bacterial growth and biofilm formation. These results hold pro-

mise for the development of effective approaches to combat bacterial infections, benefiting diverse fields where biofilm-related risks are a concern, such as healthcare and surgical implant applications.

Cancer Cells Growth On Binary Metal Oxide Thin Films

After conducting extensive research on stem cells and bacterial growth on metal oxides, our focus shifted to investigating the cytotoxicity of various metal oxides. Specifically, we examined the effects of ZnO, Al₂O₃, CuO_x, VO_x, and TiO₂ on cancer cells derived from the chondrosarcoma cell line (SW1353) and the ovarian carcinoma (SKOV3) cell line. In this chapter, our focus was on the adhesion and proliferation of cancer cells in relation to thin films made of metal oxides. We aimed to understand why certain metal thin films exhibit toxicity while others are biocompatible. Cell culture and toxicity assessment was done by Dr. Laurent Poulain and Dr. Emilie Brotin with the help of Mr. A. Lebrun in the Comprehensive Cancer Centre F. Baclesse lab at the University of Caen, Normandie with the help of Dr. Maria Khokhlova.

6.1 Introduction

The growing interest in binary oxide thin films has led to their exploration in many medical applications, with particular emphasis on Copper oxide (CuO_x), Titanium dioxide (TiO₂), Aluminum oxide (Al₂O₃), and Vanadium oxide (VO_x) owing to their unique characteristics. These thin films have attracted considerable interest in the areas of wound healing, antimicrobial coatings, and biosensors.[118] In their study, Wang et al. (2019) utilized pulsed laser deposition (PLD) to create a CuO_x thin film. This film demonstrated

the ability to improve cell proliferation and collagen synthesis, which are important factors in the process of wound healing. Li et al. (2018) found that a TiO_2 thin film, created by PLD, facilitated the movement and growth of fibroblasts, hence aiding in the process of wound healing.[119]

Simultaneously, researchers have intensively investigated binary oxide thin films in the field of cancer research, where they have proven to be useful in examining the proliferation of human cancer cells. Due to their inherent biocompatibility, they are very suitable for conducting experiments on cancer cells in a controlled environment, providing a distinct opportunity to study the proliferation, programmed cell death, and transportation of drugs in cancer cells.[120] Moreover, these thin films exhibit unique optical and electrical characteristics that make them extremely pertinent to several aspects of cancer research. For example, studies have demonstrated that ZnO thin films can hinder the growth of cancer cells and trigger programmed cell death (apoptosis) in human cancer cells like HeLa and MCF-7.[121, 122] On the other hand, TiO_2 thin films have been found to enhance the growth of cancer cells and prevent programmed cell death (apoptosis) in human cancer cells such as A549 and HCT-116.[123]

Expanding on these scientific principles, Guangman et al. discovered a fascinating phenomenon in their research. It was noted that two breast cancer cell lines with aggressive behavior showed faster growth and more dissemination when exposed to a flat layer of graphene oxide. This event was accompanied by negligible cytotoxicity. The synergistic interaction between the high loading capacity of Graphene Oxide, conformational changes in cellular proteins upon contact with this material, and the abundant presence of oxygenated functional groups in the Graphene Oxide structure were identified as the underlying mechanisms.[124]

Huang et al. successfully synthesized a transparent monolayer thin film consisting of hollow nanospheres constituted of MnO_2 in a separate experiment. This novel substance was carefully engineered to serve as a platform for the effective gathering and subsequent discharge of cancer cells. After capturing, a meticulous purification procedure was carried out, involving the frequent substitution of the cell culture medium, which resulted in the elimination of leukocytes and dead cancer cells. The rigorous process resulted in cancer cell populations that had exceptional levels of purity, reaching as high as 98%, and outstanding vitality, reaching 90%. Moreover, the MnO_2 -based thin film's exceptional transparency is a crucial characteristic that allows for direct observation of the growth patterns of released

circulating tumor cells. This makes it an ideal window for furthering cancer therapy and research, with significant potential.[125]

Cancer cells, known for their exceptional ability to adapt, exhibit different behaviors depending on the individual matrices they are cultivated on, including natural substrates or synthetic materials such as plastic, glass, fibronectin (FN), vitronectin (VN), or collagen (coll). The matrix environments have a crucial impact in regulating the behavior of cancer cells, affecting important parameters such as cell growth, movement, and reactions to treatment drugs. The diverse behaviors arise from differences in the mechanical, biological, and topographical characteristics of the matrices.[126, 127]

In addition, modern cancer research has initiated the investigation of cancer cells producing their own extracellular matrix (ECM)-like structures, which is a unique method to facilitate their growth and development. The velocity and effectiveness of this matrix formation are intricately affected by the nature of the surrounding medium. The medium contains chemical and physical signals that can control the secretion and arrangement of matrix components by cancer cells. This process influences the structure and characteristics of the matrix that is produced by the cells themselves. Understanding the complexities of the interactions between cancer cells and their matrix environments is of utmost significance, as it enhances our understanding of cancer biology and facilitates the creation of more effective therapeutic options.[128, 129]

Within this particular framework, the act of applying a layer of non-reactive materials onto supportive substances becomes a crucial approach with the objective of augmenting the attachment, growth, and diverse capabilities of cells. This strategic approach is based on the understanding that cells interact with their surroundings through a variety of surface receptors, which attach to specific molecules inside the extracellular matrix (ECM). The extracellular matrix (ECM) serves as both a structural support and a provider of regulatory signals that control cell behavior.

When there is a lack of natural extracellular matrix (ECM), using inert supports such as plastic culture dishes may not effectively support cell adhesion and growth. Applying ECM-mimicking materials to these inactive substrates is crucial, as it offers a range of attachment sites and signals that enhance cell adherence and activity. A wide range of materials, such as collagen, laminin, fibronectin, polylysine, polyornithine, and hydrogels made from cross-linked polymer chains, are used to efficiently mimic the natural extracellular matrix.[130]

This coating technique not only expands the advantages to other cell types, including those that are difficult to culture and primary cultures but also shows significant potential in growing tumor cells. Tumor cells frequently display modified cell surface receptors and extracellular matrix (ECM) interactions, making their culture a challenging task. Applying materials on inactive supports that have the ability to offer the necessary binding sites for tumor cells can greatly improve cell adhesion, growth, and overall performance.

An example of this is the research conducted by Bernhardt et al. (2008), which demonstrates the advantages of applying collagen to plastic culture dishes while creating primary cell lines from bovine ocular malignancies. The application of a collagen coating significantly enhanced the process of cell adhesion and proliferation, leading to the creation of cell lines that are more stable and easier to handle when compared to those grown on substrates without any coating. This method is an important tool in the field of cell culture, especially for achieving excellent results, particularly when working with tumor cells that have unique extracellular matrix (ECM) connections.[131]

The proposed study is to examine the process of creating, describing, and understanding the development of human cancer cells, specifically SW1353 generated from human chondrosarcoma and SKOV3 from human serous ovarian adenocarcinoma. This will be done by cultivating these cells on binary oxide thin films that have been deposited on glass substrates. The binary oxide thin films of interest, namely Al_2O_3 , TiO_2 , ZnO , and CuO_x , are synthesized using the pulsed laser deposition (PLD) technique.

The PLD technology was selected for its ability to generate high-quality thin films, providing fine manipulation of their structural and optical characteristics. The characteristics of PLD make it a perfect technique for the formation of binary oxide layers. The study will investigate the cellular activity of cancer cells on various supports, including an analysis of their morphological properties, adhesion, proliferation, and other pertinent factors. The main emphasis is on performing a thorough kinetic study to clarify the mechanisms by which cells interact with these substrates over a period of time.

The observations will be methodically compared to the outcomes obtained from cells cultivated on plastic (polyethylene terephthalate or PET), a widely used benchmark material for these cell lines, and on glass, which serves as a standard reference material in cell culture operations. The objective is to identify and highlight the significant differences in cellular behavior observed when cancer cells are cultivated on binary oxide thin films as opposed to the established reference materials. This will provide insights into the potential

implications and applications of these findings in the field of cancer research.

6.2 Experimental techniques

6.2.1 Films preparation and characterization

Binary oxide thin films of ZnO, Al₂O₃, CuO_x, VO_x, and TiO₂ were deposited on glass substrates using pulsed laser deposition (PLD) technique.[132] A series of thin films with various thicknesses were deposited on a glass substrate (12 mm diameter) using PLD. Before introduction in the growth chamber, the glass was cleaned ultrasonically with ethanol, then rinsed in deionized water, and finally dried with compressed air. The targets (ZnO, Al₂O₃, VO_x, CuO_x, TiO₂) were prepared using a standard solid-state process. Briefly, the respective powders for the target were ground to the desired stoichiometry and heated several times at 800 °C. The final product was pressed and sintered at 1100 °C for 24 hours.

To produce the film, a KrF excimer laser ($\lambda = 248$ nm, 3 Hz) is scanned over the target at a fluence of 2.45 J/cm². During the deposition, the substrate is placed at 4.5 cm from the target and maintained at 300 °C under a base average pressure of 1.1×10^{-7} bar.

The structural quality of the films is characterized by X-ray reflectometry (XRR) using a Bruker D8 Discover diffractometer (CuK α_1 $\lambda = 1.5405$ Å) in the $2\theta = 0^\circ$ - 5° range. Thickness is obtained from the relative position of oscillation maxima versus the square of their order number as described in Chapter 3.

Culture of SW1353" and SKOV3 cancer cells

The chondrosarcoma cell line SW1353 (ATCC[®] HTB-94) was grown in high glucose-Dulbecco's modified Eagle's medium (HG-DMEM, Biowest, Nuaille, France) supplemented with 10

The ovarian carcinoma SKOV3 cell line was purchased from ATCC. SKOV3 cells were grown in RPMI 1640 medium supplemented with 2 mmol/L Glutamax, 10% FCS, 20 mmol/L HEPES, and 33 mmol/L sodium bicarbonate (Gibco). All cell lines were maintained in a 5% CO₂ humidified atmosphere at 37°C. Cancer cell lines were certified Mycoplasma-free on a regular basis (MycoAlert Mycoplasma Detection Kit, Lonza).

6.2.2 Real-time cell imaging of cell morphology

The IncuCyte S3 system (Sartorius) is an automated imaging platform providing real-time images and quantitative data generated throughout the proliferation process. 2.10^4 SKOV3 cells or SW1353 cells were seeded per well in 24-well plates on glass slides coated with thin films of oxides. Cells were placed into the device maintained in a 5% CO₂ humidified atmosphere at 37°C. Cells were monitored in the IncuCyte, acquiring images every hour for 90 hours in 16 separate regions per well (objective $\times 10$). The live-cell phase contrast images were used to calculate confluence using the IncuCyte software.

6.2.3 Cell death and real-time quantification

2.10^4 SKOV3 cells were seeded per well in 24-well plates on glass slides coated with thin films of oxides. The CellTox™ Green Cytotoxicity Assay reagent (Promega) was added, and baseline images were taken using a 10x objective. Cells were monitored using an IncuCyte® S3 (Sartorius). The plate was scanned, and fluorescent and phase-contrast images were acquired in real time every 1 hour from 2 separate regions per well. The CellTox™ Green reagent labels dead cells, yielding green fluorescence. The live-cell phase contrast images were used to calculate confluence using the IncuCyte® software and to provide morphology information. The accumulation of CellTox™ Green over time was normalized to the confluence of cells.

6.2.4 Nuclei counting after staining by DAPI

2.10^4 SW1353 cells were seeded per well in 24-well plates on glass slides coated with thin films of oxides. Cells were placed into the incubator maintained in a 5% CO₂ humidified atmosphere at 37°C for 90 hours. All samples were fixed in 70% ethanol, then incubated with 1 μ g/ml DAPI solution (Roche), washed in water, and stored at 4°C. The plate was scanned, and fluorescent images were acquired using the Zeiss Cell Discoverer 7 imaging system (Zeiss, Jena, Germany). The images and the number of nuclei were generated using Zeiss Zen 3.3 software.

6.3 Results and discussion

6.3.1 Structure and surface topography of thin films

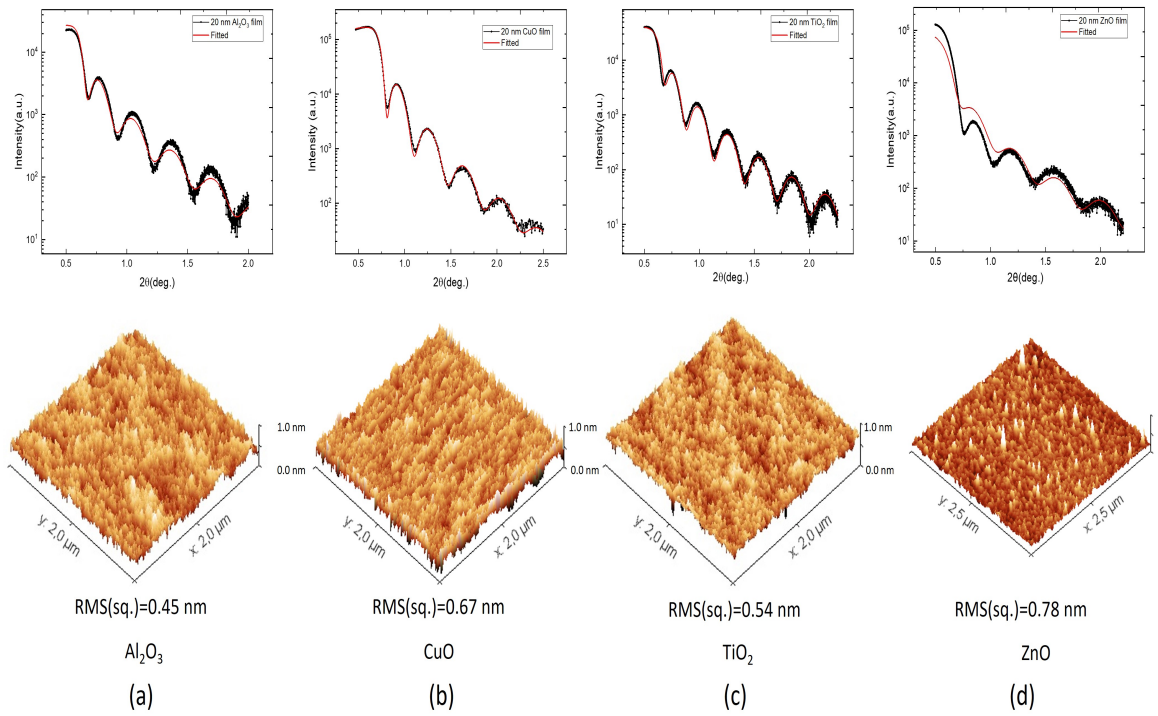


FIGURE 6.1 – Typical XRR curves and $2\mu\text{m} \times 2\mu\text{m}$ AFM image of 20 nm of Al_2O_3 (a), CuO_x (b), TiO_2 (c), and ZnO (d) thin films. XRR recorded from 0 to 2.5, including experimental (black) and fitted (red) curves.

The surface of the deposited Al_2O_3 , CuO_x , TiO_2 , and VO_x films was characterized by XRR, AFM, and contact angle techniques. The film thickness was determined by XRR and fitted using GenX2.4.10 software and was 20 nm (see Fig. 2, red curve : fitted data and black curve : experimental data). In addition, the surface roughness was recorded by AFM technique and determined to be 0.45 nm, 0.67 nm, 0.54 nm, and 0.38 nm for Al_2O_3 , CuO_x , TiO_2 , and VO_x RMS (squared), respectively (see Fig. 6.1). The surfaces imaged by AFM have uniform coverage, a yellow transparent color, and are free of pinhole defects. The surfaces imaged by AFM have uniform coverage, a yellow transparent color, and are free of pinhole defects. All layers are amorphous (see Appendix 1), and all recorded roughness was below 1 nm, confirming a smooth surface.

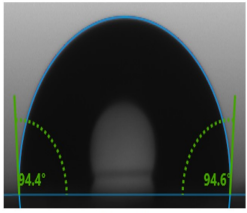
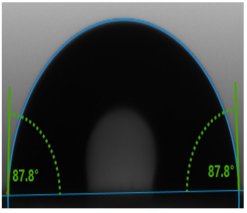
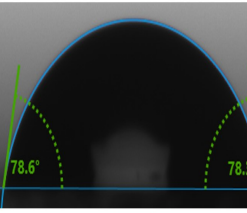
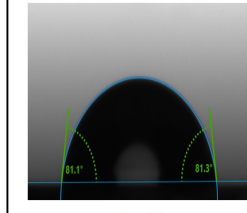
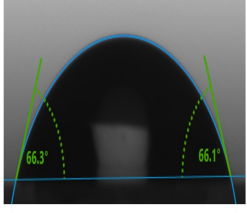
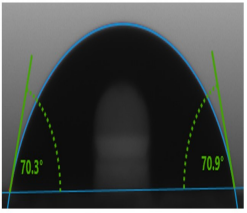
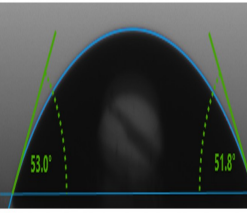
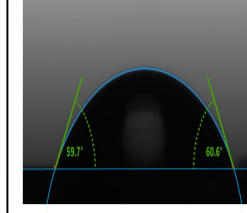
Testing liquid	Al_2O_3	CuO	TiO_2	ZnO
Water	 94.5°	 87.09°	 78.44°	 81.2°
Ethylene Glycol	 66.2°	 70.60°	 52.39°	 60.1°

FIGURE 6.2 – Systematic plot of the contact angle with water and ethylene glycol as the test liquids.

Figure 6.2 displays the systematic plot of the contact angle when testing with water and ethylene glycol as the liquids. The contact angle measurements for Al_2O_3 , CuO_x , TiO_2 , and ZnO with water are 94.5° , 87.09° , 78.4° , and 81.2° , respectively. Similarly, the contact angle measurements for the same materials with ethylene glycol are 66.2° , 70.60° , 52.39° , and 60.1° , respectively.

Amorphous thin films generally have a higher surface energy compared to crystalline thin films of the same material due to the lack of ordered structures at the surface. This can lead to a higher contact angle and reduced wetting of the surface. However, the exact effect of amorphousness on the contact angle of these materials can depend on various factors, such as surface roughness, chemical composition, and preparation method.^[133]

6.3.2 Cell proliferation and cell death on oxide films

The usual cell culture support is PET, which shows surface properties convenient for cell adhesion and spreading. PET thus constituted our reference. Glass slices were used for oxide film deposition. The cells' behavior (adhesion, spreading, proliferation, cell death) on various surfaces was compared to these two references, i.e., PET and glass slices. We first analyzed the confluence of ovarian SKOV3 cancer cells on these supports (Figures

6.3 and 6.4) and observed similar growth curves on PET, Glass, TiO₂, and Al₂O₃. In contrast, CuO_{xx} reduces cell confluence over time, and zinc even more so.

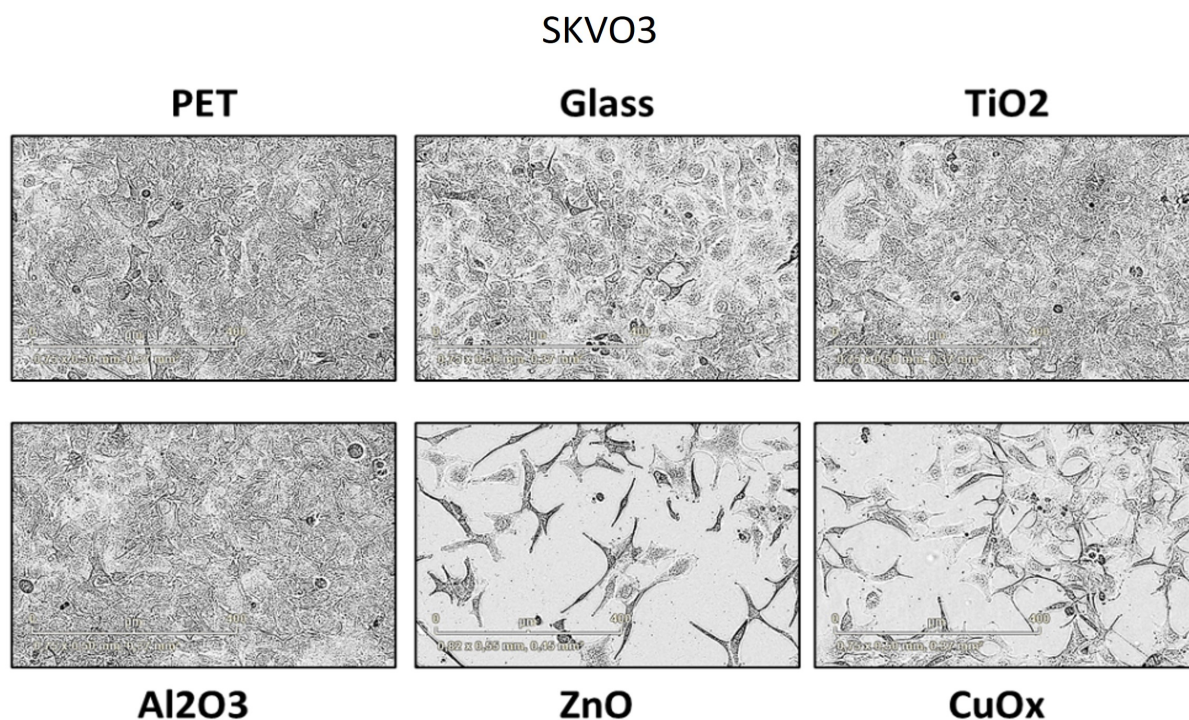


FIGURE 6.3 – SKVO3 cells growth on PET, Glass, TiO₂, Al₂O₃, ZnO and CuO_{xx}.

We then observed cell morphologies and identified major changes depending on the culture support. Whereas TiO₂ and Al₂O₃ showed similar cell morphologies as compared to PET, the cells grown on glass appeared less numerous and more spread out, suggesting that both TiO₂ and Al₂O₃ constitute advantageous surfaces for the growth of these ovarian cancer cells. More drastic changes were observed on ZnO and CuO_x. Cells grown on these oxides were much less numerous and less spread out than on other supports and showed more elongated morphologies (fibroblast-like morphologies). Moreover, the monitoring of cell death occurring through the quantification of CellTox Green positive cells (cell death probe) showed that after 48h, cells cultured on ZnO are mainly positive and showed altered morphology (cell shrinkage and blebbing highly evocative of apoptotic cell death), whereas cells cultured on PET, glass or CuO_x did not. Proliferation slowdown is also confirmed by the counting of the cell nuclei, which showed a decreased number of cells in glass, ZnO, and CuO_x culture conditions (Figure 6.5(B)). Of note, no apoptotic cell death was observed in these conditions, suggesting that these supports do not favor cell proliferation but are not cytotoxic.

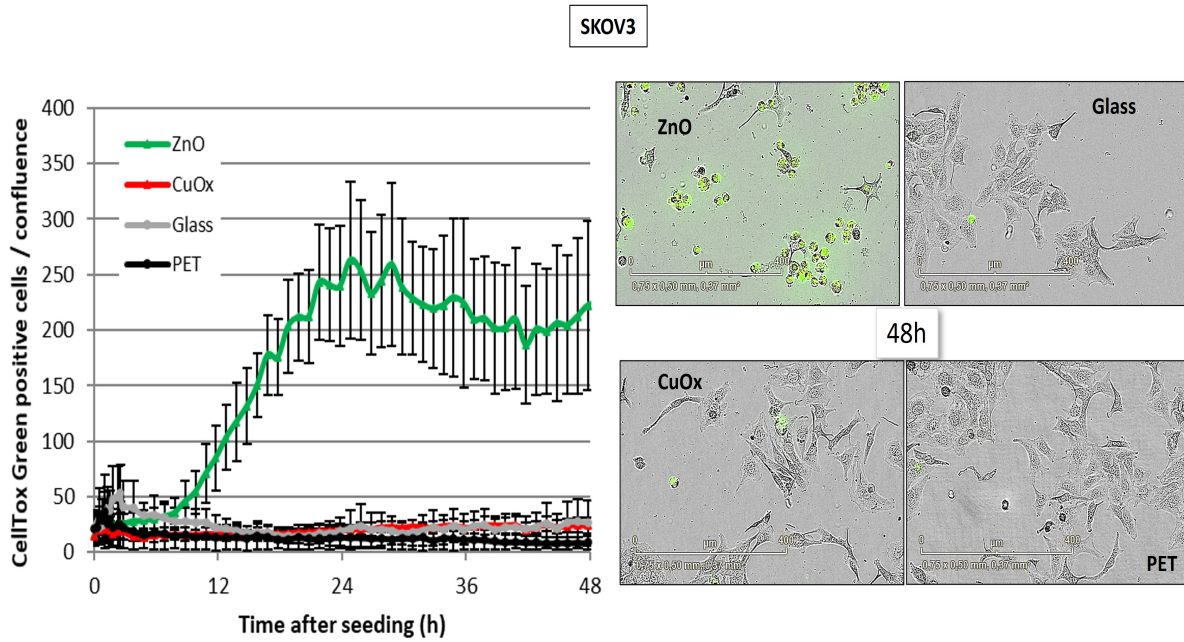


FIGURE 6.4 – Temporal Assessment of SKOV3 Cell Confluence Post-Seeding and After 48 Hours. The Presence of Green Dots on ZnO and CuO_x Indicates Cell Death Relative to Reference Conditions.

We performed similar experiments on another cancer cell line, the SW1353 cell line derived from chondrosarcoma, and observed very similar results. The cell culture on PET, TiO₂, and Al₂O₃ led to strong proliferation and spreading, whereas the culture on glass, ZnO, and CuO_x seemed to induce a decrease in both cell proliferation and spreading (Figures 6.5 and 6.6).

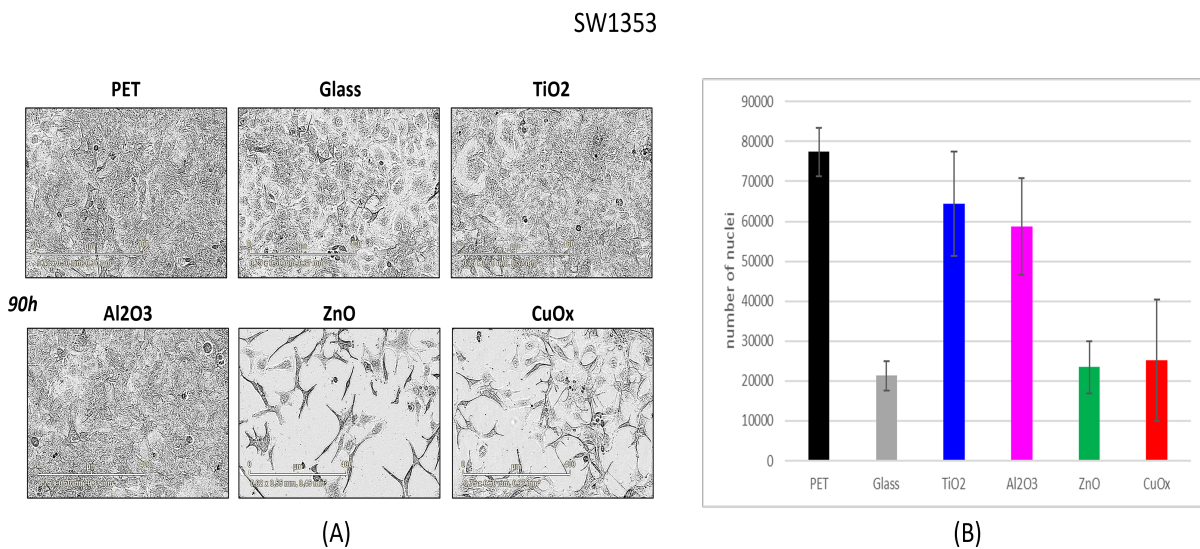


FIGURE 6.5 – SW1353 Cell proliferation and nuclei count on metal oxide thin films after 90 hrs.

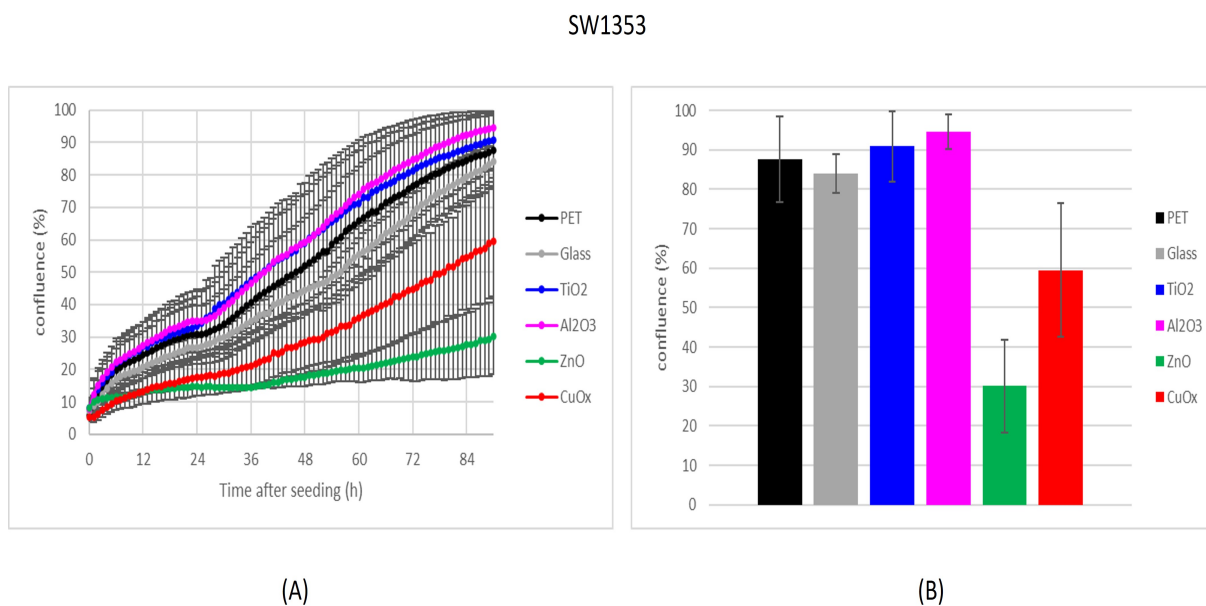


FIGURE 6.6 – Cell Confluence (%) of SW1353 Cells Over Time Since Seeding.

We then observed the adhesion kinetics of SKOV3 and SW1353 cells on the various supports and measured the confluence level after 0, 6, and 24h. In both cell lines, a marked decrease in adhesion and spreading processes was observed when cells were cultivated on CuO_x, and to a lesser extent, on ZnO, as compared to other support (Figure 6.7 and 6.8)

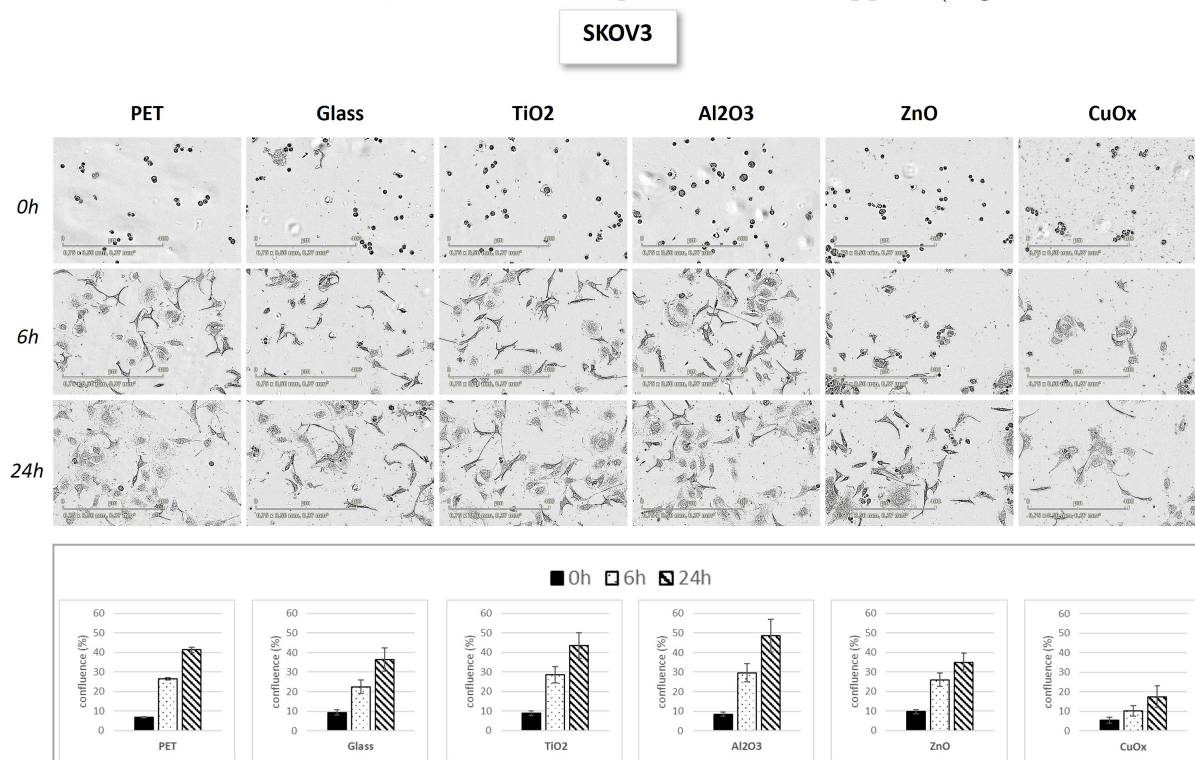


FIGURE 6.7 – Kinetics of SKOV3 cells on different metal oxides, plastic and glass coverslips.

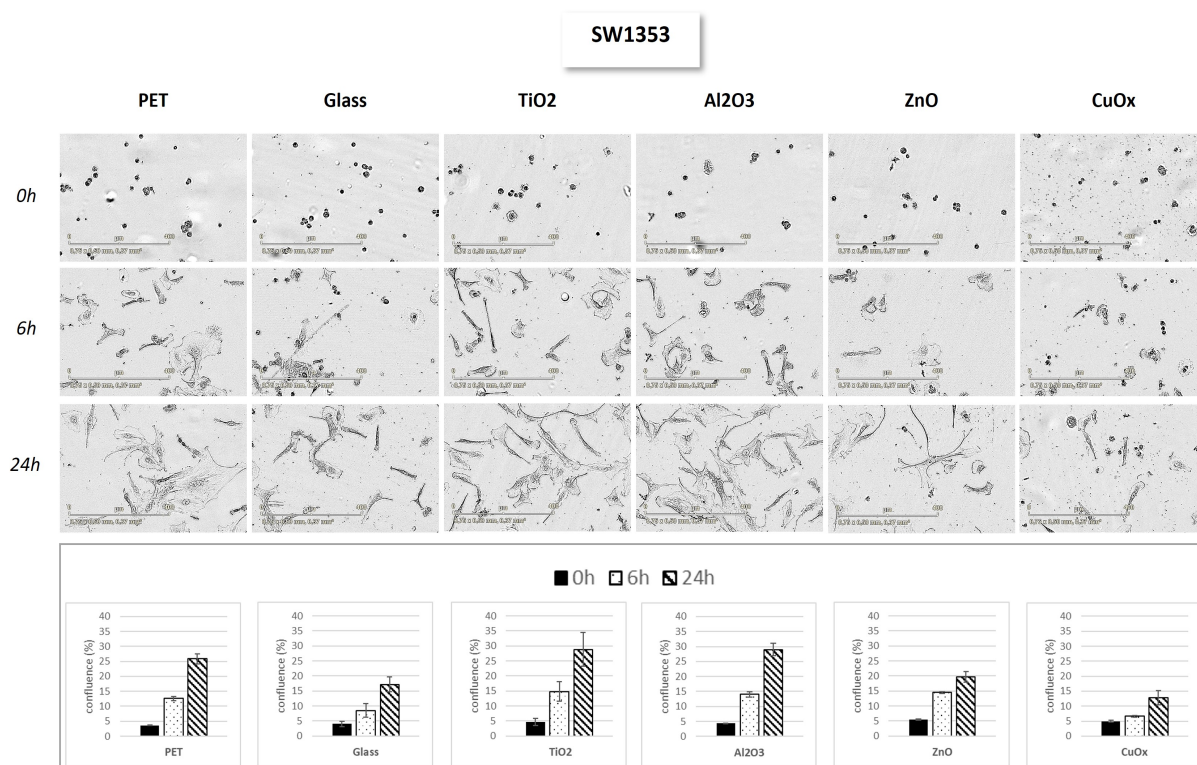


FIGURE 6.8 – Kinetics of SW1353 cells on different metal oxides, plastic and glass coverslips.

6.4 Discussion

Cell behavior is profoundly influenced by interactions with extracellular matrix (ECM) proteins, such as collagens, vitronectin, or fibronectin. ECM facilitates adhesion, spreading, and proliferation through membrane receptors, notably integrins, and subsequent activation of cell signaling pathways. Cell culture supports coated with matrix proteins are often required for certain cell types, such as neurons or primary cells, challenging to cultivate on conventional PET substrates. Commercially available solutions address this need. Notably, cells cultured on glass may require an extended duration to attain typical growth levels and reach confluence, with reports suggesting that ovarian cancer cells synthesize their matrix for adhesion and spreading on glass. This study aimed to elucidate how various binary metal oxide thin films deposited on glass slices influence cell behavior. Our findings reveal that TiO₂ and Al₂O₃ facilitate favorable adhesion, spreading, and proliferation on glass, comparable to or slightly exceeding observations on standard PET support.

The factors contributing to the facilitation of favorable adhesion, spreading, and pro-

liferation of cancer cells by TiO_2 and Al_2O_3 can be outlined as follows :

1. The surface topography of TiO_2 and Al_2O_3 thin films has a greater resemblance to the surface topography of extracellular matrix (ECM) proteins when compared to the surface topography of glass. The observed similarities between cancer cells may potentially offer additional anchoring locations and cues for adhesion and dissemination.
2. The hydrophilicity of TiO_2 and Al_2O_3 thin films' surface chemistry surpasses that of glass. The hydrophilic nature of the material may enhance the creation of a water layer at the boundary between the film and the cells, hence potentially facilitating the process of cell attachment and spreading.
3. The surface charge of titanium dioxide (TiO_2) and aluminum oxide (Al_2O_3) thin films exhibits a higher positive polarity compared to that of glass. The presence of a positive charge has the potential to create an attractive force towards negatively charged cell membranes, hence facilitating the process of cell adhesion.

Furthermore, it is plausible that thin films of TiO_2 and Al_2O_3 may release ions or other compounds that exhibit a favorable impact on the behavior of cancer cells. One example is titanium dioxide (TiO_2), which has been seen to generate reactive oxygen species (ROS) through photogeneration, potentially leading to the stimulation of cell proliferation. Moreover, it has been demonstrated that Al_2O_3 has anti-inflammatory characteristics, hence potentially influencing cancer cell behavior beneficially.[\[134\]](#)

The results showed that ZnO and CuO_x had a significantly different effect on cell behavior than TiO_2 and Al_2O_3 . Cells grown on ZnO and CuO_x were much less numerous, less spread out, and showed more elongated morphologies (fibroblast-like morphologies) than cells grown on TiO_2 or Al_2O_3 . The number of cells in glass, ZnO , and CuO_x culture conditions was also decreased.

The neutral influence of ZnO on cell behavior can be attributed to its surface features, which are characterized by a comparatively inert nature. The surface topography of ZnO is rougher compared to TiO_2 or Al_2O_3 , but it does not exhibit such a high level of roughness that would entirely impede cell attachment. Moreover, the surface chemistry of ZnO exhibits hydrophobic characteristics for a bio-molecule, although not to the extent of full water molecule repulsion. The surface charge of ZnO is characterized by negative polarity, however not to an extent that would result in full repulsion of negatively charged cell membranes.

In contrast, CuO_x exhibits surface characteristics that are more deleterious to cellular well-being. The surface chemistry of CuO_x leads to the production of reactive oxygen species (ROS), which have the potential to cause cellular damage. Moreover, it has been demonstrated that thin films composed of CuO_x exhibit the capability to discharge copper ions, which possess cytotoxic properties. The observed phenomenon of cell death induced by CuO_x might be attributed to a combination of variables, which are likely to be responsible for this effect, especially in the context of the SKOV3 ovarian cancer cell line.

Conclusions and Perspectives

7.1 Conclusion

In conclusion, this study delves into the application of thin films composed of various metal oxides, specifically VO_x , CuTiO , Al_2O_3 , ZnO , and TiO_2 , as substrates for cultivating human cells, including bone marrow-derived mesenchymal stem cells (hBM-MSCs), cancer cells, and bacterial cells. The selection of oxide thin films as substrates is rooted in their ability to influence biocompatibility, enhance mechanical properties, and potentially serve as inhibitors to mitigate the release of detrimental ions.

The oxide thin films, fabricated using Pulsed Laser Deposition (PLD), exhibited an exceptionally low surface roughness of less than 1 nm. Additionally, wettability assessments revealed hydrophilic characteristics, ensuring suitability for cell adhesion and allowing an isolated examination of surface chemistry's impact.

The investigation focused on the interaction between human bone marrow-derived mesenchymal stem cells (hBM-MSCs) and vanadium oxide (VO_x) thin films. Significantly, VO_x films deposited at different temperatures had advantageous adhesion and proliferation characteristics. More precisely, the film created at a temperature of 400°C exhibited better adhesion when compared to the substrates used as a reference. Although the VO_x films had no impact on the adhesion and proliferation of hBM-MSCs, they strongly promoted chondrogenesis differentiation.

Moreover, the knowledge obtained from this research can be extended to improve our comprehension of the interactions between cells and materials, specifically in relation to the titanium-aluminum-vanadium (TiALV) alloy, which is frequently utilized in transplants. By utilizing the information gained by studying the interaction between hBMMSCs and VO_x , we can enhance the quality of materials used in biomedical applications. This has the potential to enhance the effectiveness and compatibility of implants in clinical environments.

Subsequently, attention shifted to antibacterial characteristics, particularly $\text{Cu}_{0.75}\text{Ti}_{0.25}\text{O}_2$ thin films. These films exhibited hydrophilic, smooth surfaces with active Cu^+ and Cu^{2+} ions, effectively impeding bacterial proliferation. Light sheet microscopy revealed a 20% reduction in bacterial proliferation on $\text{Cu}_{0.75}\text{Ti}_{0.25}\text{O}_2$ surfaces, indicating a notable ability to prevent biofilm formation. Furthermore, the knowledge acquired from the antibacterial properties of $\text{Cu}_{0.75}\text{Ti}_{0.25}\text{O}_2$ thin films has wider applications in the realm of biomedical materials. This knowledge can be utilized to further our comprehension of addressing bacterial infections on implants. Through the exploration of the antibacterial properties exhibited by the $\text{Cu}_{0.75}\text{Ti}_{0.25}\text{O}_2$ thin films, we can potentially aid in the advancement of implant surfaces that are highly resistant to bacterial colonization. This, in turn, has the potential to significantly decrease the likelihood of infections linked to implantable medical devices.

Expanding the scope, the study explored the effects of additional metal oxides on cancer cells, focusing on SW1353 and SKOV3 cells. TiO_2 and Al_2O_3 thin films promoted favorable adhesion, spreading, and proliferation, comparable to or surpassing normal PET support. In contrast, CuO_x and ZnO demonstrated limitations, with CuO_x and ZnO leading to cell death in some instances.

In summary, this research offers valuable insights into the complex relationship between oxide thin films and various cell types. The findings highlight the importance of surface chemistry and material characteristics in shaping cellular behavior, with potential applications in biomedicine, orthopedic prosthesis design, and cancer cell research. The rigorous approach utilized in this study makes a valuable contribution to the current understanding of how oxide thin films affect cellular responses.

7.2 Future perspective

The extensive investigation of the interactions between different metal oxide thin films and a range of cellular entities, including stem cells, bacteria, and cancer cells, reveals numerous exciting possibilities for future interdisciplinary research. One potential path involves incorporating the gained knowledge into the improvement and advancement of biomedical materials, specifically surfaces designed for medical devices like prostheses and orthopedic implants. The main objective is to enhance the compatibility with living organisms and reduce the chances of infection. Furthermore, the utilization of metal oxide thin films in the coatings of medical devices shows great potential for improving operational capabilities.

Surface engineering plays a crucial role in the development of medical devices, making it a key area of focus for harnessing this expertise. The deliberate alteration of surface properties to enhance performance, functionality, and biocompatibility in medical devices, such as orthopedic implants and prosthetics, is a practical application. It is crucial to thoroughly investigate different methods of incorporating metal oxide thin films into medical device coatings to enhance their performance.

Additional areas of investigation can be found in the field of antimicrobial strategies. Further investigation into the antibacterial properties of metal oxide thin films has the potential to enhance their effectiveness in fighting against different types of bacteria. The exploration of these films' potential in developing antimicrobial surfaces for healthcare environments, laboratories, and public spaces is a crucial area for practical impact.

Considering the field of cancer therapeutics and diagnostics, it is necessary to further explore the complex interactions between cancer cells and various metal oxide thin films. This investigation seeks to discover substances that possess specific anti-cancer properties and evaluate their potential for use in drug delivery systems or as coatings for cancer diagnostic devices.

The use of these scientific findings in clinical settings represents yet another intriguing path of investigation. This involves the creation of customized surfaces for individualized treatments or coatings for implants, highlighting the significant potential in the field of personalized medicine. In addition, it is crucial to conduct a comprehensive evaluation of the ecological consequences of metal oxide thin films in medical devices throughout their entire lifecycle. This includes the incorporation of environmental impact studies to

fully understand the implications. It is crucial to foster interdisciplinary collaborations among materials scientists, biologists, clinicians, and engineers in order to address the intricate challenges involved in the development and application of these groundbreaking materials. By bringing together knowledge from various disciplines, there is great potential for significant progress in both the theoretical and practical aspects of this rapidly growing field.

Appendix 1

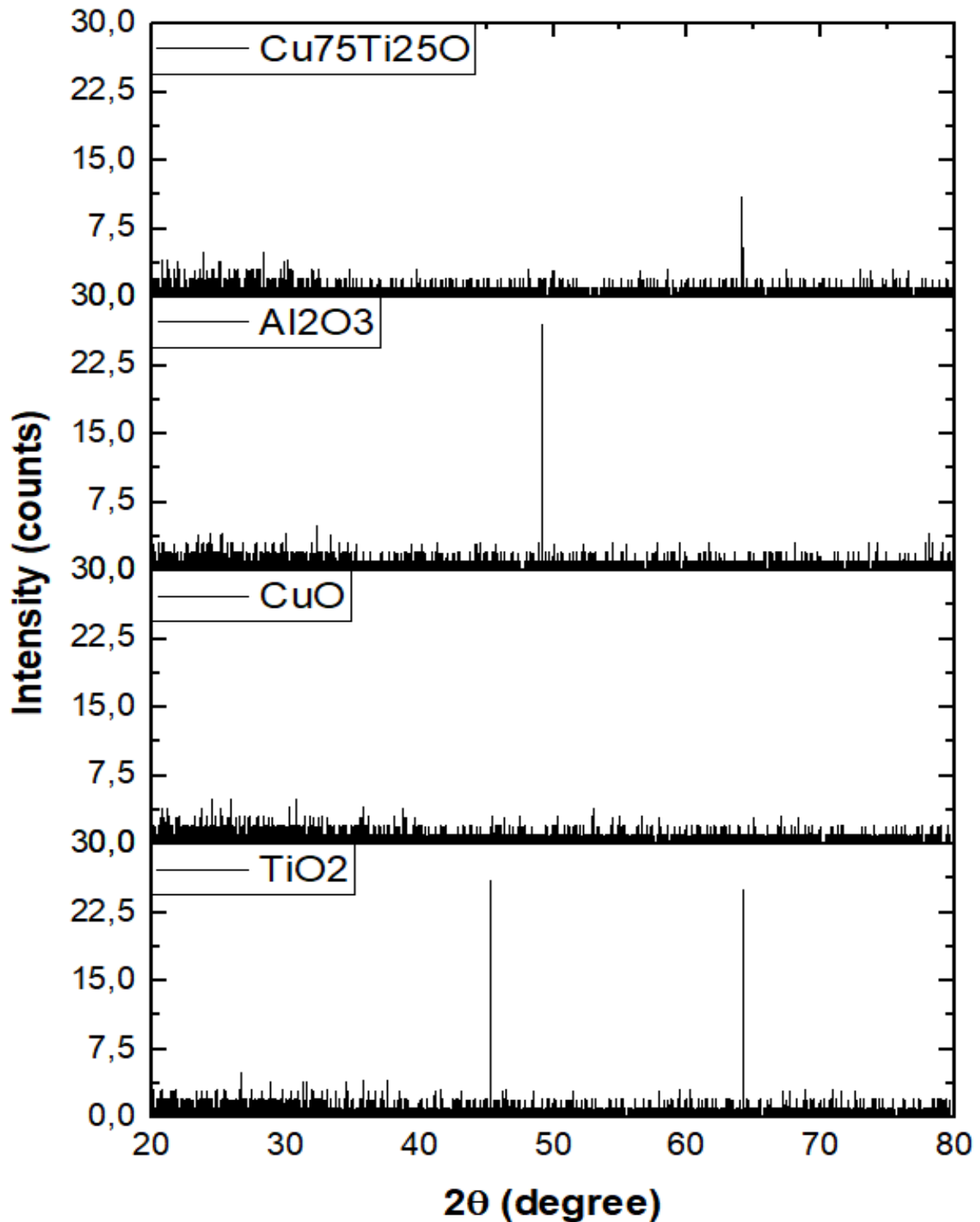


FIGURE 7.1 – XRD profile of various samples of thin films.

The θ - 2θ profile of the various thin film samples reveals distinct characteristics : a near absence or very low intensity of peaks. This observation indicates that all samples are amorphous films rather than crystalline. In X-ray diffraction, high-intensity peaks typically correspond to a well-defined crystalline structure, whereas amorphous films,

lacking long-range order, produce diffuse spectra or very broad and weak peaks.

Bibliographie

- [1] A. Rastogi, P. Singh, F. A. Haraz, A. Barhoum, Biological synthesis of nanoparticles : An environmentally benign approach, in : Fundamentals of Nanoparticles, Elsevier, 2018, pp. 571–604.
- [2] R. D. Umrani, K. M. Paknikar, et al., Jasada bhasma, a zinc-based ayurvedic preparation : Contemporary evidence of antidiabetic activity inspires development of a nanomedicine, Evidence-Based Complementary and Alternative Medicine 2015 (2015).
- [3] M. J. Limo, A. Sola-Rabada, E. Boix, V. Thota, Z. C. Westcott, V. Puddu, C. C. Perry, Interactions between metal oxides and biomolecules : from fundamental understanding to applications, Chemical reviews 118 (22) (2018) 11118–11193.
- [4] P. A. Koyale, D. K. Panda, S. D. Delekar, Metal oxide engineering, in : Advances in Metal Oxides and Their Composites for Emerging Applications, Elsevier, 2022, pp. 3–56.
- [5] S. Saha, M. Ali, M. Khaleque, M. Bacchu, M. A. S. Aly, M. Khan, Metal oxide nanocarrier for targeted drug delivery towards the treatment of global infectious diseases : A review, Journal of Drug Delivery Science and Technology (2023) 104728.
- [6] H. Saravanan, T. Subramani, S. Rajaramon, H. David, A. Sajeevan, S. Sujith, A. P. Solomon, Exploring nanocomposites for controlling infectious microorganisms : charting the path forward in antimicrobial strategies, Frontiers in Pharmacology 14 (2023) 1282073.

- [7] O. Ishchenko, V. Rogé, G. Lamblin, D. Lenoble, I. Fechete, TiO_2 , ZnO , and SnO_2 -based metal oxides for photocatalytic applications : principles and development, *Comptes Rendus. Chimie* 24 (1) (2021) 103–124.
- [8] S. Aththanayaka, G. Thiripuranathar, S. Ekanayake, Emerging advances in biomimetic synthesis of nanocomposites and potential applications, *Materials Today Sustainability* 20 (2022) 100206.
- [9] A. M. Negrescu, M. S. Killian, S. N. Raghu, P. Schmuki, A. Mazare, A. Cimpean, Metal oxide nanoparticles : Review of synthesis, characterization and biological effects, *Journal of Functional Biomaterials* 13 (4) (2022) 274.
- [10] R. Augustine, A. P. Mathew, A. Sosnik, Metal oxide nanoparticles as versatile therapeutic agents modulating cell signaling pathways : linking nanotechnology with molecular medicine, *Applied Materials Today* 7 (2017) 91–103.
- [11] M. Eshed, J. Lellouche, A. Gedanken, E. Banin, A Zn -doped CuO nanocomposite shows enhanced antibiofilm and antibacterial activities against *Streptococcus mutans* compared to nanosized CuO , *Advanced Functional Materials* 24 (10) (2014) 1382–1390.
- [12] M. Moros, J. Idiago-López, L. Asín, E. Moreno-Antolín, L. Beola, V. Grazú, R. M. Fratila, L. Gutiérrez, J. M. de la Fuente, Triggering antitumoural drug release and gene expression by magnetic hyperthermia, *Advanced drug delivery reviews* 138 (2019) 326–343.
- [13] M. P. Nikolova, M. S. Chavali, Metal oxide nanoparticles as biomedical materials, *Biomimetics* 5 (2) (2020) 27.
- [14] A. B. Sengul, E. Asmatulu, Toxicity of metal and metal oxide nanoparticles : a review, *Environmental Chemistry Letters* 18 (2020) 1659–1683.
- [15] A. Abdal Dayem, M. K. Hossain, S. B. Lee, K. Kim, S. K. Saha, G.-M. Yang, H. Y. Choi, S.-G. Cho, The role of reactive oxygen species (ROS) in the biological activities of metallic nanoparticles, *International journal of molecular sciences* 18 (1) (2017) 120.
- [16] P. C. Ray, H. Yu, P. P. Fu, Toxicity and environmental risks of nanomaterials : challenges and future needs, *Journal of Environmental Science and Health Part C* 27 (1) (2009) 1–35.

- [17] B. Kasemo, J. Lausmaa, Biomaterial and implant surfaces : a surface science approach., *International Journal of Oral & Maxillofacial Implants* 3 (4) (1988).
- [18] T. R. Nayak, H. Andersen, V. S. Makam, C. Khaw, S. Bae, X. Xu, P.-L. R. Ee, J.-H. Ahn, B. H. Hong, G. Pastorin, et al., Graphene for controlled and accelerated osteogenic differentiation of human mesenchymal stem cells, *ACS nano* 5 (6) (2011) 4670–4678.
- [19] M. H. Lamm, P. C. Ke, Cell trafficking of carbon nanotubes based on fluorescence detection, *Carbon Nanotubes : Methods and Protocols* (2010) 135–151.
- [20] E. Elena, et al., Aj friedenstein, founder of the mesenchymal stem cell concept, *Cellular Therapy and Transplantation* 1 (3) (2009) 35–38.
- [21] W. Jiang, J. Xu, Immune modulation by mesenchymal stem cells, *Cell proliferation* 53 (1) (2020) e12712.
- [22] M. Gebauer, J. Saas, F. Sohler, J. Haag, S. Söder, M. Pieper, E. Bartnik, J. Beninga, R. Zimmer, T. Aigner, Comparison of the chondrosarcoma cell line sw1353 with primary human adult articular chondrocytes with regard to their gene expression profile and reactivity to $il-1\beta$, *Osteoarthritis and cartilage* 13 (8) (2005) 697–708.
- [23] J. Fogh, *Human tumor cells in vitro*, Springer Science & Business Media, 2013.
- [24] S. Chevalier, E. Bouffartigues, J. Bodilis, O. Maillot, O. Lesouhaitier, M. G. Feuilloley, N. Orange, A. Dufour, P. Cornelis, Structure, function and regulation of *Pseudomonas aeruginosa* porins, *FEMS microbiology reviews* 41 (5) (2017) 698–722.
- [25] P. Pachori, R. Gothalwal, P. Gandhi, Emergence of antibiotic resistance *Pseudomonas aeruginosa* in intensive care unit ; a critical review, *Genes & diseases* 6 (2) (2019) 109–119.
- [26] B. Nebe, F. Luethen, R. Lange, U. Beck, Cellular activity and biomaterial's surface topography, in : *Materials science forum*, Vol. 539, Trans Tech Publ, 2007, pp. 517–522.
- [27] V. Bodiou, P. Moutsatsou, M. J. Post, Microcarriers for upscaling cultured meat production, *Frontiers in nutrition* 7 (2020) 10.
- [28] Z. Alhalili, Metal oxides nanoparticles : General structural description, chemical, physical, and biological synthesis methods, role in pesticides and heavy metal removal through wastewater treatment, *Molecules* 28 (7) (2023) 3086.

- [29] M. Khokhlova, M. Hammad, E. Lhuissier, R. Retoux, D. Goux, A. Fouchet, A. David, U. Lüders, K. Boumediene, W. Prellier, Differentiation of mesenchymal stem cells using metal oxide thin films, *Journal of Physics D : Applied Physics* 54 (23) (2021) 235402.
- [30] H. J. Haugen, M. Monjo, M. Rubert, A. Verket, S. P. Lyngstadaas, J. E. Ellingsen, H. J. Rønold, J. C. Wohlfahrt, Porous ceramic titanium dioxide scaffolds promote bone formation in rabbit peri-implant cortical defect model, *Acta biomaterialia* 9 (2) (2013) 5390–5399.
- [31] M. Orazizadeh, A. Khodadadi, V. Bayati, S. Saremy, M. Farasat, L. Khorsandi, In vitro toxic effects of zinc oxide nanoparticles on rat adipose tissue-derived mesenchymal stem cells, *Cell Journal (Yakhteh)* 17 (3) (2015) 412.
- [32] M. De, P. S. Ghosh, V. M. Rotello, Applications of nanoparticles in biology, *Advanced Materials* 20 (22) (2008) 4225–4241.
- [33] M. Jeyaraj, S. Gurunathan, M. Qasim, M.-H. Kang, J.-H. Kim, A comprehensive review on the synthesis, characterization, and biomedical application of platinum nanoparticles, *Nanomaterials* 9 (12) (2019) 1719.
- [34] E. A. McLaren, A. Maharishi, S. N. White, Influence of yttria content and surface treatment on the strength of translucent zirconia materials, *The Journal of prosthetic dentistry* (2021).
- [35] M. Z. Ibrahim, A. A. Sarhan, F. Yusuf, M. Hamdi, Biomedical materials and techniques to improve the tribological, mechanical and biomedical properties of orthopedic implants—a review article, *Journal of Alloys and Compounds* 714 (2017) 636–667.
- [36] B. D. Ratner, Replacing and renewing : synthetic materials, biomimetics, and tissue engineering in implant dentistry, *Journal of dental education* 65 (12) (2001) 1340–1347.
- [37] F. Silver, *Biomaterials, Medical Devices and Tissue Engineering : An Integrated Approach : An Integrated Approach*, Springer Science & Business Media, 1993.
- [38] A. Bui, S. G. Guillen, A. Sua, T. C. Nguyen, A. Ruiz, L. Carachure, M. D. Weber, A. Cortez, F. Tian, Iron-containing metal-organic framework thin film as a drug delivery system, *Colloids and Surfaces A : Physicochemical and Engineering Aspects* 650 (2022) 129611.

- [39] A. M. Oliveira, M. Machado, G. A. Silva, D. B. Bitoque, J. Tavares Ferreira, L. A. Pinto, Q. Ferreira, Graphene oxide thin films with drug delivery function, *Nanomaterials* 12 (7) (2022) 1149.
- [40] C. Angelé-Martínez, K. V. T. Nguyen, F. S. Ameer, J. N. Anker, J. L. Brumaghim, Reactive oxygen species generation by copper (ii) oxide nanoparticles determined by dna damage assays and epr spectroscopy, *Nanotoxicology* 11 (2) (2017) 278–288.
- [41] P. V. Gnaneshwar, S. V. Sudakaran, S. Abisegapriyan, J. Sherine, S. Ramakrishna, M. H. A. Rahim, M. M. Yusoff, R. Jose, J. R. Venugopal, Ramification of zinc oxide doped hydroxyapatite biocomposites for the mineralization of osteoblasts, *Materials Science and Engineering : C* 96 (2019) 337–346.
- [42] M. Laurenti, V. Cauda, Zno nanostructures for tissue engineering applications, *Nanomaterials* 7 (11) (2017) 374.
- [43] S. Zahoor, S. Sheraz, D. F. Shams, G. Rehman, S. Nayab, M. I. A. Shah, M. Ateeq, S. K. Shah, T. Ahmad, S. Shams, et al., Biosynthesis and anti-inflammatory activity of zinc oxide nanoparticles using leaf extract of *senecio chrysanthemoides*, *BioMed research international* 2023 (2023).
- [44] K. Alvarez, H. Nakajima, Metallic scaffolds for bone regeneration, *Materials* 2 (3) (2009) 790–832.
- [45] S. Mondal, U. Pal, 3d hydroxyapatite scaffold for bone regeneration and local drug delivery applications, *Journal of Drug Delivery Science and Technology* 53 (2019) 101131.
- [46] R. P. van Hove, I. N. Sierevelt, B. J. van Royen, P. A. Nolte, et al., Titanium-nitride coating of orthopaedic implants : a review of the literature, *BioMed research international* 2015 (2015).
- [47] Y. Wang, X. Yang, X. Zhang, Y. Wang, W. Pei, Implantable intracortical microelectrodes : reviewing the present with a focus on the future, *Microsystems & Nanoengineering* 9 (1) (2023) 7.
- [48] A. R. West, *Solid state chemistry and its applications*, John Wiley & Sons, 2022.
- [49] C. Vahlas, B. Caussat, P. Serp, G. N. Angelopoulos, Principles and applications of cvd powder technology, *Materials Science and Engineering : R : Reports* 53 (1-2) (2006) 1–72.

- [50] H.-U. Krebs, M. Weisheit, J. Faupel, E. Süske, T. Scharf, C. Fuhse, M. Störmer, K. Sturm, M. Seibt, H. Kijewski, et al., Pulsed laser deposition (pld)—a versatile thin film technique, *Advances in Solid State Physics* (2003) 505–518.
- [51] H. M. Christen, G. Eres, Recent advances in pulsed-laser deposition of complex oxides, *Journal of Physics : Condensed Matter* 20 (26) (2008) 264005.
- [52] G. Hajdok, J. Battista, I. Cunningham, Fundamental x-ray interaction limits in diagnostic imaging detectors : Spatial resolution, *Medical physics* 35 (7Part1) (2008) 3180–3193.
- [53] L. Elton, D. F. Jackson, X-ray diffraction and the bragg law, *American Journal of Physics* 34 (11) (1966) 1036–1038.
- [54] A. Gibaud, S. Hazra, X-ray reflectivity and diffuse scattering, *Current Science* (2000) 1467–1477.
- [55] N. Gadegaard, Atomic force microscopy in biology : technology and techniques, *Biotechnic & Histochemistry* 81 (2-3) (2006) 87–97.
- [56] J. D. Andrade, X-ray photoelectron spectroscopy (xps), *Surface and Interfacial Aspects of Biomedical Polymers : Volume 1 Surface Chemistry and Physics* (1985) 105–195.
- [57] J. Halim, An X-ray Photoelectron spectroscopy study of multilayered transition metal carbides (MXenes), Drexel University, 2016.
- [58] D. K. Owens, R. Wendt, Estimation of the surface free energy of polymers, *Journal of applied polymer science* 13 (8) (1969) 1741–1747.
- [59] D. Kaelble, Dispersion-polar surface tension properties of organic solids, *The Journal of Adhesion* 2 (2) (1970) 66–81.
- [60] N. Z.-J. Khong, Y. Zeng, S.-K. Lai, C.-G. Koh, Z.-X. Liang, K.-H. Chiam, H.-Y. Li, Dynamic swimming pattern of *pseudomonas aeruginosa* near a vertical wall during initial attachment stages of biofilm formation, *Scientific Reports* 11 (1) (2021) 1952.
- [61] B. Hames, N. Hooper, B. Hames, et al., *Biochemistry/david hames and nigel hooper.* (2005).
- [62] D. Kim, B. Choi, J. Song, S. Kim, S. Oh, E.-H. Jin, S.-S. Kang, E.-J. Jin, Titanium dioxide nanotube stimulate chondrogenic differentiation of limb mesenchymal cells by modulating focal activity, *Experimental & Molecular Medicine* 43 (2011) 455–461.

- [63] C. Boudot, M. Kühn, M. Kühn-Kauffeldt, J. Schein, Vacuum arc plasma deposition of thin titanium dioxide films on silicone elastomer as a functional coating for medical applications, *Materials Science and Engineering : C* 74 (2017) 508–514.
- [64] A. U. Khan, W. S. Al-Arjan, M. S. Binkadem, H. Mehboob, A. Haider, M. A. Raza, S. I. Abd Razak, A. Hasan, R. Amin, Development of biopolymeric hybrid scaffold-based on aac/go/nhap/titanium dioxide nanocomposite for bone tissue engineering : In-vitro analysis, *Nanomaterials (Basel, Switzerland)* 11 (2021) 1319.
- [65] O. A. Ogunmefun, B. L. Bayode, T. Jamiru, P. A. Olubambi, A critical review of dispersion strengthened titanium alloy fabricated through spark plasma sintering techniques, *Journal of Alloys and Compounds* (2023) 170407.
- [66] R. Pederson, Microstructure and phase transformation of ti-6al-4v, Ph.D. thesis, Luleå tekniska universitet (2002).
- [67] J. Elmer, T. Palmer, S. Babu, E. Specht, In situ observations of lattice expansion and transformation rates of α and β phases in ti-6al-4v, *Materials Science and Engineering : A* 391 (1-2) (2005) 104–113.
- [68] M. M. Dykas, S. K. Desai, A. Patra, M. R. Motapothula, K. Poddar, L. J. Kenney, T. Venkatesan, Identification of biofilm inhibitors by screening combinatorial libraries of metal oxide thin films, *ACS applied materials & interfaces* 10 (15) (2018) 12510–12517.
- [69] J. Park, K. Ahn, S. Yu, J. An, T. H. Lee, M.-G. Kim, Oxidation state control of solution-processed vanadium oxide thin-films and resistive switching of vanadium dioxide thin-film in a metastable state, *Thin Solid Films* (2018) 69–75.
- [70] D. Barrio, M. Braziunas, S. Etcheverry, A. Cortizo, Maltol complexes of vanadium (iv) and (v) regulate in vitro alkaline phosphatase activity and osteoblast-like cell growth, *Journal of trace elements in medicine and biology* 11 (2) (1997) 110–115.
- [71] B. Moretti, V. Pesce, G. Maccagnano, G. Vicenti, P. Lovreglio, L. Soleo, P. Apostoli, Peripheral neuropathy after hip replacement failure : is vanadium the culprit ?, *The Lancet* 379 (9826) (2012) 1676.
- [72] Q. Zhou, Z. Zhao, Z. Zhou, G. Zhang, R. C. Chiechi, P. van Rijn, Directing mesenchymal stem cells with gold nanowire arrays, *Advanced Materials Interfaces* 5 (14) (2018) 1800334.

- [73] L. Tang, P. Thevenot, W. Hu, Surface chemistry influences implant biocompatibility, *Current topics in medicinal chemistry* 8 (4) (2008) 270–280.
- [74] M. Miyauchi, A. Nakajima, T. Watanabe, K. Hashimoto, Photocatalysis and photoinduced hydrophilicity of various metal oxide thin films, *Chemistry of Materials* 14 (6) (2002) 2812–2816.
- [75] Z. Liang, L. Zhao, W. Meng, C. Zhong, S. Wei, B. Dong, Z. Xu, L. Wan, S. Wang, Tungsten-doped vanadium dioxide thin films as smart windows with self-cleaning and energy-saving functions, *Journal of Alloys and Compounds* 694 (2017) 124–131.
- [76] E. Müller, W. Vogelsberger, H.-G. Fritsche, The dependence of the surface energy of regular clusters and small crystallites on the particle size, *Crystal Research and Technology* 23 (9) (1988) 1153–1159.
- [77] L. Yang, Z. Jiang, L. Zhou, K. Zhao, X. Ma, G. Cheng, Hydrophilic cell-derived extracellular matrix as a niche to promote adhesion and differentiation of neural progenitor cells, *RSC advances* 7 (72) (2017) 45587–45594.
- [78] M. Khokhlova, A. Yadav, M. Hammad, E. Lhuissier, R. Retoux, D. Goux, A. Fouchet, A. David, U. Luders, K. Boumediene, et al., Controlling mesenchymal stem cell differentiation using vanadium oxide thin film surface wettability, *APL Materials* 11 (7) (2023).
- [79] G. P. Bodey, R. Bolivar, V. Fainstein, L. Jadeja, Infections Caused by *Pseudomonas aeruginosa*, *Reviews of Infectious Diseases* 5 (2) (1983) 279–313.
- [80] W. Kim, F. K. Tengra, Z. Young, J. Shong, N. Marchand, H. K. Chan, R. C. Pangule, M. Parra, J. S. Dordick, J. L. Plawsky, et al., Spaceflight promotes biofilm formation by *pseudomonas aeruginosa*, *PloS one* 8 (4) (2013) e62437.
- [81] N. Rabin, Y. Zheng, C. Opoku-Temeng, Y. Du, E. Bonsu, H. O. Sintim, Biofilm formation mechanisms and targets for developing antibiofilm agents, *Future medicinal chemistry* 7 (4) (2015) 493–512.
- [82] M. Jamal, W. Ahmad, S. Andleeb, F. Jalil, M. Imran, M. A. Nawaz, T. Hussain, M. Ali, M. Rafiq, M. A. Kamil, Bacterial biofilm and associated infections, *Journal of the chinese medical association* 81 (1) (2018) 7–11.
- [83] V. Stanić, D. Janačković, S. Dimitrijević, S. B. Tanasković, M. Mitrić, M. S. Pavlović, A. Krstić, D. Jovanović, S. Raičević, Synthesis of antimicrobial monophase

- silver-doped hydroxyapatite nanopowders for bone tissue engineering, *Applied Surface Science* 257 (9) (2011) 4510–4518.
- [84] J. Palmer, S. Flint, J. Brooks, Bacterial cell attachment, the beginning of a biofilm, *Journal of Industrial Microbiology and Biotechnology* 34 (9) (2007) 577–588.
- [85] L. K. Vestby, T. Grønseth, R. Simm, L. L. Nesse, Bacterial biofilm and its role in the pathogenesis of disease, *Antibiotics* 9 (2) (2020) 59.
- [86] I. Ostrov, A. Harel, S. Bernstein, D. Steinberg, M. Shemesh, Development of a method to determine the effectiveness of cleaning agents in removal of biofilm derived spores in milking system, *Frontiers in microbiology* 7 (2016) 1498.
- [87] G. Midelet, B. Carpentier, Impact of cleaning and disinfection agents on biofilm structure and on microbial transfer to a solid model food, *Journal of applied microbiology* 97 (2) (2004) 262–270.
- [88] K. Bruellhoff, J. Fiedler, M. Möller, J. Groll, R. E. Brenner, Surface coating strategies to prevent biofilm formation on implant surfaces, *The International journal of artificial organs* 33 (9) (2010) 646–653.
- [89] C. Cattò, F. Cappitelli, Testing anti-biofilm polymeric surfaces : where to start ?, *International journal of molecular sciences* 20 (15) (2019) 3794.
- [90] K. K. Amirtharaj Mosas, A. R. Chandrasekar, A. Dasan, A. Pakseresht, D. Galusek, Recent advancements in materials and coatings for biomedical implants, *Gels* 8 (5) (2022) 323.
- [91] Y.-H. Kim, Y.-r. Choi, K.-M. Kim, S.-Y. Choi, Evaluation of copper ion of antibacterial effect on pseudomonas aeruginosa, salmonella typhimurium and helicobacter pylori and optical, mechanical properties, *Applied surface science* 258 (8) (2012) 3823–3828.
- [92] M. Mansour lakouraj, G. Rahpaima, S. M. Mohseni, Synthesis, characterization, and biological activities of organosoluble and thermally stable xanthone-based polyamides, *Journal of Materials Science* 48 (2013) 2520–2529.
- [93] N. L. Brown, D. A. Rouch, B. T. Lee, Copper resistance determinants in bacteria, *Plasmid* 27 (1) (1992) 41–51.
- [94] Y. Seo, J. Hwang, E. Lee, Y. J. Kim, K. Lee, C. Park, Y. Choi, H. Jeon, J. Choi, Engineering copper nanoparticles synthesized on the surface of carbon nanotubes for anti-microbial and anti-biofilm applications, *Nanoscale* 10 (33) (2018) 15529–15544.

- [95] J. K.-M. Knobloch, S. Tofern, W. Kunz, S. Schütze, M. Riecke, W. Solbach, T. Wuske, “life-like” assessment of antimicrobial surfaces by a new touch transfer assay displays strong superiority of a copper alloy compared to silver containing surfaces, *PLoS one* 12 (11) (2017) e0187442.
- [96] H. Michels, J. Noyce, C. W. Keevil, Effects of temperature and humidity on the efficacy of methicillin-resistant staphylococcus aureus challenged antimicrobial materials containing silver and copper, *Letters in applied microbiology* 49 (2) (2009) 191–195.
- [97] M. Vincent, P. Hartemann, M. Engels-Deutsch, Antimicrobial applications of copper, *International journal of hygiene and environmental health* 219 (7) (2016) 585–591.
- [98] A. Lazary, I. Weinberg, J.-J. Vatine, A. Jefidoff, R. Bardenstein, G. Borkow, N. Ohana, Reduction of healthcare-associated infections in a long-term care brain injury ward by replacing regular linens with biocidal copper oxide impregnated linens, *International Journal of Infectious Diseases* 24 (2014) 23–29.
- [99] M. Amiri, Z. Etemadifar, A. Daneshkazemi, M. Nateghi, Antimicrobial effect of copper oxide nanoparticles on some oral bacteria and candida species, *Journal of Dental Biomaterials* 4 (1) (2017) 347.
- [100] D. Longano, N. Ditaranto, L. Sabbatini, L. Torsi, N. Cioffi, Synthesis and antimicrobial activity of copper nanomaterials, *Nano-antimicrobials : progress and prospects* (2012) 85–117.
- [101] G. Mary, S. Bajpai, N. Chand, Copper (ii) ions and copper nanoparticles-loaded chemically modified cotton cellulose fibers with fair antibacterial properties, *Journal of Applied Polymer Science* 113 (2) (2009) 757–766.
- [102] L. Randolph, M. Banjafar, T. R. Preston, T. Yabuuchi, M. Makita, N. P. Dover, C. Rödel, S. Göde, Y. Inubushi, G. Jakob, et al., Nanoscale subsurface dynamics of solids upon high-intensity femtosecond laser irradiation observed by grazing-incidence x-ray scattering, *Physical Review Research* 4 (3) (2022) 033038.
- [103] N. Popovici, E. Jimenez, R. Da Silva, W. Branford, L. Cohen, O. Conde, Optical and magnetic properties of co-doped tio₂ thin films grown by pulsed laser deposition, *Journal of non-crystalline solids* 352 (9-20) (2006) 1486–1489.

- [104] X. Huang, T. Li, X. Zhang, J. Deng, X. Yin, Bimetallic palladium@ copper nanoparticles : Lethal effect on the gram-negative bacterium *pseudomonas aeruginosa*, *Materials Science and Engineering : C* 129 (2021) 112392.
- [105] Z. Dwidjosiswojo, J. Richard, M. M. Moritz, E. Dopp, H.-C. Flemming, J. Winger, Influence of copper ions on the viability and cytotoxicity of *pseudomonas aeruginosa* under conditions relevant to drinking water environments, *International journal of hygiene and environmental health* 214 (6) (2011) 485–492.
- [106] D. Mitra, M. Li, E.-T. Kang, K. G. Neoh, Transparent copper-based antibacterial coatings with enhanced efficacy against *pseudomonas aeruginosa*, *ACS applied materials & interfaces* 11 (1) (2018) 73–83.
- [107] I. Salah, I. P. Parkin, E. Allan, Copper as an antimicrobial agent : Recent advances, *RSC advances* 11 (30) (2021) 18179–18186.
- [108] B. Bhushan, Y. C. Jung, Micro-and nanoscale characterization of hydrophobic and hydrophilic leaf surfaces, *Nanotechnology* 17 (11) (2006) 2758.
- [109] T. Ghodselahi, M. Vesaghi, A. Shafiekhani, A. Baghizadeh, M. Lameii, Xps study of the cu@ cu₂o core-shell nanoparticles, *Applied Surface Science* 255 (5) (2008) 2730–2734.
- [110] B. F. Matlaga, L. P. Yasenchak, T. N. Salthouse, Tissue response to implanted polymers : the significance of sample shape, *Journal of biomedical materials research* 10 (3) (1976) 391–397.
- [111] A. Taubert, J. F. Mano, et al., *Biomaterials surface science*, John Wiley & Sons, 2013.
- [112] M. Vincent, R. E. Duval, P. Hartemann, M. Engels-Deutsch, Contact killing and antimicrobial properties of copper, *Journal of applied microbiology* 124 (5) (2018) 1032–1046.
- [113] I. B. Gomes, M. Simões, L. C. Simões, Copper surfaces in biofilm control, *Nanomaterials* 10 (12) (2020) 2491.
- [114] K. P. Pontin, K. A. Borges, T. Q. Furian, D. Carvalho, D. E. Wilsman, H. R. P. Cardoso, A. K. Alves, G. Z. Chitolina, C. T. P. Salle, H. L. de Souza Moraes, et al., Antimicrobial activity of copper surfaces against biofilm formation by *salmonella enteritidis* and its potential application in the poultry industry, *Food Microbiology* 94 (2021) 103645.

- [115] M. J. Vargas-Straube, S. Beard, R. Norambuena, A. Paradela, M. Vera, C. A. Jerez, High copper concentration reduces biofilm formation in acidithiobacillus ferrooxidans by decreasing production of extracellular polymeric substances and its adherence to elemental sulfur, *Journal of proteomics* 225 (2020) 103874.
- [116] C. Molteni, H. K. Abicht, M. Solioz, Killing of bacteria by copper surfaces involves dissolved copper, *Applied and environmental microbiology* 76 (12) (2010) 4099–4101.
- [117] A. Yadav, S. Pradhan, M. Khokhlova, O. El Khaloufi, N. Z. J. Khong, S. K. Lai, A. Fouchet, A. David, U. Lüders, H.-Y. Li, M. S. R. Rao, W. Prellier, Enhancing implant performance : 20 bacterial initial formation with $\text{Cu}_{0.75}\text{Ti}_{0.25}\text{O}_2$ coating, *AIP Advances* 13 (9) (2023) 095008.
- [118] A. Khani, N. Talebian, In vitro bactericidal effect of ultrasonically sol–gel-coated novel $\text{CuO}/\text{TiO}_2/\text{PEG}/\text{cotton}$ nanocomposite for wound care, *Journal of Coatings Technology and Research* 14 (3) (2017) 651–663.
- [119] J. Li, D. Zhai, F. Lv, Q. Yu, H. Ma, J. Yin, Z. Yi, M. Liu, J. Chang, C. Wu, Preparation of copper-containing bioactive glass/eggshell membrane nanocomposites for improving angiogenesis, antibacterial activity and wound healing, *Acta biomaterialia* 36 (2016) 254–266.
- [120] J. W. Rasmussen, E. Martinez, P. Louka, D. G. Wingett, Zinc oxide nanoparticles for selective destruction of tumor cells and potential for drug delivery applications, *Expert opinion on drug delivery* 7 (9) (2010) 1063–1077.
- [121] M. Ahamed, M. J. Akhtar, M. M. Khan, H. A. Alhadlaq, Enhanced anticancer performance of eco-friendly-prepared $\text{Mo-ZnO}/\text{rGO}$ nanocomposites : Role of oxidative stress and apoptosis, *ACS omega* 7 (8) (2022) 7103–7115.
- [122] S.-H. Moon, W. J. Choi, S.-W. Choi, E. H. Kim, J. Kim, J.-O. Lee, S. H. Kim, Anti-cancer activity of ZnO chips by sustained zinc ion release, *Toxicology Reports* 3 (2016) 430–438.
- [123] N. R. Kukia, Y. Rasmi, A. Abbasi, N. Koshoridze, A. Shirpoor, G. Burjanadze, E. Saboory, Bio-effects of TiO_2 nanoparticles on human colorectal cancer and umbilical vein endothelial cell lines, *Asian Pacific journal of cancer prevention : APJCP* 19 (10) (2018) 2821.

- [124] G. Cui, J. Wu, J. Lin, W. Liu, P. Chen, M. Yu, D. Zhou, G. Yao, Graphene-based nanomaterials for breast cancer treatment : promising therapeutic strategies, *Journal of Nanobiotechnology* 19 (2021) 1–30.
- [125] Q. Huang, B. Chen, R. He, Z. He, B. Cai, J. Xu, W. Qian, H. L. Chan, W. Liu, S. Guo, et al., Capture and release of cancer cells based on sacrificeable transparent mno₂ nanospheres thin film., *Advanced healthcare materials* 3 (9) (2014) 1420–1425.
- [126] K. Wang, F. Wu, B. R. Seo, C. Fischbach, W. Chen, L. Hsu, D. Gourdon, Breast cancer cells alter the dynamics of stromal fibronectin-collagen interactions, *Matrix Biology* 60 (2017) 86–95.
- [127] S. Libring, A. Shinde, M. K. Chanda, M. Nuru, H. George, A. M. Saleh, A. Abdullah, T. L. Kinzer-Ursem, S. Calve, M. K. Wendt, et al., The dynamic relationship of breast cancer cells and fibroblasts in fibronectin accumulation at primary and metastatic tumor sites, *Cancers* 12 (5) (2020) 1270.
- [128] H. Raskov, S. Gaggar, A. Tajik, A. Orhan, I. Gögenur, The matrix reloaded—the role of the extracellular matrix in cancer, *Cancers* 15 (7) (2023) 2057.
- [129] N. V. Popova, M. Jücker, The functional role of extracellular matrix proteins in cancer, *Cancers* 14 (1) (2022) 238.
- [130] A. Aazmi, D. Zhang, C. Mazzaglia, M. Yu, Z. Wang, H. Yang, Y. Y. S. Huang, L. Ma, Biofabrication methods for reconstructing extracellular matrix mimetics, *Bioactive Materials* 31 (2024) 475–496.
- [131] B.-J. Kang, Y. Kim, S. H. Lee, W. H. Kim, H.-M. Woo, O.-K. Kweon, Collagen i gel promotes homogenous osteogenic differentiation of adipose tissue-derived mesenchymal stem cells in serum-derived albumin scaffold, *Journal of Biomaterials Science, Polymer Edition* 24 (10) (2013) 1233–1243.
- [132] R. Dietsch, T. Holz, H. Mai, M. Panzner, S. Völlmar, Pulsed laser deposition (pld)—an advanced state for technical applications, *Optical and quantum electronics* 27 (1995) 1385–1396.
- [133] R. D. Schulman, M. Trejo, T. Salez, E. Raphaël, K. Dalnoki-Veress, Surface energy of strained amorphous solids, *Nature communications* 9 (1) (2018) 982.
- [134] E.-H. M. El-Hussainy, A. M. Hussein, A. Abdel-Aziz, I. El-Mehasseb, Effects of aluminum oxide (al₂o₃) nanoparticles on ecg, myocardial inflammatory cytokines, redox state, and connexin 43 and lipid profile in rats : possible cardioprotective effect

of gallic acid, Canadian journal of physiology and pharmacology 94 (08) (2016) 868–878.